Toward Value-Added Applications of Asphaltenes

by

Kenny Xu

A thesis submitted in partial fulfillment of the requirements for the degree of

Doctor of Philosophy

Department of Chemistry

University of Alberta

Abstract

Asphaltenes are the heaviest fraction of crude oils. Asphaltenes are composed of carbon rings with aliphatic side chains, and they are precipitated from crude oils with small-chain alkanes, such as pentane or heptane. This complex class of molecules can be problematic during oil extraction, production, and transportation because asphaltenes are known to precipitate and adsorb onto surfaces. Therefore, there is extensive motivation to better understand the chemistry and behaviour of asphaltenes. The literature of asphaltene research is long and extensive. However, the vast majority of the research is motivated by understanding its chemistry. There is very little research into applications of this material. This dissertation strives to remedy this by exploring several different applications of asphaltenes.

Asphaltene is a rich source of carbon atoms and can be used as a precursor for graphitic carbon. Two different graphitic materials are made from asphaltenes: asphaltene-derived thin films and electrospun carbon fibres. The electrochemical reactivities of these materials are found to be comparable to glassy carbon. Asphaltene is also used as an additive to electrospin composite fibres with polyethylene oxide, polyvinylpyrrolidone, and polyacrylonitrile. Smooth fibres are successfully spun with polyvinylpyrrolidone and polyacrylonitrile, and subsequently carbonized in an inert atmosphere. Asphaltene is found to have a positive effect on carbon yield, increasing the diameter of carbonized fibres, compared to those without any asphaltene additive. Finally, an asphaltene coating is used to construct a simple solid-phase microextraction device for the extraction and detection of four polycyclic aromatic hydrocarbons (fluorene, fluoranthene, pyrene, benz[a]anthracene) using HS-SPME-GC. The limits of detection for the asphaltene-coating is lower than commercially available SPME fibres,

such as PDMS and PA, and also superior to many advanced nanomaterials such as MWCNTs. These applications show asphaltenes can be more than just a problematic fraction of crude oils. Its properties can be exploited to create useful, value-added materials.

Preface

This thesis is an original work by Kenny Xu under the supervision of Dr. Mark T. McDermott. No part of this thesis has been previously published.

Acknowledgements

My degree would not be possible without the kindness and the help I've received from people along the way. In the McDermott research group, students mostly work independently without our research projects overlapping too much. This means that we each have our own areas of expertise. During occasions when I need to use an instrument I'm not familiar with, fellow group members will gladly offer a helping hand. I also want to acknowledge and thank Dr. Cagri Ayranci, Dr. James Harynuk, and their research groups. Dr. Ayranci helped me tremendously with electrospinning, and Dr. Harynuk allowed me to use the GC in his research lab. Lastly, I want to thank Dr. McDermott, the Department of Chemistry, and Alberta Innovates for funding me to complete my degree.

Table of Contents

List of Tables

List of Figures

Glossary of terms

ADF	Asphaltene-derived films
AFM	Atomic force microscopy
CNT	Carbon nanotube
CV	Cyclic voltammetry
DMF	Dimethylformamide
HS	Headspace
GC	Glassy carbon
GC-FID	Gas chromatography-flame ionization detector
HOPG	Highly-oriented pyrolytic graphite
LOD	Limit of detection
MWCNT	Multi-walled carbon nanotube
PA	Polyacrylate
PAH	Polyaromatic hydrocarbon

PAN	Polyacrylonitrile
PDMS	Polydimethylsiloxane
PEO	Polyethylene oxide
PPF	Pyrolyzed photoresist film
PVB	Polyvinyl butyral
PVP	Polyvinylpyrrolidone
SEM	Scanning electron microscopy
SPME	Solid-phase microextraction
XPS	X-ray photoelectron spectroscopy

Chapter 1

Introduction

1.1 Overview

Carbon is one of the most abundant and versatile elements in the universe. The versatility of carbon is seen across its many allotropes and forms, including graphite, graphene, diamond, nanotubes, nanoparticles, and others, each with its own unique properties than can be exploited. Perhaps even more importantly, carbon is responsible for all forms of life. Without carbon, there would be no carbohydrates, proteins, nucleic acids, or any organic macromolecules that are necessary for the existence of life. As such, carbon has a broad and extensive history in research across many different disciplines.

The interest in carbon materials arises from their various advantageous properties. Diamond, or sp^3 carbon, is well-known since antiquity for its exceptional hardness and transparency. Graphitic carbon, or sp^2 carbon, has traditionally been valued for its conductivity. Because of its abundance, stability, and conductivity, graphite is commonly used in energy related applications such lithium-ion batteries,[1–3] in electrochemistry,[4,5] and supercapacitors.[6,7] In recent decades, with the advent of nanotechnology, there has been growing interest in carbon nanomaterials, including graphene, carbon nanotubes, and carbon nanoparticles. Graphene and carbon nanotubes are exciting, novel materials with many potential applications. Carbon nanotubes, which are essentially folded graphene sheets, have impressive mechanical properties. Single-walled carbon nanotubes (SWNTs) have exhibited Young's moduli and tensile strengths that are greater than that of steel wires.[8,9] Their conductivity and strength allow carbon nanotubes to act as additives to synthesize composite materials with superior mechanical and electrical properties. Carbon nanotubes have been added to make composites with thermoplastics,[10–12] stainless steel,[13] epoxies,[14–16] aluminum,[17,18] and many other

materials. Furthermore, carbon nanotubes have excellent potential as supercapacitors due to their high surface area to volume ratio and conductivity.[19–21] Other carbon nanomaterials such as graphene and carbon nanoparticles also have their own unique properties that can be exploited. However, this thesis will not aim to discuss all carbon materials in detail. Carbon is studied extensively and there is a myriad of exhaustive reviews available in literature.

Because of their various properties and allotropes, carbon materials can be used in a wide range of applications including, but not limited to, sensing, biomedicine, energy, composites, and electrochemistry. Hence, carbon materials are an exciting and valuable area of research. The purpose of this thesis is using asphaltenes as a carbon source to synthesize useful, value-added carbon materials.

1.2 Introduction to asphaltenes

Asphaltenes are a complex class of hydrocarbon molecules found in crude oils. The term asphaltene was coined by J. B. Boussingault in 1837 when he noticed that the distillation residue of bitumen resembled asphalt.[22] Today, asphaltenes are defined by their solubility. Specifically, asphaltenes that are precipitated in pentane are known as C_5 asphaltenes whereas those that are precipitated in heptane are C_7 asphaltenes. Among the SARA fractions of heavy crude oil, which are saturates, aromatics, resins, and asphaltenes, the asphaltene fraction has the highest molecular weight. Because they are not defined by their structure, but rather by solubility, and coupled with high molecular weights, asphaltenes are difficult to study and characterize. Even the most basic physical properties, such as molecular weights and chemical structure, are still up for debate. Hence, asphaltenes are not well-understood and this poses a significant problem in industry.

Asphaltenes have long been known for causing problems in the crude oil industry. At certain temperatures and pressures, which are not consistent across different oil fields, asphaltenes can precipitate and adsorb onto surfaces. This precipitation can lead to obstructed pipelines during oil extraction and transportation,[22] as well as catalyst deactivation during treatment and refining.[23] The maintenance of equipment as well as production issues caused by asphaltene precipitate pose a significant financial impact. Hence, there is strong impetus to better understand the structure, chemistry, and behaviour of asphaltenes.

1.3 Asphaltene structure

The complexity and controversy surrounding asphaltene structure arise from the fact that asphaltenes are not a single molecule. Asphaltenes encompass countless possible isomers, which means there is no unique structure, composition, or molecular weight. This is why asphaltene properties are usually given as an average, or a range of values. The basic structure of asphaltene molecules have long been a topic of debate. The first comprehensive theory on asphaltene structure was given by professor Teh Fu Yen, known as the Yen model.[24] He proposed an average structure with aromatic nuclei, which are substituted with alkyl side chains. The substituents are mostly methyls, with no second or tertiary carbons. This proposed asphaltene microstructure is shown in Figure 1.1. He also proposed a bulk, macrostructure of multiple asphaltene molecules stacked together due to π-π interactions.

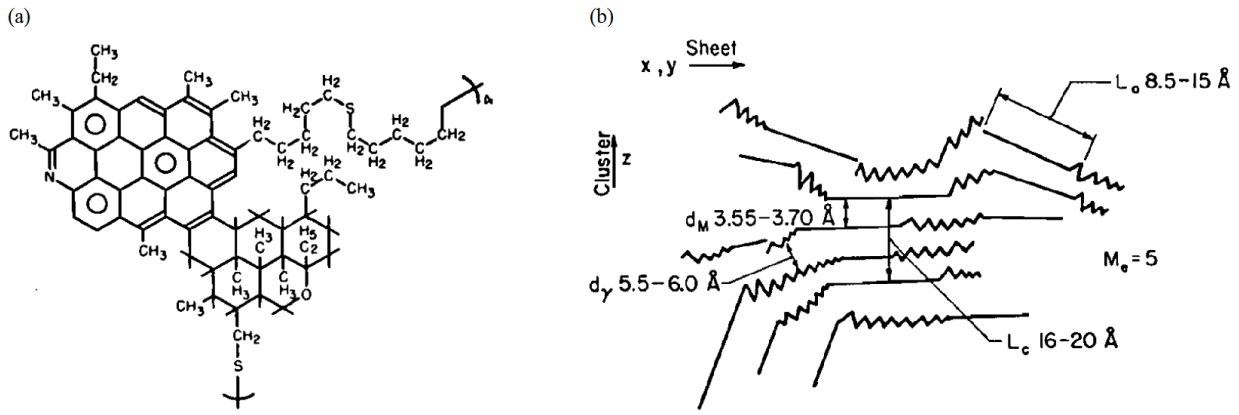

Figure 1.1 a) proposed asphaltene microstructure b) cross-sectional view of proposed asphaltene macrostructure. Zig-zag line represents saturated carbon chains; straight line represents edge of flat sheets of condensed aromatic rings. Reprinted with permission from "Yen, T. F. Structure of Petroleum Asphaltene and Its Significance. *Energy Sources* **1,** 447–463 (1974)".

The Yen model of asphaltene structure was proposed in 1974, and since then there has been tremendous advancement in asphaltene science. The current, predominant theory on asphaltene structure is known as the Yen-Mullins model, which is an updated model proposed by Dr. Oliver Mullins.[25] In the Yen-Mullins model, as shown in Figure 1.2, the average asphaltene molecule contains a central polycyclic aromatic hydrocarbon (PAH) system with 4 to 10 fused rings, with alkane substituents as sidechains. These PAHs are the primary sites of intermolecular interaction and they contribute to the formation of asphaltene nanoaggregates. These nanoaggregates, also known as primary aggregation, are roughly ~2 nm in diameter. At higher concentrations starting at ~2 g/L, these nanoaggregates will form clusters in the range of 100-300 nm in diameter. This aggregation of asphaltene molecules is responsible for causing the aforementioned production problems in the oil industry. Hence, the motive behind the vast majority of asphaltene research is to better understand their chemistry and behaviour in order to mitigate the financial impact of asphaltenes. However, this thesis explores asphaltenes in a

different direction. Asphaltenes are known for their problematic behaviour, but currently have little to no useful application. The purpose behind this thesis is using asphaltenes as a carbon source to synthesize useful, value-added materials.

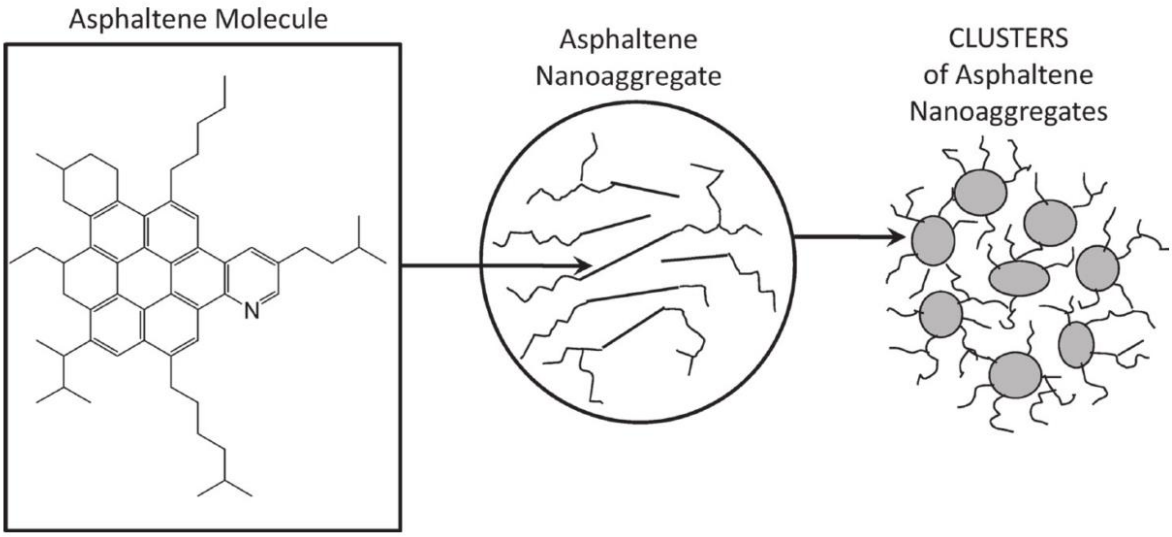

Figure 1.2 Proposed asphaltene structure and aggregation from the Yen-Mullins model. Reprinted with permission from "Mullins, O. C. The Modified Yen Model. *Energy & Fuels* **24,** 2179–2207 (2010)".

1.4 Pyrolysis for the production of graphitic materials

Graphitic carbon materials are widely found in application such as electrochemistry, supercapacitors, batteries, and other energy-related areas. This is because graphitic carbon is an inexpensive, versatile, and conductive material. The properties of graphite derive from its planes of sp^2 carbon. Because of the sp^2 structure, delocalized electrons can freely move in the basal plane of the graphite crystal. Graphitic materials are hence conductive and behave like semimetals or metals, depending on the conditions under which the material was made. For highly oriented pyrolytic graphite (HOPG), which is highly ordered and has large crystals, there is only a small overlap between the valence and conduction band. HOPG behaves like a

semimetal because of its low density of states. In contrast, disordered graphite, which is more electrochemically active than the basal plane of HOPG, has a greater density of states because of defect energy levels introduced by disorder in the sp^2 structure. Despite having greater resistivity for disordered graphitic materials such as glassy carbon compared to HOPG, glassy carbon actually exhibits higher electron transfer rates because of the difference in the density of states between the two materials.[26] It has been established that graphitic materials can exhibit vastly different behaviours depending on how they are made. Factors such as pressure, temperature, and the precursor material can influence graphite's structure, conductivity, and electrochemical reactivity.

The processes of synthesizing graphitic carbon are well-understood and diverse. Graphitic materials have been synthesized by electron beam evaporation,[27,28] chemical vapour deposition,[29,30] electron cyclotron resonance sputtering,[31,32] and pyrolysis of various precursors. In plain terms, pyrolysis means the heat treatment of a carbon source material, generally up to temperatures between 1000 to 3000 ^{o}C. For all of these methods, a high temperature is required for the formation and rearrangement of carbon atoms in a sp^2 structure. However, pyrolysis has the advantage of not requiring complicated and expensive equipment. These various methods to synthesize graphite material may result in vastly different properties, as seen in Table 1.1.[26] The electrode material, synthesized via different methods and conditions, as well as the pre-treatment step, can all drastically affect the electrochemical reactivity. For the two redox systems shown in Table 1.1, the electron transfer rates for the basal plane of HOPG is two to five orders of magnitude lower than that of glassy carbon, even though both materials are sp^2 carbon. It is evident that not all graphitic materials are the same. The

development of new graphitic materials with unique properties is still an exciting and valuable area of research. Specifically, we aim to develop an inexpensive graphitic substrate with comparable properties to materials that are typically made with complex equipment and expensive precursors.

Electrode material	pretreatment	k^o, $Ru(NH_3)_6^{3+/2+}$ cm/s	k^o, $Fe(CN)_6^{3-/4-}$ cm/s
HOPG basal plane		0.0014	$<10^{-7}$
HOPG edge plane			0.06-0.1
GC20	conventional polish		0.005±0.003
GC20	ultraclean polish	0.51	0.14
GC20	polish+laser	>0.4	0.46
GC20	IPA/AC	0.11	0.090
PPF	IPA/AC	0.02	
e-beam carbon	IPA/AC	0.046	
electron cyclotron resonance carbon film		close to reversible limit	0.012

Table 1.1 Electrode kinetics for $Ru(NH_3)_6^{3+/2+}$ and $Fe(CN)_6^{3-/4-}$. Reprinted with permission from "McCreery, R. L. Advanced carbon electrode materials for molecular electrochemistry. *Chem. Rev.* **108,** 2646–2687 (2008)."

1.5 Precursors for pyrolytic graphite

Pyrolytic graphite is the product of high temperature treatment of a carbon precursor material. Pyrolysis is a common method of producing graphite because it does not require complex equipment, it can mass produce materials, and it is versatile since different precursor materials can be used. To make pyrolytic graphite, the precursor material must contain carbon atoms. At high temperatures, thermal decomposition of the precursor will occur and carbon-carbon bonds will be formed, mostly as sp^2. Hence, the exact identity of the precursor material does not matter significantly, as long as it provides a rich source of carbon atoms.

The synthesis of pyrolytic graphite has a long and extensive history in literature. The process of depositing carbon was first patented in 1880 by William Sawyer, in which a carbon pencil was "immersed in a hydrocarbon gas or, liquid and heated to an extremely high temperature".[33] After that, no significant development occurred until the middle of the 20th century, during which small hydrocarbons were used as precursors for pyrolytic graphite. In the 1960s, Karu and Beer produced very thin graphite films from the pyrolysis of methane.[34] Graphite was formed when methane gas came in contact with a hot nickel plate heated to 900 ^{o}C. Similar methods of producing graphite were performed using acetylene,[35,36] propane,[37,38] ethane,[38] ethylene,[38] benzene,[38] and cyclohexane[38] as the carbon source. For all of these gaseous precursors, a hot surface was required for the deposition. However, it was found that often times a specific temperature or pressure range were required to produce a graphite coating. For example, Karu and Beer found that no graphite formed below a temperature of 700 ^{o}C or above a temperature of 1100 ^{o}C.[34] Yajimi et al. also found that the rate of graphite deposition is dependent upon the pressure, and does not have a clear, linear relationship.[37] The

highly ordered form of graphite, HOPG, can be made by stress annealing pyrolytic graphite at 3000 ^{o}C.[39] In recent years, the vapour deposition method has been focused on producing very thin graphite films that are only a few graphene layers thick. This has been motivated by graphene's impressive mechanical, electrical, and chemical properties. The process to deposit these very thin graphite films is analogous to the methods mentioned above. Obraztsov et al. synthesized graphite films with 1.5±0.5 nm thickness by using methane gas and a nickel or zinc substrate heated to 950 ^{o}C.[40] Reina et al. also synthesized films of 1.2 – 3.0 nm in thickness by the deposition of a methane/hydrogen gas mixture onto a heated nickel substrate.[41]

In contrast to vapour deposition, the pyrolysis of solid or liquid precursors does not require a metal surface to catalyze the reaction. Glassy carbon, a common reference material used in electrochemistry, is made by the pyrolysis of a non-gaseous precursor. Glassy carbon is a hard, electrically conductive sp^2 carbon material made by the pyrolysis of a carbonaceous polymer or resin in an inert atmosphere. It was first discovered and patented by Bernard Redfern, who pyrolyzed phenol-aldehyde resins at 1400 ^{o}C.[42] Glassy carbon has also been made from precursors such as polyfurfuryl alcohol, acetone-furfural polymers, and other aromatic resins.[43] The Whitesides group used polymers of phenol-formaldehyde and furfuryl alcohol-phenol to make glassy carbon microstructures with tunable electrical properties.[44] The Madou group used SU-8 photoresist to make similar carbon micro and nano-electromechanical systems that have potential applications in batteries and fuel cells.[45–47] Photoresist is a commonly used precursor for graphitic materials because it is light sensitive and thus can be patterned into unique structures. Other than carbon micro-electromechanical systems, photoresist has also been used to produce conductive carbon films. A nearly atomically flat carbon film was

produced from the pyrolysis of photoresist and found to have similar electrochemical reactivity as compared to glassy carbon.[48] Furthermore, pyrolyzed photoresist carbon films were shown to be more stable in air compared to glassy carbon, with the O/C ratio for the photoresist-derived film to be less than 2% after 4 days of air exposure.[48]

1.6 Crude oils as precursors

There is a myriad of different molecules and polymers, both gaseous and non-gaseous, that can be used as precursors to produce carbonaceous, graphitic materials. The one thing in common among them is that the precursor must be carbon based, so it can provide a source of carbon atoms. Hence, it is not unfeasible that crude oils, a complex mixture of carbon based molecules, can be used as a carbon source. Crude oils are composed of organic molecules ranging from small alkanes to complex aromatic ring systems, and these can be separated into fractions known as asphaltenes and maltenes (saturates, aromatics, resins). Pyrolysis of these fractions, including asphaltenes, is not new. In fact, pyrolysis is a common technique used to analyze crude oils, especially asphaltenes.

The structure of the complex asphaltene fraction of crude oils is a popular topic of debate. One technique that has been used to analyze asphaltene structure is pyrolysis coupled with mass spectroscopy and chromatography. Pyrolysis will induce the decomposition of asphaltene molecules into their smaller substituents. These substituents can then be analyzed to shed light on the original structure of the asphaltenes. For example, thermal cracking of asphaltenes first produces volatile light gases, such as methane, ethane, butane, and at higher temperatures, effluents include a complex mixture of paraffins, naphthenes and aromatics.[49] This is consistent with the general known structure of asphaltenes. There are numerous

examples in literature on the pyrolysis or thermal cracking of asphaltenes, but they will not be reviewed in depth because they focus on the gaseous species evolved from the asphaltenes. There is currently no research done on the application of carbonaceous material remaining after asphaltene pyrolysis. However, other petroleum-derived liquids have been used as precursors for carbon materials.

Pitch is a general term describing viscous, carbonaceous liquids derived from petroleum processing. It has been used as a precursor for various applications. Pitch has been widely studied as a binder material for lithium ion batteries. This is because carbon materials can insert lithium reversibly and are also conductive. Pitch provides a rich source of carbon and is a viable option for this application. For example, Wen et al. made a composite material from pitch, graphite, and silicon and pyrolyzed it at 1000 ^{o}C to use it as the anode.[50] Pitch-based carbon fibres have also been incorporated into the anode of lithium ion batteries.[51] These batteries show high reversible capacity up to 800–900 mAh/g, but cyclic stability and efficiency still needs improvement. Pyrolyzed petroleum pitch has also been used as active carbon with desulphurization properties,[52] carbon foam with high thermal conductivity,[53] and carbon/carbon composite materials.[54] As a precursor, petroleum pitch has the benefit of being inexpensive, abundant, and having a high carbon content. This is akin to asphaltenes since both are derived from crude oils. The difference between them being that asphaltenes are a specific class of materials defined by solubility whereas pitch is a general term enveloping an inconsistent group of viscous petroleum-derived liquids. Despite this difference, asphaltenes should also be a viable precursor for carbon materials.

1.7 Carbon films

Carbon is an attractive material for many applications due to its electrical and thermal conductivity, versatility, and stability. Perhaps one of the simplest forms of a carbon material is a thin film. Graphitic carbon films are often used in electrochemistry, sensing, and energy applications since graphitic carbon is a conductor. As mentioned previously, the conductivity of graphite arises from its delocalized electrons of sp^2 carbon. This allows graphitic carbon to act as an effective conductor, similar to semi-metals and metals.

An important and active area of research is in energy and in particularly, the advancement of lithium ion batteries. Lithium ion batteries are ubiquitous in the modern world and there is persistent need to develop novel materials to improve the efficiency and longevity of batteries. Graphitic carbon is one such material used in lithium ion batteries. Even though graphite-based lithium ion batteries do not have great capacity, due to limited intercalation, they are prized for their low expansion during lithium insertion. For example, Datta et al. prepared a lithium ion battery anode with a thin amorphous carbon film in contact with another silicon layer.[55] This additional presence of a thin carbon film resulted in improved capacity retention and longevity compared to an anode with only a silicon layer. The carbon film acts as a buffer to relieve stress during charge and discharge cycles. Similarly, Li et al. constructed an anode with silicon spheres embedded in a carbon film.[56] This again showed the benefit of a carbon film to improve the cyclic efficiency of the lithium ion batteries.

Another area where carbon films are prevalent is electrochemistry. A glassy carbon electrode, which can be thought of as a thick glassy carbon film, is a reference material commonly used in the laboratory to probe the electrochemical reactivity of various systems.

However, there are a few disadvantages to glassy carbon, including high surface oxygen content and the requirement of high temperatures of up to 3000 ^{o}C during production. There is an ongoing need to manufacture alternative carbon films with excellent electrochemical reactivity and chemical stability. One such alternative carbon film was made by Blackstock et al. An ultra-flat film was prepared using electron beam evaporation.[28] The carbon film was 1-4 Å in roughness and 7 nm in thickness. Electron transfer rates for this carbon film were measured to be comparable to that of glassy carbon and better than many other thin-film carbon electrodes in literature.[28] Ranganathan et al. produced a similar, flat carbon film using photoresist.[48] The pyrolyzed photoresist film was 1 nm in rms roughness and also very stable in air, with low surface oxygen composition. These characteristics minimize the double layer capacitance and faradaic capacitance from surface active groups. Ranganathan et al. found that the pyrolyzed photoresist film had fast electron-transfer rates for two common redox systems (hexaaminеruthenium and ferri/ferrocyanide) that are comparable to glassy carbon. These electrochemically active, low capacitance carbon films are not only useful in electrochemistry, but also have potential applications in molecular electronics and analytical settings where background current is an issue. For example, the aforementioned photoresist film was incorporated into a molecular junction where a layer of stilbene was sandwiched between the carbon film and mercury.[57] The characteristic of this molecular junction is that the resistance of the monolayer varies with respect to voltage. Carbon films are promising materials for molecular electronics because of their conductivity and propensity for surface modification.

Electroanalysis is the detection of analytes via electrochemistry. Carbon film electrodes have the benefit of a wide potential window and being resistant to oxidation. Hence, the use of

carbon films in electroanalysis is extensive because of their desirable properties. Hydrazine is an environmental toxin and Hadi et al. developed a pyrolytic carbon film electrode as an electrochemical sensor for its detection.[58] This carbon film sensor has a low limit of detection and high sensitivity compared to surface modified glassy carbon electrodes. A further benefit is the simplicity and lack of surface modification required for this hydrazine sensor. Carbon films have also been doped with metal nanoparticles to improve their electroanalytical capability. Platinum and iridium doped carbon films have been studied for the detection of hydrogen peroxide.[59,60] You et al. found that compared to a platinum metal electrode, whose electrochemical reactivity gradually decreases due to oxidation, a carbon film electrode embedded with platinum nanoparticles is more resistant to oxidation and is very active for the oxidation of hydrogen peroxide.[59] The detection of important biomolecules such as glucose, acetylcholine, and choline is hence possible since hydrogen peroxide is a by-product of enzymatic reactions of these biomolecules. From this short overview of carbon films, it is clear that carbon films have tremendous potential in energy and electrochemistry related areas. The development of new and unique carbon-based films and materials is a relevant and exciting area of research.

1.8 Methods of fabrication for carbon films

There are various methods of fabricating carbon films, and some of them have been briefly touched upon. These methods can be generally categorized into pyrolysis and non-pyrolysis techniques. Non-pyrolysis techniques include methods such as chemical vapour deposition, sputtering, or electron beam evaporation. The ultra-flat carbon film fabricated by Blackstock et al. was fabricated via electron beam evaporation, where an electron beam was

used to evaporate a graphite source onto a silicon substrate.[28] This technique has the benefit of a slow and controllable deposition rate, thus resulting in an atomically flat surface. Sputtering is a similar process, but instead of evaporation, the target atoms are ejected due to the bombardment of energetic gas particles. Since the target is not being evaporated, high temperatures are not required for sputtered films. This is especially useful for the fabrication of composite carbon/metal films. You et al. created carbon/platinum and carbon/iridium film electrodes by cosputtering metal and carbon targets onto a silicon substrate.[59,60] Homogeneous carbon films produced by sputtering have ranged from being graphite-like to diamond-like. Rossnagel et al. found that the resistivity of sputtered carbon films depend on the sputtering gas pressure, with higher pressure depositions being more insulating and diamond-like.[61] A conductive, graphite-like sputtered carbon film was prepared by Schlesinger et al. and found to have similar electron transfer rates to glassy carbon for ferri/ferrocyanide.[62] Other methods of fabrication found in literature include chemical vapour deposition,[40,63] laser ablation,[64,65] and ion-beam deposition.[66] These techniques can produce a wide range of carbon films, from conductive to insulating, with homogeneous, flat morphologies. However, they require complex and expensive machinery, and often also require vacuum conditions.

Pyrolysis is a simpler, and more economical solution to fabricating carbon films compared to the techniques mentioned above. Pyrolysis does not require complex instruments such as magnets or lasers because only a furnace is required for heat treatment. Vacuum conditions are also not required because pyrolysis is often done under an inert or reducing atmosphere. Two important factors for pyrolysis are the temperature and atmosphere. The pyrolysis temperature determines the degree of graphitization and hence it determines the

conductivity and electrochemical reactivity of the film. The affects of temperature can be seen in the photoresist films made by Ranganathan et al..[48] Table 1.2 shows the ΔE_p for ferri/ferrocyanide and hexaammineruthenium redox systems both decrease with respect to an increase in pyrolysis temperature. A decrease in ΔE_p is indicative of improved conductivity and graphitization. It is evident that graphitization does not readily occur under 800 ^oC, and that temperatures of 1000 ^oC or above are required for significant graphitization. Table 1.2 also shows that the atmosphere also affects ΔE_p. The ΔE_p for films pyrolyzed under forming gas are all lower than the same films pyrolyzed under vacuum. Forming gas is composed of an inert gas with a small amount of hydrogen. It creates a reducing effect, which increases the amount of hydrogen-terminated carbons and lowers the amount the surface oxygen groups. A hydrogen-terminated carbon surface can improve electron transfer rates for certain redox system as listed in Table 1.2, but an oxygen-rich surface could also be beneficial for certain redox systems that require adsorption or catalysis by surface oxygen groups. Pyrolysis has the benefit of being a very simple process, and the conductivity and the surface composition of the film can be manipulated through temperature and atmosphere conditions.

Curing temperature (°C)	1 mM $[Ru(NH_3)_6]^{+3/+2}$ in 1 M KCl Scan rate: = 200 mV/s ΔE_p (Forming gas, mV)	ΔE_p (Vacuum, mV)	1 mM $Fe(CN)_6^{3-/4-}$ in 0.1 M H_2SO_4 Scan rate: = 200 mV/s ΔE_p (Forming gas, mV)	0.1 mM $[Ru(NH_3)_6]^{+3/+2}$ in 1 M KCl Scan rate: = 200 mV/s ΔE_p (Forming gas, mV)	ΔE_p (Vacuum, mV)	0.1 mM $Fe(CN)_6^{3-/4-}$ in 0.1 M H_2SO_4 Scan rate: = 200 mV/s ΔE_p (Forming gas, mV)
600	—	—	—	—	—	—
700	—	87	—	—	158	339
800	146	92	142	88	100	77
900	109	93	101	72	90	69
1000	88	98	90	70	84	80
1100	70	—	84	70	—	63

Table 1.2. Effects of curing temperature on ΔE_p for AZ4330 photoresist films by Ranganathan *et al*. Reprinted with permission from "Ranganathan, S., Mccreery, R., Majji, S. M. & Madou, M. Photoresist-Derived Carbon for Microelectromechanical Systems and Electrochemical Applications. *J. Electrochem. Soc.* **147,** 277–282 (2000)."

1.9 Electrochemical reactivity of carbon films

As discussed earlier, electrochemistry is a major application for conductive, carbon films. The electrochemical reactivity for carbon films is heavily dependent on the carbon structure as well as the surface composition. The electronic properties of carbon films can vary widely from insulating undoped diamond to electroactive graphitic films. The difference in electroactivity is due to the density of states of varying materials. Among carbon materials, graphitic carbon exhibits high density of states because of defects in its sp^2 structure. A high density of states means that it is more likely to have an appropriate energy state to either accept or donate electrons during a redox reaction. This makes electron transfer possible for graphitic film electrodes.

A common redox system to evaluate an electrode is hexaammineruthenium ($Ru(NH_3)_6^{3+/2+}$). Hexaammineruthenium is an outer-sphere redox system because it does not require adsorption or bond formation with surface moieties. Its electron transfer rate is also largely independent of surface cleanliness or surface composition. Surface modification of a glassy carbon electrode with surface oxides, methylene blue, nitrophenyl, and anthraquinone-2,6-disulfonate all had

very little impact on the electron transfer rate of $Ru(NH_3)_6^{3+/2+}$.[4] Unless for surface layers with large molecules that can hinder electron tunneling, a surface monolayer will not affect outer-sphere reactions. Hence, hexaammineruthenium can used to probe the basic conductivity of an electrode and is useful for comparing various carbon films.

1.10 Electrospinning

Electrospinning is a simple method of manufacturing carbon fibres, polymer fibres, or composite fibres. Electrospinning has a long history dating back to the 1940s, during which Anton Formhals was issued a series of patents on producing fine fibres in an electric field.[67–69] In the 1960s, Geoffrey Taylor described the theoretical framework behind electrospinning, to what is now known as the Taylor cone.[70,71] Taylor describes in his paper that "Fine jets of slightly conducting viscous fluids…can be drawn from conducting tubes by electric forces".[70] This is the driving force behind electrospinning. When an electric field is applied to a conducting liquid at an orifice, a charged droplet will form as charged ions collect on the surface of the droplet. The electrostatic forces and the surface tension are in balance to form a cone shaped droplet known as the Taylor cone. If the strength of the electric field further increases, it will overcome the surface tension of the liquid and jets of the solution will eject from the tip of the Taylor cone. As the solvent evaporates, fibrous material can be formed. Figure 1.3 shows the basic electrospinning process where a high voltage is applied between a solution and a conducting substrate. At a sufficient voltage, solvent evaporation of charged jets may form fibrous materials on the conducting substrate. The formation of electrospun fibres depends on the applied voltage, the polymer solution, and other factors such as flow rate and distance.

However, as a whole, electrospinning is very simple, powerful, and versatile solution to making a wide range of polymer fibres.

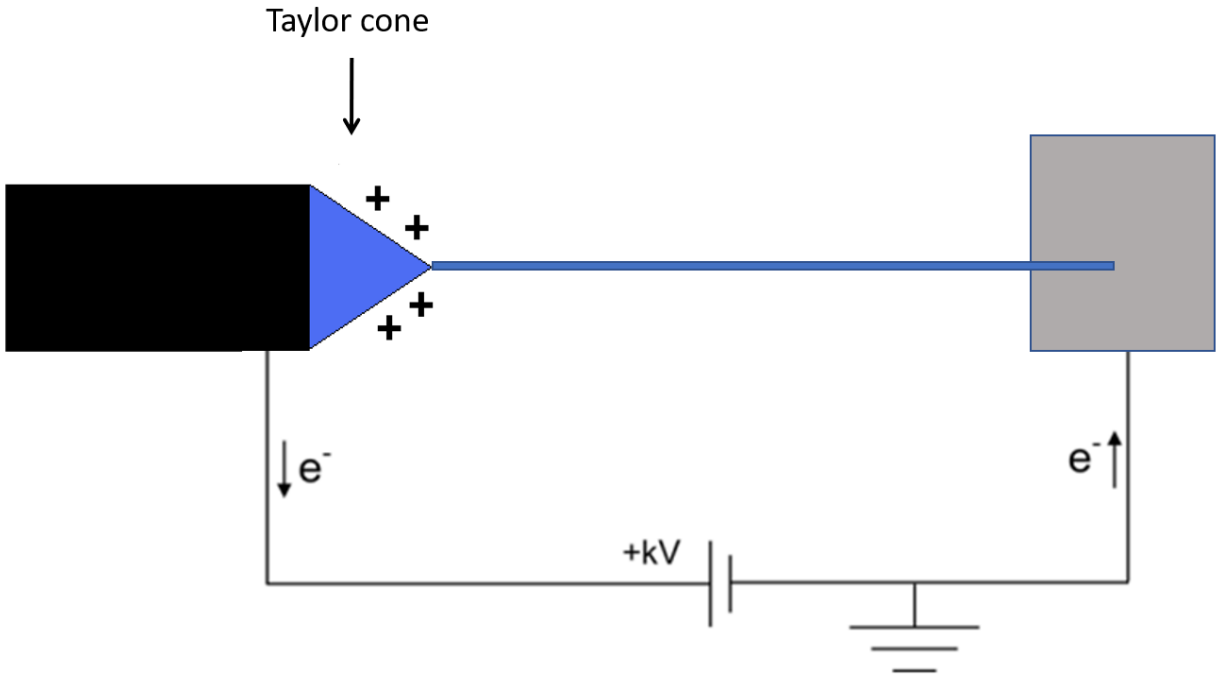

Figure 1.3 Basic electrospinning schematic

1.11 Electrospinning of carbon fibres

Electrospinning is a simple, economical method of producing carbon fibres or nanofibres. Perhaps the most widely known type of carbon nanofibres is carbon nanotubes. Carbon nanotubes has been studied extensively and are renowned for their mechanical properties. However, the synthesis of carbon nanotubes is a complicated and expensive process involving chemical vapour deposition. Electrospinning provides an alternative method of producing carbon nanofibres without the need for complicated machinery.

Electrospinning cannot directly produce carbon nanofibres because electrospun material originates from the polymer that is dissolved in solution. Instead, heat treatment after electrospinning is required for the carbonization of nanofibres. The most common polymer used for this purpose is polyacrylonitrile, but other polymers have also been demonstrated as precursors. Wang *et al.* use a three-step heat treatment process to carbonize polyvinylpyrrolidone nanofibres that were produced from electrospinning.[72] Poly(amic acid) was electrospun and carbonized by Kim *et al.* and tested for its capacitance.[73] Highly porous carbonized fibres based on polyvinylidene fluoride was shown by Yang *et al*.[74] All of these examples share stabilization treatment in air at a lower temperature followed by carbonization in an inert atmosphere. However, not all electrospun polymers can be successfully carbonized. The polymer must be able to be electrospun into smooth fibres while maintaining their morphology during heat treatment. Polyacrylonitrile is perhaps the most popular polymer used as a carbon precursor because it can be easily electrospun into nanofibres, and does not require complicated multi-step stabilization. It has been shown that polyacrylonitrile nanofibres require a stabilization step between 200-300 ^{o}C in air for the polymer to undergo dehydrogenation, cyclization, and oxidation.[75,76] This stabilization step is crucial for carbonization at higher temperatures.

Electrospun carbon fibres are often used in energy-related applications due to their conductivity. Electrospun carbon fibres derived from polyacrylonitrile have higher reversible capacities compared to graphite, which is traditionally used in lithium ion batteries.[77] Polyacrylonitrile-derived carbon fibres also have high capacitance because of their high surface area. Compared to activated carbon, polyacrylonitrile fibres treated at 1000 ^{o}C have superior

capacitance over a wider range of current densities.[78] Electrospun carbon fibres have great potential in high power capacitors and as anode material for high performance batteries. Not only do these fibres show great electrical properties, electrospinning provides a simple, cost-effective method of fabricating these materials.

Another interesting area for electrospun carbon fibres is for the extraction and detection of analytes by solid-phase microextraction. Solid-phase microextraction uses a thin polymer film coated on a support to extract analytes from a sample either directly or the headspace above it. A high surface area with active surface moieties for analyte adsorption are desirable traits for an adsorptive SPME coating. Carbonized fibres from electrospun photoresist were used to extract volatile organic compounds using SPME.[79] Compared to commercial SPME coatings, such as polydimethylsiloxane, carbonized electrospun fibres show improved extraction efficiency.[79] A carbonized SU-8 photoresist coating exhibits an extraction efficiency of up to three times greater than that of commercial PDMS coatings for the extraction of benzene, toluene, and ethylbenzene.[79] Though not carbonized, other electrospun polymers that have been used in SPME include polyetherimide,[80] polyamide,[81] and polystyrene.[82]

1.12 Electrospinning of composite fibres

Electrospun composite fibres are derived from solutions of more than a single polymer. Composite fibres aim to improve upon thermal, mechanical, electrical, or other properties of electrospun fibres. Also, some materials cannot be, or are very difficult to be, electrospun on their own, so the addition of a second polymer is necessary to facilitate the electrospinning process. One such example are carbon nanotubes. Dissolved carbon nanotubes do not have the viscosity to form fibres on their own. However, carbon nanotubes are often added as a

secondary polymer to increase the electrical or mechanical properties of electrospun fibres. Hou *et al*. showed that the addition to MWCNTs to polyacrylonitrile can increase the tensile strength and modulus of electrospun sheets by up to 75% (at 5% MWCNTs) and 144% (at 20% MWCNTs).[83] Sen *et al*. showed similar improvements in mechanical properties for composite SWCNTs electrospun membranes with polystyrene and polyurethane.[84] Similar to carbon nanotubes, graphene can also be used as a secondary polymer in electrospinning to improve mechanical and electrical properties. Recently, TiO_2-graphene composite nanofibres have shown to exhibit superior electrical properties compared to pure TiO_2 nanofibres, with potential application as a high capacity battery.[85] The electrospinning of composite fibres is not limited to these prominent carbon nano-materials. The versatility and ease of electrospinning means that almost any polymer can be added to make composite fibres, as long as there is a high molecular weight polymer to facilitate the fibre forming process. The electrospinning of asphaltenes can be accomplished on its own, but the process is not ideal due asphaltenes' low molecular weight. By adding a high molecular weight polymer to asphaltenes, composite asphaltene fibres with better spinnability can be achieved.

1.13 Summary

This thesis will explore various types of materials that can be synthesized from asphaltenes. Asphaltenes are a rich source of carbon and have promising potential as a precursor for graphitic materials. Both carbon films and carbon fibres can be derived from asphaltenes, and they will be investigated for their electrochemical reactivity. The electrospinning of composite asphaltene fibres with various polymers will be explored, and

finally, asphaltenes will be used for the detection of polycyclic aromatic hydrocarbons using solid-phase microextraction.

1.14 References

1. Mohri, M. *et al.* Rechargeable lithium battery based on pyrolytic carbon as a negative electrode. *J. Power Sources* **26,** 545–551 (1989).
2. Peled, E. Improved Graphite Anode for Lithium-Ion Batteries Chemically. *J. Electrochem. Soc.* **143,** L4 (1996).
3. Zhang, W. J. A review of the electrochemical performance of alloy anodes for lithium-ion batteries. *J. Power Sources* **196,** 13–24 (2011).
4. Chen, P. & McCreery, R. L. Control of Electron Transfer Kinetics at Glassy Carbon Electrodes by Specific Surface Modification. *Anal. Chem.* **68,** 3958–3965 (1996).
5. McDermott, M. T., McDermott, C. a. & McCreery, R. L. Scanning Tunneling Microscopy of Carbon Surfaces - Relationships Between Electrode-Kinetics, Capacitance, and Morphology for Glassy-Carbon Electrodes. *Anal. Chem.* **65,** 937–944 (1993).
6. Chen, Z. *et al.* High-performance supercapacitors based on hierarchically porous graphite particles. *Adv. Energy Mater.* **1,** 551–556 (2011).
7. Gao, W. *et al.* Direct laser writing of micro-supercapacitors on hydrated graphite oxide films. *Nat. Nanotechnol.* **6,** 496–500 (2011).
8. Thostenson, E. T., Ren, Z. & Chou, T.-W. Advances in the science and technology of carbon nanotubes and their composites: a review. *Compos. Sci. Technol.* **61,** 1899–1912 (2001).
9. Dalton, A. B. *et al.* Super-tough carbon-nanotube fibres. *Nature* **423,** 703–703 (2003).
10. Kashiwagi, T. *et al.* Thermal degradation and flammability properties of poly(propylene)/carbon nanotube composites. *Macromol. Rapid Commun.* **23,** 761–765 (2002).
11. McNally, T. *et al.* Polyethylene multiwalled carbon nanotube composites. *Polymer (Guildf).* **46,** 8222–8232 (2005).
12. Qian, D., Dickey, E. C., Andrews, R. & Rantell, T. Load transfer and deformation mechanisms in carbon nanotube-polystyrene composites. *Appl. Phys. Lett.* **76,** 2868 (2000).
13. Baltzis, D., Orfanidis, S., Lekatou, A. & Paipetis, A. S. Stainless steel coupled with carbon nanotube- modified epoxy and carbon fibre composites : Electrochemical and mechanical study Stainless steel coupled with carbon nanotube- modified epoxy and carbon fibre composites : *Plast. Rubber Compos.* **8011,** 95–105 (2016).
14. Sandler, J. K. W., Kirk, J. E., Kinloch, I. A., Shaffer, M. S. P. & Windle, A. H. Ultra-low electrical percolation threshold in carbon-nanotube-epoxy composites. *Polymer (Guildf).* **44,** 5893–5899 (2003).

15. Schadler, L. S., Giannaris, S. C. & Ajayan, P. M. Load transfer in carbon nanotube epoxy composites. *Appl. Phys. Lett.* **73,** 3842–3844 (1998).

16. Gojny, F. H., Wichmann, M. H. G., Köpke, U., Fiedler, B. & Schulte, K. Carbon nanotube-reinforced epoxy-composites: Enhanced stiffness and fracture toughness at low nanotube content. *Compos. Sci. Technol.* **64,** 2363–2371 (2004).

17. Xu, C. L. *et al.* Fabrication of aluminum / carbon nanotube composites and their electrical properties. *Carbon N. Y.* **37,** 855–858 (1999).

18. George, R., Kashyap, K. T., Rahul, R. & Yamdagni, S. Strengthening in carbon nanotube/aluminium (CNT/Al) composites. *Scr. Mater.* **53,** 1159–1163 (2005).

19. Brabec, Christoph J., et al. Origin of the open circuit voltage of plastic solar cells. *Adv. Funct. Mater.* **11,** 374–380. (2001).

20. Yu, D. & Dai, L. Self-assembled graphene/carbon nanotube hybrid films for supercapacitors. *J. Phys. Chem. Lett.* **1,** 467–470 (2010).

21. Fan, Z. *et al.* A three-dimensional carbon nanotube/graphene sandwich and its application as electrode in supercapacitors. *Adv. Mater.* **22,** 3723–3728 (2010).

22. Zhang, D. *et al.* Asphaltenes — Problematic but Rich in Potential. *Oilf. Rev.* 22–43 (2007).

23. Stanislaus, A. Coke formation on catalysts during the hydroprocessing of heavy oils ’. *Appl. Catal.* **72,** 193–215 (1991).

24. Yen, T. F. Structure of Petroleum Asphaltene and Its Significance. *Energy Sources* **1,** 447–463 (1974).

25. Mullins, O. C. The Modified Yen Model. *Energy & Fuels* **24,** 2179–2207 (2010).

26. McCreery, R. L. Advanced carbon electrode materials for molecular electrochemistry. *Chem. Rev.* **108,** 2646–2687 (2008).

27. Kiema, G. K. & Brett, M. J. Electrochemical Characterization of Carbon Films with Porous Microstructures. *J. Electrochem. Soc.* **150,** E342 (2003).

28. Blackstock, J. J. *et al.* Ultraflat carbon film electrodes prepared by electron beam evaporation. *Anal. Chem.* **76,** 2544–2552 (2004).

29. Mani, R. C. *et al.* Nanocrystalline graphite for electrochemical sensing. *J. Electrochem. Soc.* **152,** E154–E159 (2005).

30. Obraztsov, A. N. *et al.* Raman scattering characterization of CVD graphite films. *Carbon N. Y.* **46,** 963–968 (2008).

31. Jia, J. *et al.* Structure and Electrochemical Properties of Carbon Films Prepared by a Electron Cyclotron Resonance Sputtering Method. *Anal. Chem.* **79,** 893–900 (2007).

32. Hirono, S., Umemura, S., Tomita, M. & Kaneko, R. Superhard conductive carbon

nanocrystallite films. *Appl. Phys. Lett.* **80,** 425–427 (2002).

33. Sawyer, W. E. & Man, A. Patent US229335. (1880).

34. Karu, A. E. & Beer, M. Pyrolytic formation of highly crystalline graphite films. *J. Appl. Phys.* **37,** 2179–2181 (1966).

35. Baker, R. T. K., Barber, M. A., Harris, P. S., Feates, F. S. & Waite, R. J. Nucleation and growth of carbon deposits from the nickel catalyzed decomposition of acetylene. *J. Catal.* **26,** 51–62 (1972).

36. Presland, A. E. B. & Walker, P. L. Growth of single-crystal graphite by pyrolysis of acetylene over metals. *Carbon* **7,** 1–8 (1969).

37. Yajima, S., Satow, T. & Hirai, T. Mechanism of the pyrolytic graphite formation. *J. Nucl. Mater.* **17,** 116–126 (1965).

38. Bard, R. J., Baxman, H. R., Bertino, J. P. & O'Rourke, J. A. Pyrolytic Carbons Deposited in Fluidized Beds At 1200 To 1400 ° C From Various Hydrocarbons. *Carbon N. Y.* **6,** 603–616 (1967).

39. Wilson, S. D. R. & Hulme, A. Stress recrystallization of graphite. *Proc. R. Soc. A Math. Phys. Eng. Sci.* **266,** 20–32 (1962).

40. Obraztsov, A. N., Obraztsova, E. A., Tyurnina, A. V. & Zolotukhin, A. A. Chemical vapor deposition of thin graphite films of nanometer thickness. *Carbon N. Y.* **45,** 2017–2021 (2007).

41. Reina, A. *et al.* Large area, few-layer graphene films on arbitrary substrates by chemical vapor deposition. *Nano Lett.* **9,** 30–35 (2009).

42. Redfern, B. US3109712 A. (1960).

43. Fitzer, E., Schaefer, W. & Yamada, S. The formation of glasslike carbon by pyrolysis of polyfurfuryl alcohol and phenolic resin. *Carbon N. Y.* **7,** 643–648 (1969).

44. Schueller, O. J. A., Brittain, S. T. & Whitesides, G. M. Fabrication of glassy carbon microstructures by pyrolysis of microfabricated polymeric precursors. *Adv. Mater.* **9,** 477–480 (1997).

45. Wang, C. & Madou, M. From MEMS to NEMS with carbon. *Biosens. Bioelectron.* **20,** 2181–2187 (2005).

46. Malladi, K., Wang, C. & Madou, M. Fabrication of suspended carbon microstructures by e-beam writer and pyrolysis. *Carbon N. Y.* **44,** 2602–2607 (2006).

47. Wang, Y., Pham, L., Vasconcellos, G. P. S. de & Madou, M. Fabrication and characterization of micro PEM fuel cells using pyrolyzed carbon current collector plates. *J. Power Sources* **195,** 4796–4803 (2010).

48. Ranganathan, S., Mccreery, R., Majji, S. M. & Madou, M. Photoresist-Derived Carbon for

Microelectromechanical Systems and Electrochemical Applications. *J. Electrochem. Soc.* **147,** 277–282 (2000).

49. Karimi, A. *et al.* Quantitative Evidence for Bridged Structures in Asphaltenes by Thin Film Pyrolysis. *Energy & Fuels* **25,** 3581–3589 (2011).

50. Wen, Z. S., Yang, J., Wang, B. F., Wang, K. & Liu, Y. High capacity silicon / carbon composite anode materials for lithium ion batteries. *Electrochem. commun.* **5,** 165–168 (2003).

51. Endo, M. *et al.* Anode performance of a Li ion battery based on graphitized and B-doped milled mesophase pitch-based carbon fibres. *Carbon N. Y.* **37,** 561–568 (1999).

52. Davini, P. Desulphurization properties of active carbons obtained from petroleum pitch pyrolysis. *Carbon N. Y.* **37,** 1363–1371 (1999).

53. Chen, C., Kennel, E. B., Stiller, A. H., Stansberry, P. G. & Zondlo, J. W. Carbon foam derived from various precursors. *Carbon N. Y.* **44,** 1535–1543 (2006).

54. Kugatov, P. V & Zhirnov, B. S. Porous carbon / carbon composites produced from carbon black and petroleum pitch. *J. Porous Mater.* **20,** 875–882 (2013).

55. Datta, M. K. *et al.* Amorphous silicon – carbon based nano-scale thin film anode materials for lithium ion batteries. *Electrochim. Acta* **56,** 4717–4723 (2014).

56. Li, W. *et al.* Core – Shell Si / C Nanospheres Embedded in Bubble Sheet-like Carbon Film with Enhanced Performance as Lithium Ion Battery Anodes. *Small* **11,** 1345–1351 (2015).

57. Ranganathan, S., Steidel, I., Anariba, F. & Mccreery, R. L. Covalently Bonded Organic Monolayers on a Carbon Substrate : A New Paradigm for Molecular Electronics. *Nano Lett.* **1,** 491–494 (2001).

58. Hadi, M., Rouhollahi, A. & Yousefi, M. Chemical Nanocrystalline graphite-like pyrolytic carbon film electrode for electrochemical sensing of hydrazine. *Sensors Actuators B. Chem.* **160,** 121–128 (2011).

59. You, T., Niwa, O., Tomita, M. & Hirono, S. Characterization of platinum nanoparticle-embedded carbon film electrode and its detection of hydrogen peroxide. *Anal. Chem.* **75,** 2080–2085 (2003).

60. You, T. *et al.* Reductive H2O2 Detection at Nanoparticle Iridium/Carbon Film Electrode and Its Application as L-Glutamate Enzyme Sensor. *Electroanalysis* **16,** 54–59 (2004).

61. Rossnagel, S. M., Russak, M. A. & Cuomo, J. J. Pressure and plasma effects on the properties of magnetron sputtered carbon films. *J. Vac. Sci. Technol. A Vacuum, Surfaces, Film.* **5,** 2150–2153 (1987).

62. Schlesinger, R., Bruns, M. & Ache, H. J. Development of thin film electrodes based on sputtered amorphous carbon. *J. Electrochem. Soc.* **144,** 6–15 (1997).

63. Matsubara, H., Yamaguchi, Y., Shioya, J. & Murakami, S. Preparation and properties of

graphite grown in vapor phase. *Synth. Met.* **18,** 503–507 (1987).

64. Sato, T., Furuno, S., Iguchi, S. & Hanabusa, M. Deposition of Diamond-like Carbon Films by Pulsed-Laser Evaporation. *Jpn. J. Appl. Phys.* **26,** L1487 (1987).

65. Rode, A. V., Luther-Davies, B. & Gamaly, E. G. Ultrafast ablation with high-pulse-rate lasers. Part II: Experiments on laser deposition of amorphous carbon films. *J. Appl. Phys.* **85,** 4222–4230 (1999).

66. Aisenberg, S. & Chabot, R. Ion-beam deposition of thin films of diamondlike carbon. *J. Appl. Phys.* **42,** 2953–2958 (1971).

67. A. Formals. Artificial Thread and Method of Producing Same. **16187,** (1940).

68. Formhals, A. Methods and apparatus for Spinning. 1–5 (1944).

69. Formhals A. Production of artifcial fibres from fibre forming liquids. 2–5 (1943).

70. Taylor, G. Electrically Driven Jets. *Proc. R. Soc. A Math. Phys. Eng. Sci.* **313,** 453–475 (1969).

71. Taylor, G. Studies in Electrohydrodynamics. I. The Circulation Produced in a Drop by Electrical Field. *Proc. R. Soc. A Math. Phys. Eng. Sci.* **291,** 159–166 (1966).

72. Wang, P. *et al.* Mesoporous carbon nanofibres with a high surface area electrospun from thermoplastic polyvinylpyrrolidone. *Nanoscale* **4,** 7199–7204 (2012).

73. Kim, C., Choi, Y. O., Lee, W. J. & Yang, K. S. Supercapacitor performances of activated carbon fibre webs prepared by electrospinning of PMDA-ODA poly(amic acid) solutions. *Electrochim. Acta* **50,** 883–887 (2004).

74. Yang, Y. *et al.* Highly porous electrospun polyvinylidene fluoride (PVDF)-based carbon fibre. *Carbon N. Y.* **49,** 3395–3403 (2011).

75. Wu, M., Wang, Q., Li, K., Wu, Y. & Liu, H. Optimization of stabilization conditions for electrospun polyacrylonitrile nanofibres. *Polym. Degrad. Stab.* **97,** 1511–1519 (2012).

76. Zhang, W. X., Wang, Y. Z. & Sun, C. F. Characterization on oxidative stabilization of polyacrylonitrile nanofibres prepared by electrospinning. *J. Polym. Res.* **14,** 467–474 (2007).

77. Kim, C. *et al.* Fabrication of electrospinning-derived carbon nanofibre webs for the anode material of lithium-ion secondary batteries. *Adv. Funct. Mater.* **16,** 2393–2397 (2006).

78. Ra, E. J., Raymundo-Piñero, E., Lee, Y. H. & Béguin, F. High power supercapacitors using polyacrylonitrile-based carbon nanofibre paper. *Carbon N. Y.* **47,** 2984–2992 (2009).

79. Zewe, J. W., Steach, J. K. & Olesik, S. V. Electrospun Fibres for Solid-Phase Microextraction. *Anal. Chem.* **82,** 5341–5348 (2010).

80. Bagheri, H., Akbarinejad, A. & Aghakhani, A. A highly thermal-resistant electrospun-

based polyetherimide nanofibres coating for solid-phase microextraction. *Anal. Bioanal. Chem.* **406,** 2141–2149 (2013).

81. Bagheri, H., Aghakhani, A., Baghernejad, M. & Akbarinejad, A. Novel polyamide-based nanofibres prepared by electrospinning technique for headspace solid-phase microextraction of phenol and chlorophenols from environmental samples. *Anal. Chim. Acta* **716,** 34–39 (2012).

82. Zali, S., Jalali, F., Es-haghi, A. & Shamsipur, M. Electrospun nanostructured polystyrene as a new coating material for solid-phase microextraction: Application to separation of multipesticides from honey samples. *J. Chromatogr. B Anal. Technol. Biomed. Life Sci.* **1002,** 387–393 (2015).

83. Hou, H. *et al.* Electrospun polyacrylonitrile nanofibres containing a high concentration of well-aligned multiwall carbon nanotubes. *Chem. Mater.* **17,** 967–973 (2005).

84. Sen, R. *et al.* Preparation of single-walled carbon nanotube reinforced polystyrene and polyurethane nanofibres and membranes by electrospinning. *Nano Lett.* **4,** 459–464 (2004).

85. Zhang, X. *et al.* Electrospun TiO 2-graphene composite nanofibres as a highly durable insertion anode for Lithium ion batteries. *J. Phys. Chem. C* **116,** 14780–14788 (2012).

Chapter 2

Synthesis and characterization of nanoparticles and thin films by the pyrolysis of asphaltenes

2.1 Introduction

Asphaltenes are a class of complex molecules defined by their solubility. Among the SARA (saturates, aromatics, resins, and asphaltenes) fractions of crude oils, asphaltenes are the heaviest fraction.[1] In addition, asphaltenes are not soluble in short-chain alkanes, such as pentane or heptane. Asphaltenes have a long and extensive history in scientific literature. This is because asphaltenes can cause significant problems during oil extraction, processing, and transportation due to their propensity to aggregate and precipitate.[2,3] Asphaltene management and associated maintenance costs have a negative economic impact on the oil industry. Hence, there is a need to better understand the chemical nature and behaviour of this complex class of molecules. However, aside from its problematic attributes, asphaltenes also possess attractive traits, such as being inexpensive and a rich source of carbon. There is currently very little research being done to explore the potential of asphaltenes as a value-added product. Asphaltenes are a carbon-rich class of molecules, and can be potentially transformed into functional carbon materials.

Carbon is one of the most common and basic elements shared by all life. As such, it is extensively studied because it plays such an important role in biology and chemistry. Carbon is a versatile element that has many different forms and allotropes with vastly different and unique properties. Graphitic carbon is one such allotrope, and it is composed of rings of sp^2 carbon. Because of its sp^2 structure, graphitic carbon is conductive, and has extensive applications in electrochemistry[4,5], sensing[6,7], batteries[8,9], and supercapacitors[10,11]. Here, asphaltenes are transformed into graphitic carbon thin films and carbon nanoparticles. Carbon film electrodes are ubiquitous in electrochemistry because of their chemical stability, wide

potential window, potential for modification, and low-cost of production. They are widely used in electrochemistry for the detection of small molecules, studying redox chemistry and kinetics, and other research purposes. Perhaps the two most common types of graphitic electrodes are glassy carbon and highly-oriented pyrolytic graphite (HOPG). These materials are often used as benchmark electrodes because their properties have been extensively studied in the literature. However, in recent years, there have been a drive to manufacture other carbon electrodes with similar performance to glassy carbon.

The primary method of synthesizing graphitic carbon materials is through the pyrolysis of a precursor at high temperatures. For example, the aforementioned glassy carbon and HOPG are produced at temperatures of up to 3000 ^{o}C with stress annealing. The degree of graphitization increases with temperature and the electrochemical behaviour generally increases as well. Hence, there is incentive to produce carbon films with similar conductivity and electrochemical reactivity at much lower temperatures. McCreery *et al.* produced conductive films by pyrolyzing photoresist up to 1100 ^{o}C.[12] The films were found to exhibit excellent electrochemical behaviour compared to standard carbon electrodes such as polished glassy carbon. Since the initial report, a number of applications of pyrolyzed photoresist films (PPF) have been reported.[12,13] In addition, the ability to pattern photoresist has led to the fabrication of a variety of micro- and nano-sized graphitic carbon structures.[14,15] Other polymers have also been employed to fabricate carbon films in a similar way. For example, carbonization of spin-coated films of polyacrylonitrile has been shown to produce porous carbon electrodes.[16] Conductive carbon films have also been produced from the pyrolysis of precursors such as cellulose[17,18] and organic polymers[19–21]. The pyrolysis of cellulose showed

that the conductivity of the carbon film increases drastically up to 1000 ^{o}C, with diminishing returns from 1000 ^{o}C to 3000 ^{o}C.[18] The pyrolysis of 3,4,9,10-perylenetetracarboxylic dianhydride produces conductive films with excellent electrochemical reactivity for various redox systems.[19,20] It is obvious that many different precursors can be used to produce conductive graphitic carbon film. As a precursor, asphaltenes have the advantage of being abundant, inexpensive, with few known applications. Hence, we report the use of asphaltenes as an alternative precursor to synthesize carbon films through pyrolysis. By taking advantage of asphaltenes' tendency to adsorb onto surfaces as nanoaggregates, carbon nanoparticles can also be produced as well. The synthesis of carbon films and nanoparticles show promise for asphaltenes as a useful material.

2.2 Experimental

2.2.1 Materials

All solutions were prepared using 18.2 megaohm-cm deionized water. No additional treatment or purification was done on any reagent. Reagents that were used include hexaammineruthenium(III) chloride (98%, Sigma-Aldrich), dopamine hydrochloride (Sigma-Aldrich), potassium ferrocyanide (99.0%, AnalaR), L-ascorbic acid (Signma-Aldrich, 99%), toluene (99.9%, Sigma-Aldrich), sulphuric acid (95.0%-98.0%, Caledon), and potassium chloride (99.0-100.5%, Sigma-Aldrich). Substrates used for pyrolysis were P-doped silicon squares. Glassy carbon (GC-20) was obtained from Tokai Carbon. Source of asphaltenes is the Athabasca oil sands in Alberta, Canada. Asphaltenes were precipitated and washed with pentane until the filtrate became only lightly in colour.

2.2.2 Elemental Analysis

The elemental composition of asphaltenes was determined using a Thermo Flash 2000 CHNS-O combustion analyzer. To determine the carbon, hydrogen, nitrogen, and sulfur composition, ~1.3 g of the asphaltene sample was pyrolyzed in the combustion reactor at 1000 ^{o}C in an oxidizing atmosphere. The C, H, N, and S in the sample were converted to CO_2, H_2O, N_2, and SO_2. These gases were separated in a Porapak QS column (4 mm ID, 2 m long) and detected using a thermal-conductivity detector. To determine the oxygen composition, ~4 grams of the asphaltene sample was pyrolyzed at 1060 ^{o}C under helium. The oxygen was converted to CO by a layer of nickel-coated carbon and is separated and detected in the same manner as above. The elemental composition of the asphaltene was determined to be C(82.52%), H(8.14%), N(1.18%), S(7.04%), and O(1.13%).

2.2.3 Pyrolysis of asphaltene nanoaggregates

Silicon substrates were cleaned in a solution of sulfuric acid and hydrogen peroxide (3:1 by volume) for 15 min and then rinsed with deionized water. For the pyrolysis of asphaltene nanoaggregates, 200 µL of a 2 ppm asphaltene solution in toluene was drop-cast on a silicon substrate and then left to sit in air for 60 s. A spin-coater was used to coat the silicon substrate with asphaltene nanoaggregates by spinning at 3000 rpm for 60 s. These substrates were imaged using SEM (Hitachi S-5500) and tapping-AFM (Veeco multimode) prior to pyrolysis. Pyrolysis was performed in a Lindberg three zone tube furnace at 1000 °C (11 °C/min) for 1.5 h in forming gas (95% argon, 5% H_2), and then left to cool to room temperature. Silicon substrates were imaged again using SEM and tapping-AFM after pyrolysis.

For high resolution TEM imaging, a small volume of the same 2 ppm asphaltene solution was drop-cast on a silicon nitride TEM grid (50 nm thick window, Norcada) and left to dry in air. The grid was pyrolyzed in a Lindberg three zone tube furnace at 1000 °C (11 °C/minute) for 1.5 h in forming gas (95% argon, 5% H_2), and then left to cool to room temperature. Imaging was performed using a JEOL 2200 TEM.

2.2.4 Pyrolysis of asphaltene-derived thin films (ADF)

Silicon substrates were cleaned in a solution of sulfuric acid and hydrogen peroxide (3:1 by volume) for 15 min and then rinsed with deionized water. For the thin films, 400 µL of a 5000 ppm asphaltene solution in toluene was drop-cast on a silicon substrate and then left to sit in air for 5 minutes, and then spun-coat at 3000 rpm for 60 s. This was repeated three times for four layers in total.

Oxidative stabilization was performed in air at 200 °C for 1 hour using a tube furnace. After stabilization, pyrolysis was performed at 1000 °C (11 °C/min) for 1.5 h in forming gas (95% argon, 5% H_2), and then left to cool to room temperature. Tapping AFM was used to image the topography of the films before and after heat treatment.

The thickness of the asphaltene film before heat treatment was determined by cross-sectional SEM. After spin-coating four layers of the 5000 ppm asphaltene solution, the sample was coated with 25 nm of Au in a thermal evaporator. The substrate was then cracked in half and the cross-section was imaged. The layer of Au on top of the layer of asphaltenes is to prevent edge effects between the asphaltene layer and air. After pyrolysis, the thickness of the graphitized layer was determined using ellipsometry. Refractive indices, *n* and *k*, were taken from Duley.[22] SEM could not be used to image the cross-section thickness of asphaltene-derived films

because of poor resolution. However, the accuracy of ellipsometry was validated by comparing to SEM cross-sections of thicker pyrolyzed asphaltene films. Thicker pyrolyzed asphaltene films were made from the same 5000 ppm asphaltene solution. After spin-coating four layers of the asphaltene solution and undergoing the same heat treatment, this process was repeated two more times, with 12 layers and 3 heat treatments in total. Ellipsometry and cross-section SEM was performed for the thicker asphaltene films for comparison. Ellipsometry modeling was done using EP4Model, where the substrate layers were Si – silicon oxide – graphite – air.

Resistivity was determined using a Lucas 4-point-probe system. For both before and after heat treatment, three different substrates were tested. Raman spectroscopy was performed using a Renishaw Raman microscope system with an argon laser operating at 514.5 nm. Operating conditions for Raman were 100 s of exposure at 30 mW power using the 20x objective lens. The D-band to G-band ratio was calculated from spectra obtained from three different samples.

X-ray photoelectron spectroscopy was used to analyze asphaltene films before and after pyrolysis. For XPS, a more concentrated solution of asphaltenes was used for spin-coating. If XPS was used to analyze our asphaltene-derived films made from a 5000 ppm solution, then the penetration would reach the silicon substrate underneath. Oxides on the silicon substrate would then distort the true oxygen/carbon ratio in the XPS spectra. Therefore, we made an asphaltene film from a 32000 ppm solution, and pyrolyzed it under the same conditions as the films made from the 5000 ppm solution. For XPS analysis, the thick pyrolyzed asphaltene was first sputtered with argon for 90 s. Survey spectra as well as high resolution spectra for the carbon 1s peak were obtained.

Cyclic voltammetry was performed using a typical three electrode cell, with a Pt mesh counter electrode and an Ag/AgCl reference electrode. An O-ring exposes approximately 28 mm^2 of the working electrode to the electrolyte solution. A PINE potentiostat and Aftermath software were used to obtain cyclic voltammograms. Experiments were done on both GC-20 and pyrolyzed asphaltene-derived thin films on doped Si as the working electrode. Redox systems used were 0.1mM $[Ru(NH_3)_6]^{3+/2+}$ in 1M KCl, 0.1mM $[Fe(CN)_6]^{3-/4-}$ in 1M KCl, 0.1 mM L-ascorbic acid in 0.1m H_2SO_4, and 0.1 mM dopamine in 0.1M H_2SO_4. The thinness of these films leads to large internal resistance, and this will widen the peak separation in cyclic voltammetry. This resistance can however be corrected by

$$\left(\Delta E_p\right)_{obs} = \left(\Delta E_p\right)_{corr} + 2|i|R_u$$

where $\left(\Delta E_p\right)_{obs}$ is the observed ΔE_p, $\left(\Delta E_p\right)_{corr}$ is the corrected ΔE_p, *i* is the peak current, and R_u is the uncompensated cell resistance. Hence, a plot of observed ΔE_p as a function of current (by altering the concentration of the redox species) will yield $\left(\Delta E_p\right)_{corr}$ as well as R_u. The uncompensated cell resistance was determined by measuring the peak current as the concentration of a dopamine solution was increased by small aliquots. The ΔE_p for each redox system was determined from three different samples. The heterogeneous rate constant, k^0, for each redox system was determined from ΔE_p obtained at 0.1 V/s, 0.2 V/s, and 0.5 V/s.

2.3 Results and discussion

2.3.1 Asphaltene-derived thin films

Asphaltenes are the components of crude oil defined by their insolubility in n-pentane (C5) or n-heptane (C7) and solubility in toluene. The dark-colored material dispersed in toluene is shown in Figure 2.1A. No single molecular structure can be assigned to asphaltenes but the material is thought to contain groups of fused aromatic and non-aromatic rings, alkane chains and heteroatoms such as sulfur, nitrogen, oxygen and some metal atoms.[23] Proposed molecular structures are shown in Figure 2.1B. Elemental analysis reveals that asphaltenes are over 80% carbon (vide infra) and our hypothesis is that they may serve as a starting material for carbon materials.

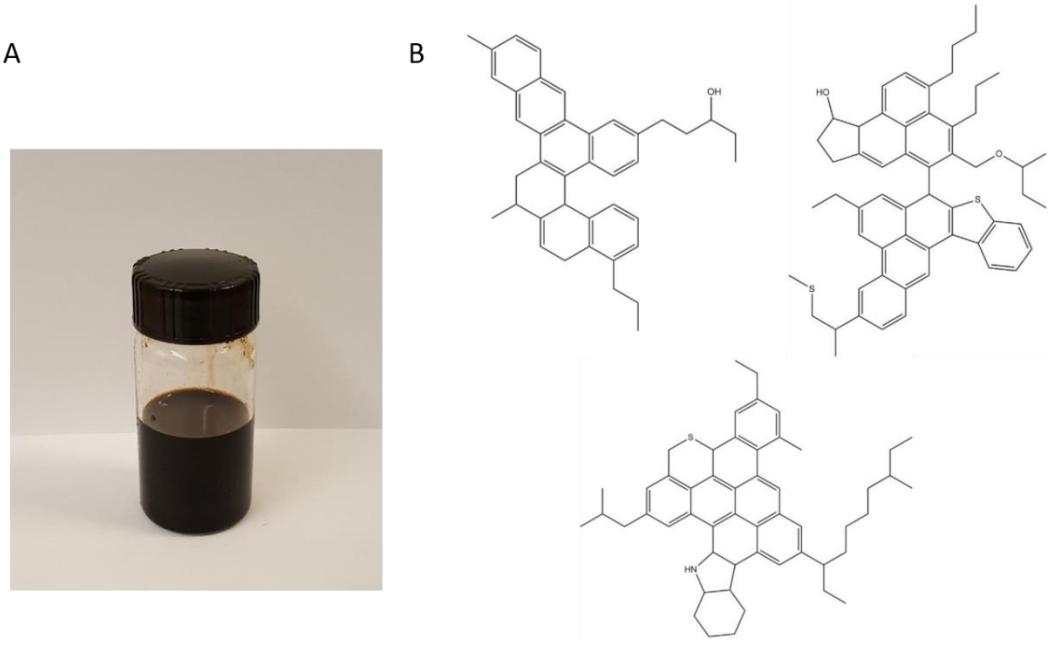

Figure 2.1 A) dissolved asphaltenes in toluene B) model structures for asphaltene molecules

2.3.2 Film Topography

Four layers of a 5000 ppm solution of asphaltene were spun-coat onto a silicon substrate. Four layers were chosen because if the film is too thin, the internal resistance would be too high and would make electrochemical analysis difficult. Figure 2.2 shows the tapping AFM images before and after pyrolysis with their corresponding line profiles. The topographies of both films are very similar. There are no cracks or defects observed in these films. The root-mean-squared roughness, determined from AFM height profiles, for both films are also very similar (0.44 and 0.46 nm for films before and after pyrolysis, respectively). This is comparable to pyrolyzed photoresist with 0.5 nm rms roughness[24], and atomically smooth basal plane HOPG with 0.24 nm rms roughness.[25]

The thickness of the original asphaltene film is 24 ± 2 nm as determined by cross-sectional SEM and ellipsometry (see experimental). After pyrolysis, the thickness of the film shrinks to 6.8 ± 0.5 nm. This is consistent with thermal gravimetric studies where asphaltenes lose about 60% of their mass after pyrolysis at 1000 °C.[26,27] Film shrinkage is also observed in the pyrolysis of other polymers.[12,28] The majority of carbon film electrodes exhibit very low roughness. The asphaltene-derived films are exceptionally smooth, which is an important characteristic for applications in molecular electronics or sensing.

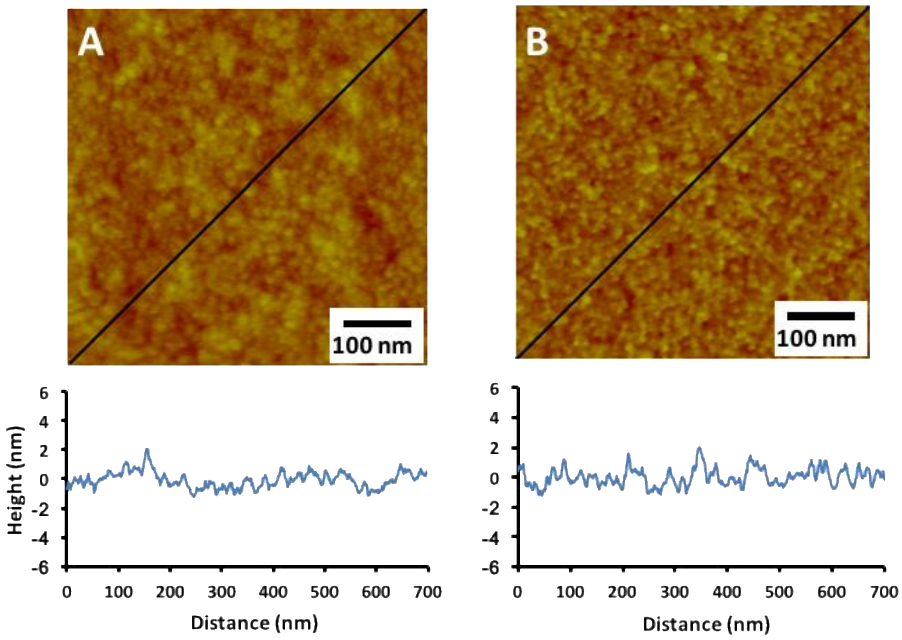

Figure 2.2 AFM images of asphaltene films and cross-section profiles. A) before pyrolysis B) after pyrolysis

2.3.3 Compositional analysis

X-ray photoelectron spectroscopy (XPS) was performed on a spin-coated asphaltene film using a 32000 ppm solution both before and after pyrolysis. The XPS survey spectrum prior to pyrolysis is shown in Figure 2.3. The two major peaks at 284.6 eV and 533.0 eV correspond to carbon 1s and oxygen 1s signals, respectively. The small peaks at 228 and 164 eV correspond to sulphur 2s and 2p, respectively. There is also a very small signal at 398 eV for nitrogen 1s. These signals are consistent with asphaltene composition. Asphaltenes are mostly composed of carbon, hydrogen, oxygen, with small amounts of sulphur, nitrogen, and trace metal atoms. Combustion analysis reveals the composition (wt%) of the original asphaltene material to be 82.5% C, 8.1% H, 1.1% O, 1.2% N and 7.0% S. Elemental analysis (see experimental) of an asphaltene sample is also consistent with this XPS survey scan. The oxygen-to-carbon ratio is approximately 12% for a non-pyrolyzed asphaltene film.

It is expected that pyrolysis of the asphaltene films results in a material that is >99% carbon. The elemental composition of the pyrolyzed films was monitored with XPS. The XPS survey spectrum of a pyrolyzed film are shown in Figure 2.4A. The two major peaks at 284.6 eV and 533.0 eV correspond to C 1s and O 1s signals, respectively. The small peak at 244 eV is the Ar 2p1/2 signal resulting from the argon sputtering used to remove impurities. Weak peaks from the Si substrate and nitrogen are observed at 150 eV (Si 2s) and 400 eV (N 1s), respectively. Sulfur, which is present in asphaltenes, was not detected in the pyrolyzed films. Figure 2.4B contains the high-resolution spectrum for the C 1s region. Usually, the C 1s peak exhibits a shoulder in the range of 286-288 eV, due to carbon atoms bonded to surface oxygen groups.[29] This shoulder is very weak in Figure 2.4B implying low oxygen content. This is expected because our asphaltene thin films are pyrolyzed in an inert, reducing atmosphere. The O/C ratio estimated from the XPS results is less than 4% for the asphaltene-derived films. This ratio is comparable to pyrolyzed photoresist (2.3-6%), and lower than polished glassy carbon (6.7%) treated by sonicating in IPA.[24]

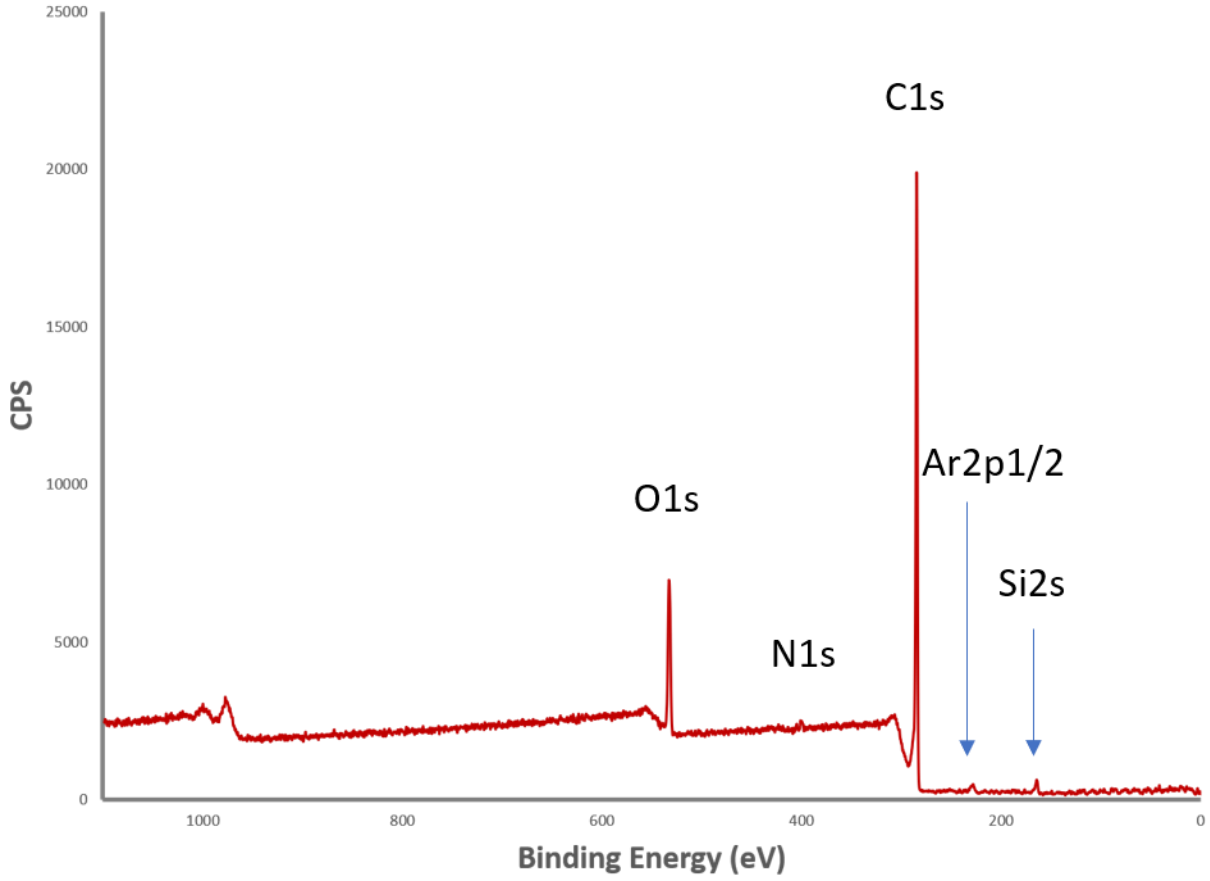

Figure 2.3 XPS spectrum for 32000 ppm spin-coated asphaltene film on silicon.

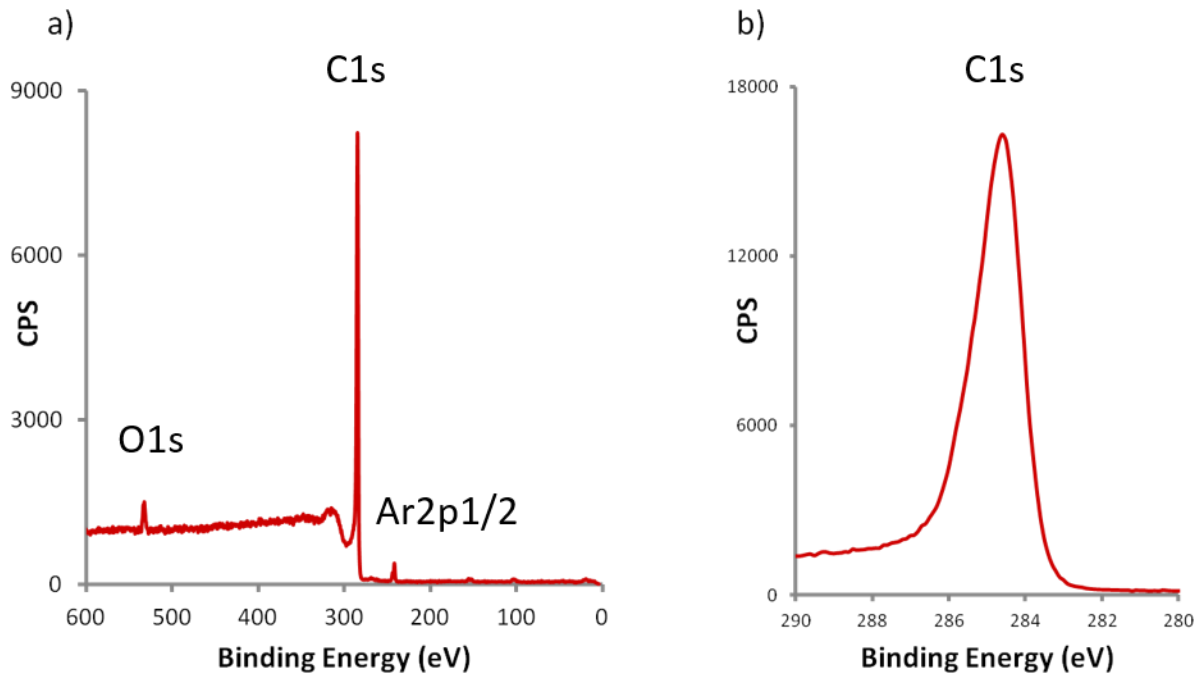

Figure 2.4 XPS spectra for pyrolyzed asphaltene-derived films. a) survey showing C1s and O1s peaks. b) high resolution C1s spectrum

2.3.4 Film Structure

Raman spectroscopy is commonly used to characterize the microstructure of graphitic materials. Two bands in the Raman spectrum of graphitic carbon are typically analyzed. These are known as the D-band and G-band. The G-band, or the "graphitic" band, is located at ~1590 cm^{-1} and is assigned to the vibration of the graphitic ring structure. The D-band is characteristic of disorder in graphitic material and is typically observed ~1360 cm^{-1}. The D-band is not attributed to any specific vibration, but rather comes from the breakdown of symmetry and the presence of edge planes.[30] The ratio of intensities of the D- and G-bands can be also used to estimate the graphite crystalline size.[31] Figure 2.5 contains the Raman spectra for asphaltene thin films before and after pyrolysis. The asphaltene film before pyrolysis shows a large, sloping background likely due to fluorescence from the asphaltenes. A small band is observed at 1600 cm^{-1} that we attribute to the vibration of the sp^2 carbon rings. The fluorescent background diminishes following pyrolysis and two bands are observed at 1370 cm^{-1} and 1601 cm^{-1} that we assign to the D-band and G-band characteristic of graphite crystallites. Using the equation proposed by Knight and White and the intensities of the D- and G-bands, L_a, the crystallite size parallel to the plane of the graphite rings, is estimated to be 6.0 ± 0.3 nm. This is typical of disordered graphitic material.[32] In contrast, highly ordered pyrolytic graphite exhibits L_a of 100 nm or greater.[32] Taken together, the combined AFM, XPS and Raman spectroscopic results discussed above provide strong confirmation that pyrolysis converts an asphaltene film into a flat graphitic film.

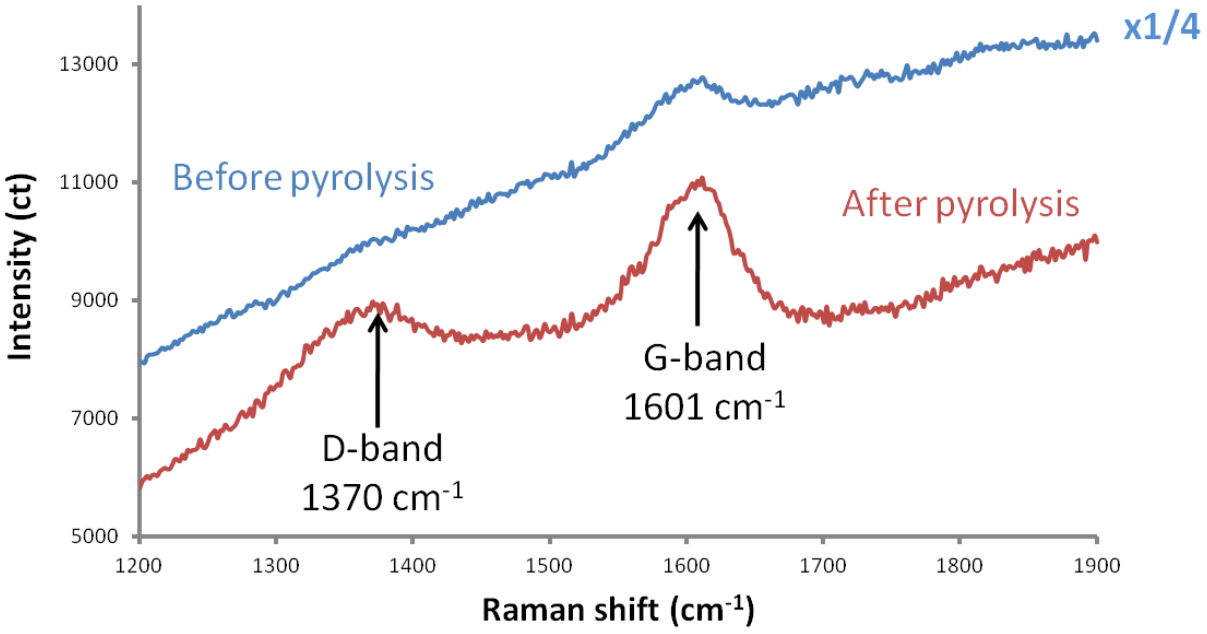

Figure 2.5 Raman spectra for asphaltene-derived films before and after pyrolysis. Laser conditions: 514.5 nm laser, 100s exposure, 30 mW

2.3.5 Film resistivity

The graphitic structure resulting from pyrolysis is expected to greatly increase the conductivity of the asphaltene films. The sheet resistance of the films was measured using a 4-point-probe. The sheet resistance and resistivity for the spin-coated asphaltene films was measured to be $(1.02 \pm 0.11) \times 10^9$ Ω/□ and 2448 Ω•cm, respectively. These very high values are characteristic of an insulating film. The pyrolyzed asphaltene-derived films have a sheet resistance and resistivity of $(1.3 \pm 0.1) \times 10^4$ Ω/□ and 0.009 ± 0.001 Ω•cm, respectively. Pyrolyzed graphitic carbon generally exhibits a resistivity on the order of 10^{-2} Ω•cm, which can vary greatly with pyrolysis temperature.[14] Conductivity is very important for electrochemical reactivity and our asphaltene-derived films are shown to have comparable conductivity to typical graphitic carbon.

2.3.6 Electrochemical reactivity

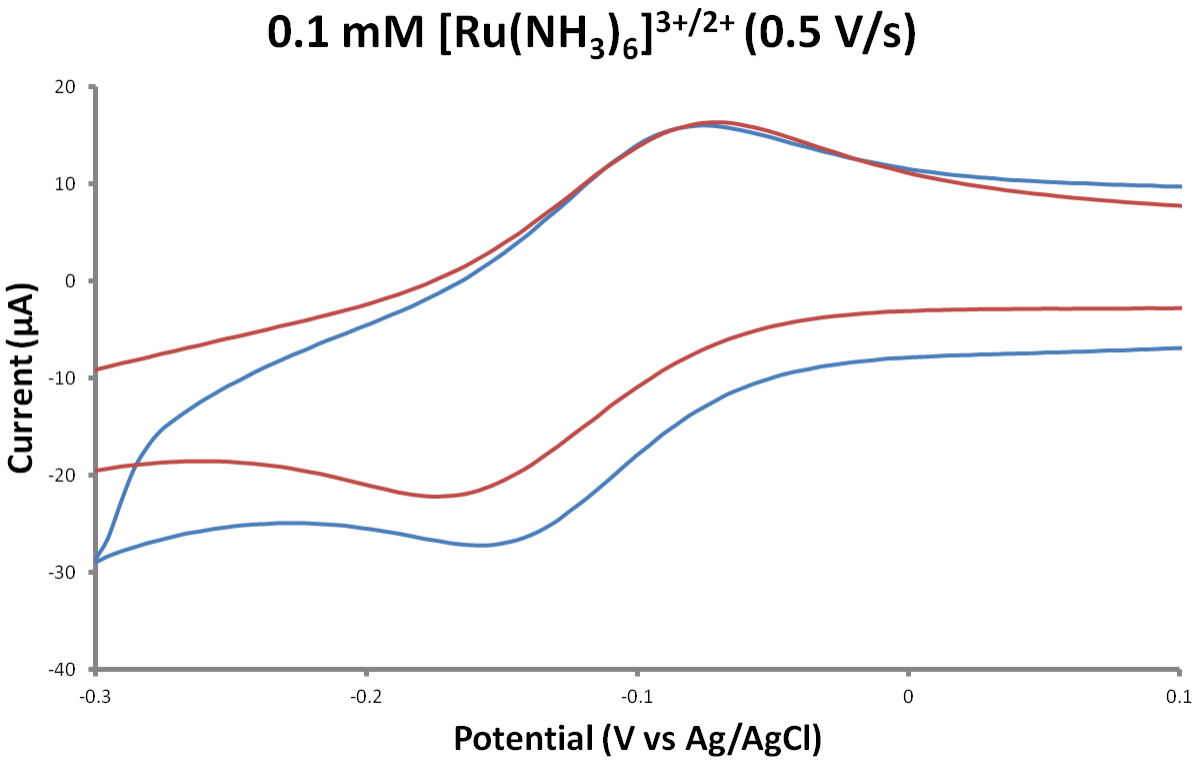

Figure 2.6 A) Cyclic voltammogram of $[Ru(NH_3)_6]^{3+/2+}$ comparing polished glassy carbon (blue) to pyrolyzed asphaltene derived thin film (red)

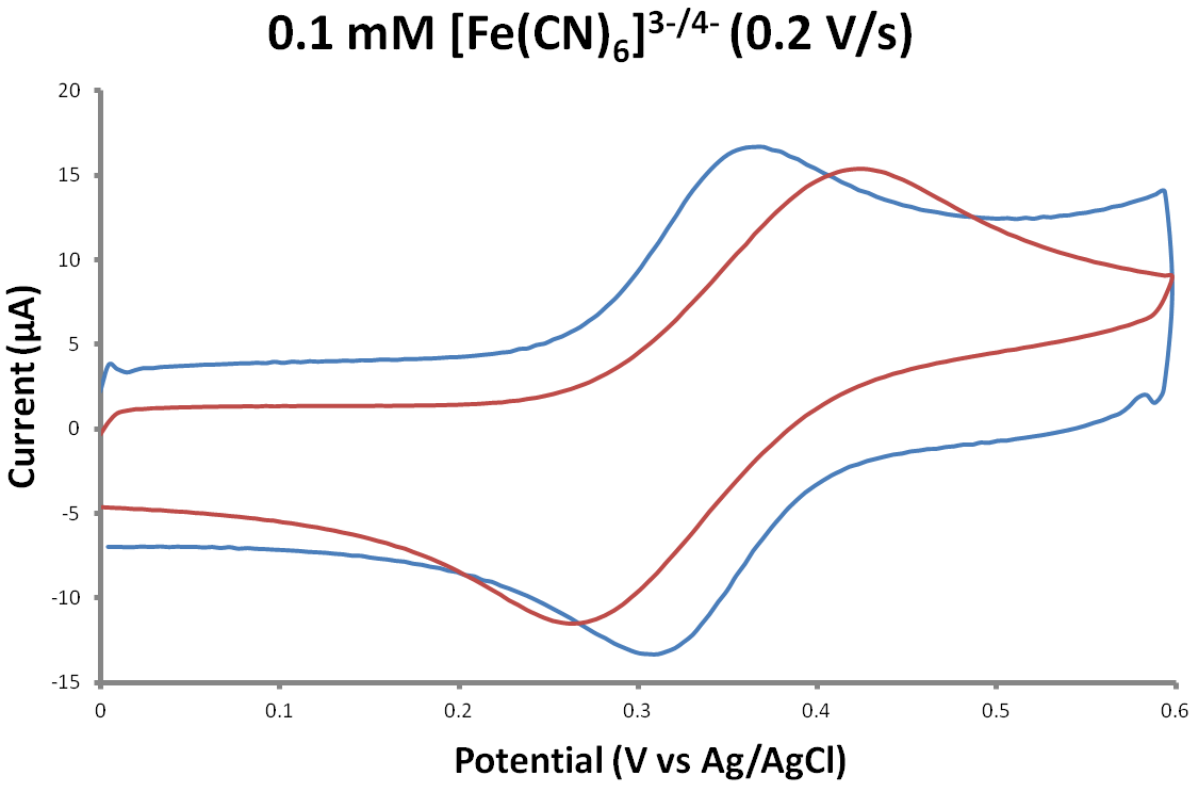

Figure 2.6 B) Cyclic voltammogram of $[Fe(CN)_6]^{3-/4-}$ comparing polished glassy carbon (blue) to pyrolyzed asphaltene derived thin film (red)

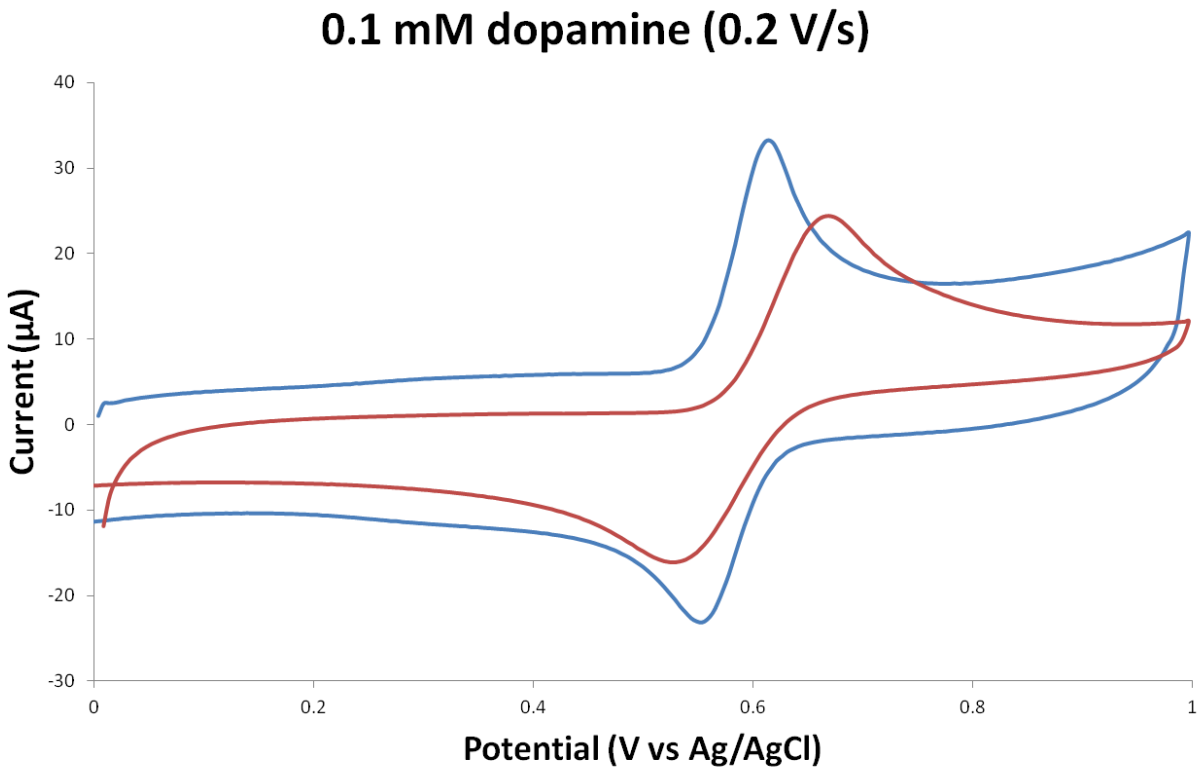

Figure 2.6 C) Cyclic voltammogram of dopamine comparing polished glassy carbon (blue) to pyrolyzed asphaltene derived thin film (red)

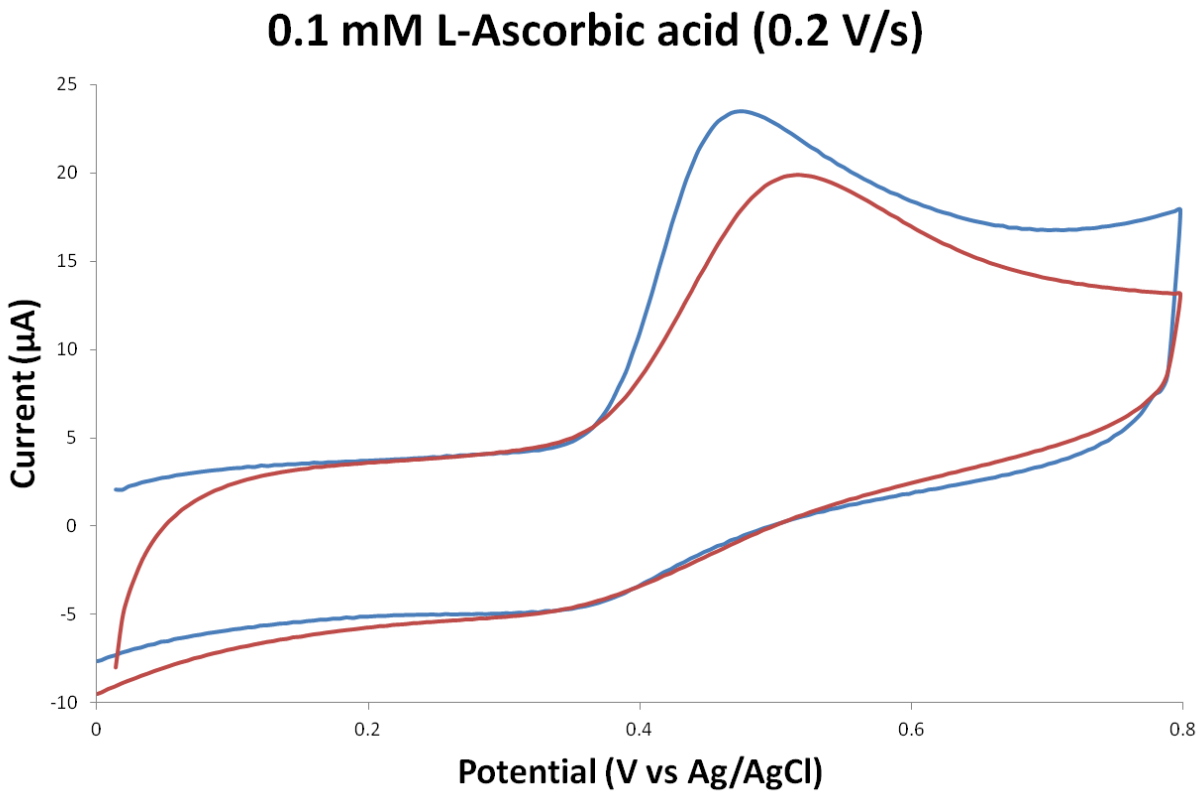

Figure 2.6 D) Cyclic voltammogram of L-ascorbic acid comparing polished glassy carbon (blue) to pyrolyzed asphaltene derived thin film (red)

The electrochemical reactivity of the asphaltene-derived carbon films (ADF) was assessed by measuring the heterogeneous electron transfer kinetics of several redox systems. Electrode kinetic parameters determined by cyclic voltammetry were compared to those observed for polished glassy carbon (GC) and to literature values for PPF. It was found that by first stabilizing our asphaltene-derived films at 200 °C in air, the electron transfer rate greatly improves. This stabilizing segment is called oxidative stabilization. Oxidative stabilization is frequently used to treat polyacrylonitrile (PAN) fibres to improve their mechanical properties.[33,34] The mechanism behind oxidative stabilization has been researched for many decades and is known to involve cross-linking, cyclization, and hydrogen elimination reactions.[35] An infrared spectroscopy study on the oxidative stabilization of polyacrylonitrile suggests the formation of C=C bonds.[36] Another IR and NMR study by Fochler *et al.* indicates a high number of C=CH bonds and also the formation of cyclized conjugated structures.[37] Asphaltenes exist as a complex mixture of carbon rings and chains of various sizes and lengths, unlike typical polymeric precursors such as photoresist or resins. We believe that oxidative stabilization acts the same way on our asphaltene-derived films as they do on PAN fibres. It is likely that oxidative stabilization of asphaltenes will also lead to cyclization and the formation of conjugated ring systems, thus improving the crystallinity of the pyrolyzed film. All electrochemistry data shown here are derived from films that were first stabilized in air.

Figure 2.6A-D shows the cyclic voltammograms for ADFs compared to polished glassy carbon. Cyclic voltammetry was performed using four different redox systems: $Ru(NH_3)_6^{3+/2+}$, $Fe(CN)_6^{3-/4-}$, dopamine, and ascorbic acid. Each of these redox systems behaves differently in regard to electron transfer at carbon electrode surfaces. Hence, it is necessary to test multiple

redox systems to assess the electrochemical capabilities of carbon electrodes. Table 2.1 lists the ΔEp and the heterogeneous electro transfer rate constant, k°. The rate constant, k°, is calculated from ΔEp using Nicholson's method.[38] The data for ADF in Table 2.1 are all corrected for internal resistance according to the method described in the experimental section.

Figure 2.6A-D shows well-defined peaks and standard shapes for voltammograms of pyrolyzed asphaltene-derived films (ADF). The peak separations are larger for ADF than for polished GC, indicating that for the redox systems tested, the electron transfer rates are generally lower for ADF. The background currents in the voltammograms are smaller for ADF compared to polished GC. This is consistent with previous AFM data where ADF are found to be very smooth, and thus exhibits lower double-layer capacitance than polished GC. The single-electron redox systems, $[Ru(NH_3)_6]^{3+/2+}$ and $[Fe(CN)_6]^{3-/4-}$, have their calculated *k°* listed in Table 2.1. The redox system for $[Ru(NH_3)_6]^{3+/2+}$ is a prototypical outer-sphere reaction, where the heterogeneous electron transfer rate does not depend on the surface conditions of the electrode. Rather, the electron transfer rate is mostly dependent upon the conductivity of the electrode. The heterogeneous electron transfer rate, k^0, for $[Ru(NH_3)_6]^{3+/2+}$ is found to be 0.013±0.001 cm/s. This is lower than polished glassy carbon (0.037±0.016 cm/s), but comparable to pyrolyzed photoresist (0.020 cm/s). This is consistent with the fact that our ADF and McCreery's PPF were both treated at 1000 °C, whereas the glassy carbon was treated at 2000 °C. The conductivity of the electrode is heavily dependent on the temperature of pyrolysis. As the temperature increases, the crystalline size and the degree of graphitization increases.[39] Since both the ADF and PPF are pyrolyzed at the same temperature, it is not surprising that they exhibit similar electron transfer rates for $[Ru(NH_3)_6]^{3+/2+}$. Another redox

system commonly used to probe the reactivity of carbon electrodes is ferri-/ferrocyanide. However, unlike $[Ru(NH_3)_6]^{3+/2+}$, $Fe(CN)_6^{3-/4-}$ is sensitive to surface conditions. Ji *et al.* found that k^0 for $Fe(CN)_6^{3-/4-}$ increases when a graphite electrode is exposed to air, suggesting that k^0 for this redox system is dependent on surface oxygen groups.[40] Electrode polishing and sonication with activated carbon also increases k^0, as found by Ranganathan *et al.*[41] In this case, the difference in k^0 is significant between polished GC and ADF. ADF has a k^0 of 0.0024±0.0007 cm/s, much lower than 0.030±0.009 cm/s for polished GC and 0.012 cm/s for PPF. This is likely because since ADF is so thin, it cannot undergo intensive cleaning such as polishing prior to analysis.

Electron transfer rate constants were not determined for DA and L-AA. The oxidation of dopamine is a multi-electron process that involves surface catalysis.[42,43] It was found by DuVall and McCreery that the electron transfer rate increases if dopamine can easily adsorb to the surface of the electrode.[43] The proposed mechanism suggests the adsorption of dopamine self-catalyzes the oxidation of dopamine in solution.[43] Because of this multi-electron mechanism, the calculation of a single $k°$ via Nicholson's method[38] would not be entirely accurate. The oxidation of dopamine is slower at ADF compared to polished GC (107±8 vs 69 mV for ΔE_p). Polished GC has a much rougher surface with a higher percent of oxygen functional groups, which could enhance the adsorption of dopamine and result in higher electron transfer rates for polished GC. Interestingly, the magnitude of ΔE_p for ADF is much closer to polished GC than to PPF (287±10 mV). This suggests reactants are more prone to adsorption on ADF than on PPF. The cyclic voltammogram for L-AA does not have a distinct cathodic peak (Figure 2.6C). Ascorbic acid oxidizes to dehydroascorbic acid, which irreversibly converts into 2,3-diketo-1-gulonic acid.

Hence, the reverse reduction of dehydroascorbic acid is not seen unless the scan rate is very high. The position of the oxidation peak for L-AA is very similar for ADF and PPF, and both are ~50 mV more positive than on polished GC. The mechanism for ascorbic acid oxidation has been suggested to involve charge transfer at surface quinoidal functionalities.[44] It was found that the oxidation of ascorbic acid is slower on a hydrophobic unactivated carbon electrode compared to a heat-treated carbon electrode with exposed polar sites.[45] Both ADF and PPF have a lower O/C ratio than polished GC, so it is reasonable the oxidation of L-AA requires a more positive potential.

It is not surprising that electron transfer rates for ADF are lower than polished GC. However, ADF is very comparable to pyrolyzed PPF. Electron transfer is very similar between ADF and PPF for $[Ru(NH_3)_6]^{3+/2+}$ and L-ascorbic acid. Both ADF and PPF are also similar in their physical characteristics. They possess lower roughness and lower capacitance background compared to polished GC. These characteristics make asphaltenes a cheap, suitable alternative as a precursor for carbon films.

	ΔEp (mV) Polished GC 0.2 V/s	ΔEp (mV)[a] pyrolyzed ADF 0.2 V/s	ΔEp (mV)[b] pyrolyzed PPF	k° (cm/s) Polished GC	k° (cm/s)[a] pyrolyzed ADF	k° (cm/s)[b] pyrolyzed PPF
$[Fe(CN)_6]^{3-/4-}$	68	150±20		0.030±0.009	0.0024±0.0007	0.012
$[Ru(NH_3)_6]^{3+/2+}$	69	85±16		0.037±0.016	0.013±0.001	0.020
Dopamine	69	107±8	287±10 (0.2 V/s)			
L-AA	453[c]	514±3[c]	505±21 (0.1 V/s)			

Table 2.1 Summary of electrode kinetics for asphaltene-derived films, with polished glassy carbon and pyrolyzed photoresist as comparison. [a]corrected for internal resistance. [b]data from McCreery et al. *Anal. Chem.* 73.5(2001): 893-900. [c]$E_{p,\ anodic}$

2.3.7 Pyrolysis of asphaltene nanoaggregates

Asphaltenes in solution are known to irreversibly adsorb onto a variety of surfaces, including silica,[46,47] gold,[46] kaolin,[48] and alumina.[49] The adsorption behaviour of asphaltenes is complex, but it is widely accepted that at low concentrations, asphaltenes will adsorb to a surface as nanoaggregates.[46,47,50] Furthermore, it is observed that asphaltene adsorption does not reach equilibrium in many circumstances. Zahabi et al. showed that no equilibrium was reached even after 1,000 minutes of adsorption on gold.[46] Xie et al. also found that for 10-200 ppm asphaltene in toluene-heptane, adsorption on gold does not reach equilibrium after 700 minutes.[51] Therefore, to ensure the adsorption of small nanoaggregates rather than large aggregates or complete monolayer coverage, a relatively short period of time (60 seconds) was chosen for adsorption prior to spin-coating. A 2 ppm solution of asphaltenes was first spin-coated onto a silicon substrate, and subsequently pyrolyzed at 1000 °C (11 °C/minute) for 1.5

hours in forming gas. Figure 2.7 shows the AFM and SEM images of nanoaggregates of asphaltenes after spin-coating. There are several small features in the SEM image of the spin-coated asphaltenes (Figure 2.7A). However, it is unlikely these are asphaltene nanoaggregates. Asphaltene is not a conductive material and is shown to have poor contrast in SEM. On the other hand, the AFM image (Figure 2.7C) shows that the surface of the silicon substrate is density populated by these nanoaggregates, with the majority between 10 and 20 nm in diameter. It is known that asphaltenes have greater adsorption on hydrophilic surfaces, possibly due to polar interactions, particularly interactions between asphaltenes and surface silanols.[49,52] Furthermore, it is widely accepted that asphaltene structure is composed of many different moieties, including aromatic rings, alkyl chains, and polar functional groups (O, S, N). It is highly likely that Van der Waals, π-π interactions, hydrogen bonding, and electrostatic interactions all contribute to asphaltene adsorption and aggregation. The abundance of nanoaggregates after just 60 seconds of adsorption on silicon from a 2 ppm solution is consistent with the literature discussed above.[46,49,51]

Figures 2.7B and 2.7D show the resulting carbon nanoparticles after pyrolysis. These nanoparticles are spherical in shape, and vary in diameter from approximately 3 to 20 nm (Figure 2.8). Figure 2.8 shows the average shifted histogram for particle diameter, where the solid curve represents the average of all shifted histograms, and the vertical lines underneath represent individual data points. Average shifted histograms eliminate any bias introduced by bin range and bin origin in traditional histograms. From the 134 particles measured, the average diameter is approximately 11 nm, with the majority of particles under 15 nm. An AFM section analysis (Figure 2.9) across several of these particles reveal that they are not perfectly

spherical in shape. These particles have an approximate aspect ratio of 1:3, suggesting that asphaltene nanoaggregates undergo a “melting” phase during pyrolysis.

Carbon nanoparticles have shown to have luminescent properties for particles that are less than 10 nm in diameter.[53] Preliminary studies did not show any luminescence for our nanoparticles, of which 40% are 10 nm in diameter or less. This could be because the density of nanoparticles is too low, or because these nanoparticles were produced in a reducing atmosphere. The luminescence of carbon nanoparticles is not completely understood, but it has been hypothesized to be related to surface oxygen groups.[54] Since the nanoparticles produced in this study was pyrolyzed in forming gas, the surface will be mostly hydrogen terminated with a very low percentage of surface oxygen.

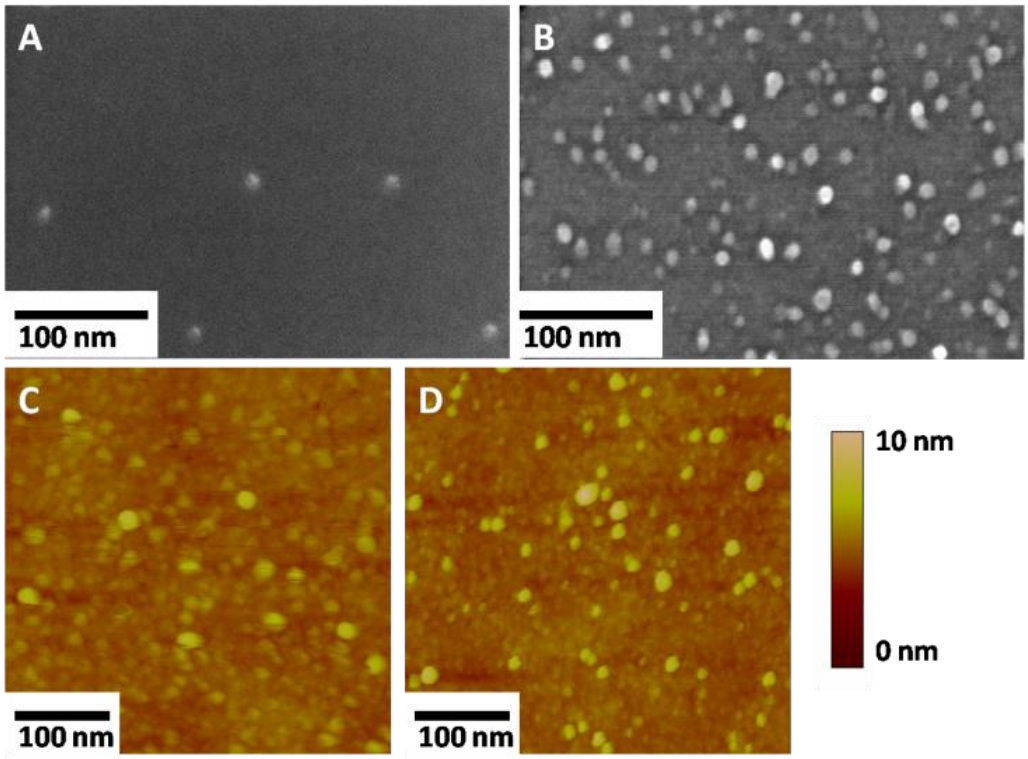

Figure 2.7 SEM images of asphaltene nanoaggregates before (A) and after (B) pyrolysis. AFM images before (C) and after (D) pyrolysis for the same sample.

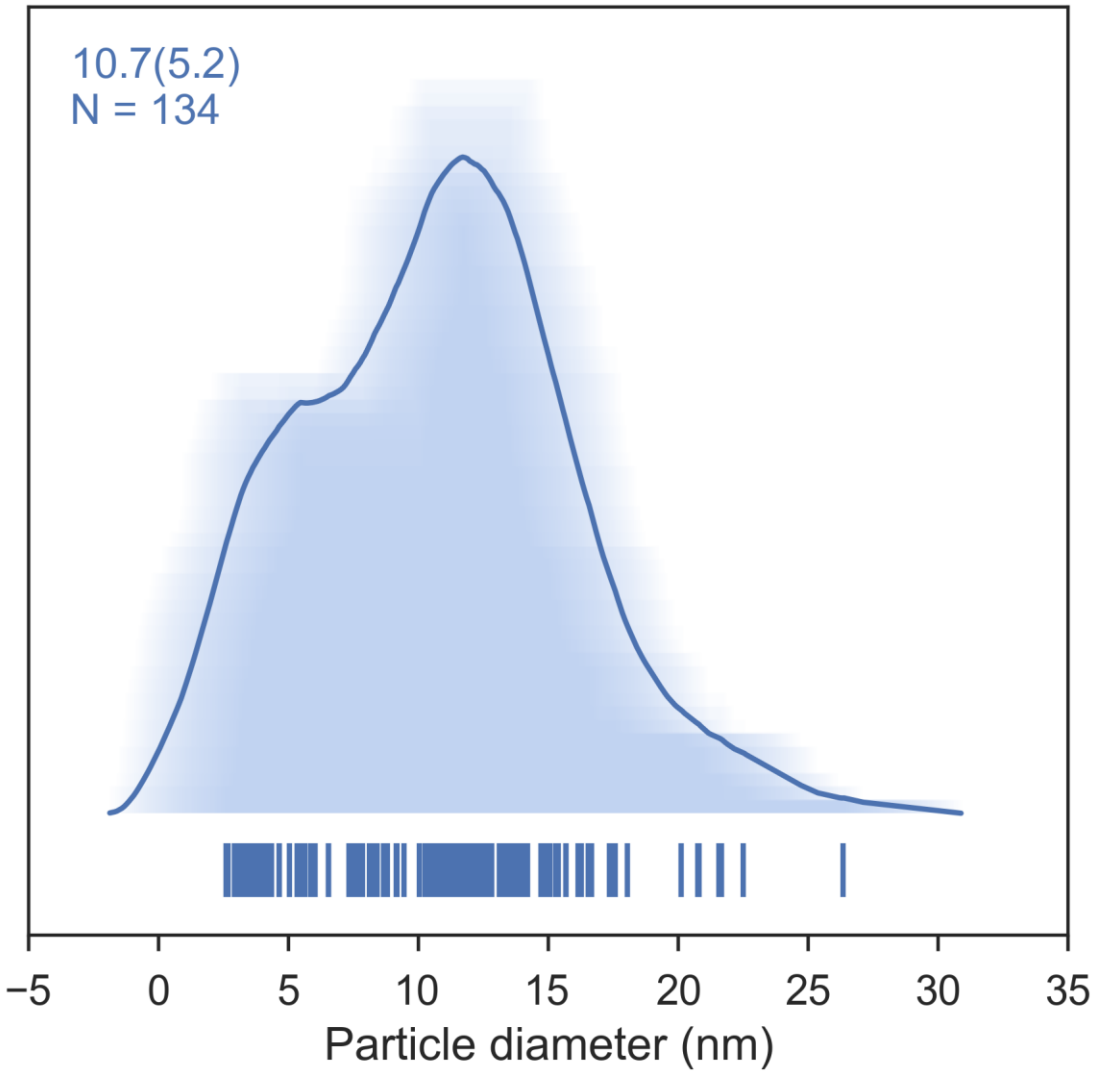

Figure 2.8 Average shifted histogram for particle diameter.

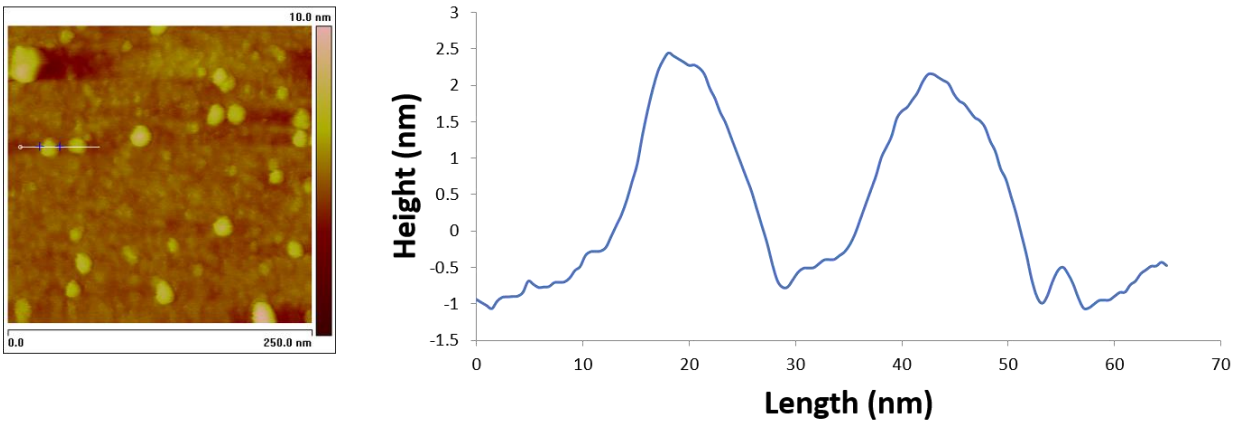

Figure 2.9 AFM section analysis for pyrolyzed asphaltene nanoaggregates.

An aliquot of the same 2 ppm asphaltene solution was drop-cast onto a silicon nitride grid and pyrolyzed under the same conditions. Figure 2.10 shows the high resolution TEM image of the resulting nanoparticles. No lattice features are seen, and the amorphous nature of these nanoparticles are consistent with carbon nanoparticles produced by laser pyrolysis.[55,56] Danumah et al. purportedly produced graphitic carbon nanoparticles after pyrolysis of asphaltenes at 200 °C.[26] However, this result is questionable since thermal decomposition only starts to occur at around 350 °C for asphaltenes.[57,58] At 200 °C, there is no decomposition of asphaltene molecules.

The mechanism of decomposition of asphaltenes is well known in literature. Decomposition begins at around 350°C. Gaseous materials generated from pyrolysis include H_2S, CO_2, CH_4, C_2H_6, and other hydrocarbons of various lengths.[27,57,58] These gases evolve from functional groups and aliphatic side chains, which are widely accepted to be components of asphaltene structure. At higher temperature, graphitization occurs and this is a complicated mechanism involving dehydrogenation, radical formation, and formation of polyaromatic hydrocarbons.[59] Previous work in our group found that pyrolysis of polymer precursor on a

silicon surface results in Si-C bond formation.[60] The nanoparticles produced in this case should also be covalently bonded to the surface of the silicon substrate by a Si-C bond.

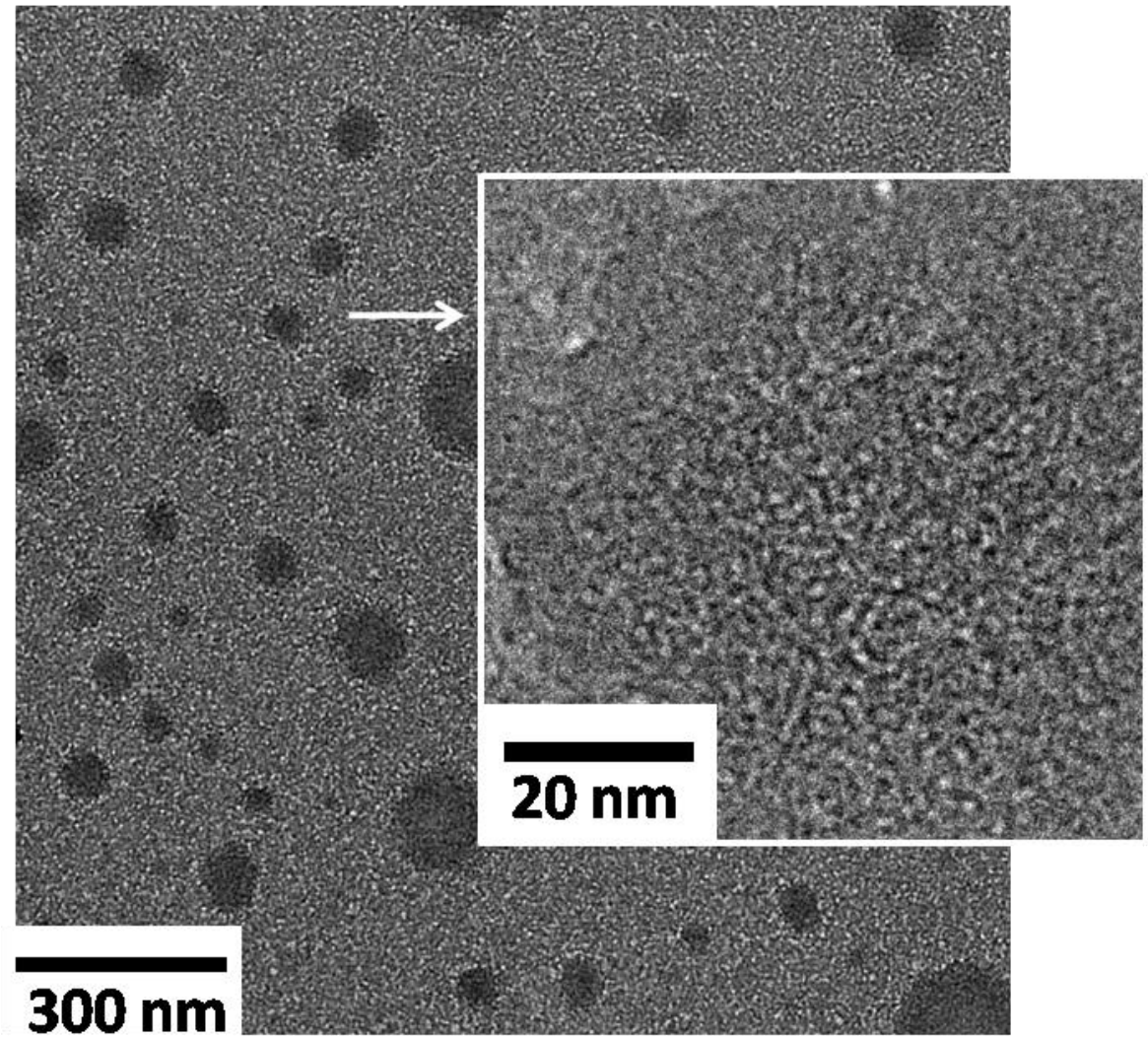

Figure 2.10 HR-TEM of a single carbon nanoparticles made by pyrolysis.

2.4 Conclusion

Asphaltenes are generally known as a problematic class of compounds in the oil industry. So far, there are not many potential applications using this material. By taking advantage of asphaltene's ability to adsorb as nanoaggregates, carbon nanoparticles were produced on the surface of a silicon substrate. These nanoparticles were not explored in detailed, but this provides an easy method of directly producing carbon nanoparticles on a surface. Similarly, by increasing the concentration of asphaltenes, a thin film was produced. This asphaltene-derived thin film (ADF) was shown to possess reasonable electrochemical activity. It is potentially possible to use asphaltenes as an inexpensive alternative to make thin film electrodes in carbon-based sensors or other applications.

2.5 References

1. Zhang, D. *et al.* Asphaltenes — Problematic but Rich in Potential. *Oilf. Rev.* 22–43 (2007).
2. Zanganeh, P. *et al.* Asphaltene deposition during CO 2 injection and pressure depletion: A visual study. *Energy and Fuels* **26,** 1412–1419 (2012).
3. Leontaritis, K. J. Asphaltene Deposition: A Comprehensive Description of Problem Manifestations and Modeling Approaches. *SPE Prod. Oper. Symp.* (1989).
4. McCreery, R. L. Advanced carbon electrode materials for molecular electrochemistry. *Chem. Rev.* **108,** 2646–2687 (2008).
5. Blackstock, J. J. *et al.* Ultraflat carbon film electrodes prepared by electron beam evaporation. *Anal. Chem.* **76,** 2544–2552 (2004).
6. Jönsson, G. & Gorton, L. An amperometric glucose sensor made by modification of a graphite electrode surface with immobilized glucose oxidase and adsorbed mediator. *Biosensors* **1,** 355–368 (1985).
7. Jönsson, G. & Gorton, L. An electrochemical sensor for hydrogen peroxide based on peroxidase adsorbed on a spectrographic graphite electrode. *Electroanalysis* **1,** 465–468 (1989).
8. Yoshio, M., Wang, H., Fukuda, K., Hara, Y. & Adachi, Y. Effect of Carbon Coating on Electrochemical Performance of Treated Natural Graphite as Lithium-Ion Battery Anode Material. *J. Electrochem. Soc.* **147,** 1245 (2000).
9. Aurbach, D., Markovsky, B., Weissman, I., Levi, E. & Ein-Eli, Y. On the correlation between surface chemistry and performance of graphite negative electrodes for Li ion batteries. *Electrochim. Acta* **45,** 67–86 (1999).
10. Gao, W. *et al.* Direct laser writing of micro-supercapacitors on hydrated graphite oxide films. *Nat. Nanotechnol.* **6,** 496–500 (2011).
11. Chen, Z. *et al.* High-performance supercapacitors based on hierarchically porous graphite particles. *Adv. Energy Mater.* **1,** 551–556 (2011).
12. Ranganathan, S., Mccreery, R., Majji, S. M. & Madou, M. Photoresist-Derived Carbon for Microelectromechanical Systems and Electrochemical Applications. *J. Electrochem. Soc.* **147,** 277–282 (2000).
13. Hebert, N. E., Snyder, B., McCreery, R. L., Kuhr, W. G. & Brazill, S. A. Performance of pyrolyzed photoresist carbon films in a microchip capillary electrophoresis device with sinusoidal voltammetric detection. *Anal. Chem.* **75,** 4265–4271 (2003).
14. Schueller, O. J. A., Brittain, S. T. & Whitesides, G. M. Fabrication of glassy carbon microstructures by pyrolysis of microfabricated polymeric precursors. *Adv. Mater.* **9,** 477–480 (1997).

15. Wang, C. & Madou, M. From MEMS to NEMS with carbon. *Biosens. Bioelectron.* **20,** 2181–2187 (2005).

16. Jain, S., Sharma, A. & Basu, B. Vertical electric field stimulated neural cell functionality on porous amorphous carbon electrodes. *Biomaterials* **34,** 9252–9263 (2013).

17. Byrne, C. E. & Nagle, D. C. Carbonization of wood for advanced materials applications. *Carbon N. Y.* **35,** 259–266 (1997).

18. Yoshino, K. *et al.* Graphite film prepared by pyrolysis of bacterial cellulose. *J. Appl. Phys.* **68,** 1720–1725 (1990).

19. Rojo, A., Rosenstratten, A. & Anjo, D. Characterization of a Conductive Carbon Film Electrode for Voltammetry. *Anal. Chem.* **58,** 2988–2991 (1986).

20. Nlwa, O. & Tabel, H. Voltammetric Measurements of Reversible and Quasi-Reversible Redox Species Using Carbon Film Based Interdigitated Array Microelectrodes. *Anal. Chem.* **66,** 285–289 (1994).

21. Ohnishi, T., Murase, I., Noguchi, T. & Hirooka, M. Preparation of graphite film by pyrolysis of polymers. *Synth. Met.* **18,** 497–502 (1987).

22. Duley, W. W. Refractive indices for amorphous carbon. *Astrophys. J.* **287,** 694–696 (1984).

23. Mullins, O. C. The Modified Yen Model. *Energy & Fuels* **24,** 2179–2207 (2010).

24. Ranganathan, S. & McCreery, R. L. Electroanalytical performance of carbon films with near-atomic flatness. *Anal. Chem.* **73,** 893–900 (2001).

25. McDermott, M. T., Kneten, K. & McCreery, R. L. Anthraquinonedisulfonate Adsorption, Electron-Transfer Kinetics, and Capacitance on Ordered Graphite-Electrodes: The Important Role of Surface Defects. *J. Phys. Chem.* **96,** 3124–3130 (1992).

26. Danumah, C., Myles, A. J. & Fenniri, H. Graphitic Carbon Nanoparticles from Asphaltenes. *MRS Proc.* **1312,** (2011).

27. Ali, M. F. & Saleem, M. Thermal Decomposition of Saudi Crude Oil Asphaltenes. *Fuel Sci. Technol. Int.* **9,** 461–484 (1991).

28. Park, B. Y., Taherabadi, L., Wang, C., Zoval, J. & Madou, M. J. Electrical Properties and Shrinkage of Carbonized Photoresist Films and the Implications for Carbon Microelectromechanical Systems Devices in Conductive Media. *J. Electrochem. Soc.* **152,** J136 (2005).

29. Kelemen, S. R. & Freund, H. XPS Characterization of Glassy-Carbon Surfaces Oxidized by O2, CO2, and HNO3. *Energy and Fuels* **2,** 111–118 (1988).

30. Endo, M. & Pimenta, M. A. Origin of dispersive effects of the raman d band in carbon materials. *Phys. Rev. B - Condens. Matter Mater. Phys.* **59,** R6585–R6588 (1999).

31. Knight, D. S. & White, W. B. Characterization of diamond films by Raman spectroscopy. *J. Mater. Res.* **4,** 385–393 (1989).

32. Wang, Y., Alsmeyer, D. C. & McCreery, R. L. Raman Spectroscopy of Carbon Materials: Structural Basis of Observed Spectra. *Chem. Mater.* **2,** 557–563 (1990).

33. Wu, M., Wang, Q., Li, K., Wu, Y. & Liu, H. Optimization of stabilization conditions for electrospun polyacrylonitrile nanofibres. *Polym. Degrad. Stab.* **97,** 1511–1519 (2012).

34. Zhang, W. X., Wang, Y. Z. & Sun, C. F. Characterization on oxidative stabilization of polyacrylonitrile nanofibres prepared by electrospinning. *J. Polym. Res.* **14,** 467–474 (2007).

35. Bashir, Z. A critical review of the stabilisation of polyacrylonitrile. *Carbon N. Y.* **29,** 1081–1090 (1991).

36. Conley, R. T. & Bieron, J. F. Examination of the oxidative degradation of polyacrylonitrile using infrared spectroscopy. *J. Appl. Polym. Sci.* **7,** 1757–1773 (1963).

37. Fochler, H. S., Mooney, J. R., Ball, L. E., Boyer, R. D. & Grasselli, J. G. Infrared and NMR spectroscopic studies of the thermal degradation of polyacrylonitrile. *Spectrochim. Acta Part A Mol. Spectrosc.* **41,** 271–278 (1985).

38. Nicholson, R. S. Theory and Application of Cyclic Voltammetry for Measurement of Electrode Reaction Kinetics. *Anal. Chem.* **37,** 1351–1355 (1965).

39. Fialkov, A. S., Baver, A. I., Sidorov, N. M., Chaikun, M. I., & Rabinovich, S. M. Pyrographite (preparation, structure, properties). *Russ. Chem. Rev.* **34,** 46–58 (1965).

40. Ji, X., Banks, C. E., Crossley, A. & Compton, R. G. Oxygenated edge plane sites slow the electron transfer of the ferro-/ferricyanide redox couple at graphite electrodes. *ChemPhysChem* **7,** 1337–1344 (2006).

41. Ranganathan, S., Kuo, T. C. & McCreery, R. L. Facile preparation of active glassy carbon electrodes with activated carbon and organic solvents. *Anal. Chem.* **71,** 3574–3580 (1999).

42. DuVall, S. H. & McCreery, R. L. Control of catechol and hydroquinone electron-transfer kinetics on native and modified glassy carbon electrodes. *Anal. Chem.* **71,** 4594–4602 (1999).

43. Duvall, S. H. & McCreery, R. L. Self-catalysis by catechols and quinones during heterogeneous electron transfer at carbon electrodes. *J. Am. Chem. Soc.* **122,** 6759–6764 (2000).

44. Hu, I. F. & Kuwana, T. Oxidative Mechanism of Ascorbic Acid at Glassy Carbon Electrodes. *Anal. Chem.* **58,** 3235–3239 (1986).

45. Deakin, M. R., Kovach, P. M., Stutts, K. J. & Wightman, R. M. Heterogeneous Mechanisms of the Oxidation of Catechols and Ascorbic Acid at Carbon Electrodes. *Anal. Chem.* **58,**

1474–1480 (1986).

46. Zahabi, A., Gray, M. R. & Dabros, T. Kinetics and properties of asphaltene adsorption on surfaces. *Energy and Fuels* **26,** 1009–1018 (2012).

47. Acevedo, S. *et al.* Importance of asphaltene aggregation in solution in determining the adsorption of this sample on mineral surfaces. *Colloids Surfaces A Physicochem. Eng. Asp.* **166,** 145–152 (2000).

48. Dubey, S. . & Waxman, M. . Asphaltene Adsorption and Desorption From Mineral Surfaces. *SPE Reserv. Eng.* **6,** 389–395 (1991).

49. Dudášová, D., Silset, A. & Sjöblom, J. Quartz crystal microbalance monitoring of asphaltene adsorption/ deposition. *J. Dispers. Sci. Technol.* **29,** 139–146 (2008).

50. Acevedo, S., Ranaudo, M. A., García, C., Castillo, J. & Fernández, A. Adsorption of asphaltenes at the toluene-silica interface: A kinetic study. *Energy and Fuels* **17,** 257–261 (2003).

51. Xie, K. & Karan, K. Kinetics and Thermodynamics of Asphaltene Adsorption on Metal Surfaces: A Preliminary Study. *Energy & fuels* **14,** 1252–1260 (2005).

52. Jada, A. & Debih, H. Hydrophobation of clay particles by asphaltenes adsorption. *Compos. Interfaces* **16,** 219–235 (2009).

53. Chandra, S., Das, P., Bag, S., Laha, D. & Pramanik, P. Synthesis, functionalization and bioimaging applications of highly fluorescent carbon nanoparticles. *Nanoscale* **3,** 1533 (2011).

54. Ray, S. C., Saha, A., Jana, N. R. & Sarkar, R. Fluorescent carbon nanoparticles: Synthesis, characterization, and bioimaging application. *J. Phys. Chem. C* **113,** 18546–18551 (2009).

55. Orlanducci, S. *et al.* Chemical/structural characterization of carbon nanoparticles produced by laser pyrolysis and used for nanotube growth. *Mater. Chem. Phys.* **87,** 190–195 (2004).

56. Bi, X.-X. *et al.* Nanoscale carbon blacks produced by CO2 laser pyrolysis. *J. Mater. Res.* **10,** 2875–2884 (1995).

57. Wang, T., Geng, A. & Li, X. Pyrolysis of one crude oil and its asphaltenes: Evolution of gaseous hydrocarbons and carbon isotope. *J. Pet. Sci. Eng.* **71,** 8–12 (2010).

58. Savage, P. E., Klein, M. T. & Kukes, S. G. Asphaltene Reaction Pathways. 1. Thermolysis. *Ind. Eng. Chem. Process Des. Dev.* **24,** 1169–1174 (1985).

59. Zhao, Y., Wei, F. & Yu, Y. Effects of reaction time and temperature on carbonization in asphaltene pyrolysis. *J. Pet. Sci. Eng.* **74,** 20–25 (2010).

60. Du, R., Ssenyange, S., Aktary, M. & McDermott, M. T. Fabrication and characterization of graphitic carbon nanostructures with controllable size, shape, and position. *Small* **5,** 1162–1168 (2009).

Chapter 3

Electrochemical Characterization of Electrospun and Carbonized Asphaltene Fibres

3.1 Introduction

In Chapter 2, asphaltenes were transformed into graphitic thin films and nanoparticles upon pyrolysis. These asphaltene-derived thin films were conductive and could be used as electrodes with comparable performance to glassy carbon, a commonly used benchmark electrode. This showed that asphaltenes can be used as a precursor to produce carbon materials. This chapter continues the exploration of asphaltenes as a basis for producing interesting, useful, value-added carbon materials.

Recently, asphaltene fibres were produced by electrospinning.[1] Natarajan *et al.* showed that smooth, micrometer diameter fibres can be electrospun from a concentrated solution of asphaltenes.[1] In electrospinning, a Taylor cone forms at the tip of a needle due to the application of a high voltage. A destabilization of the Taylor cone and solvent evaporation leads to fibre formation, and these fibres are collected on a conductive substrate. Electrospinning is very simple process for producing fibres from various kinds of polymers. For example, electrospinning has been used to form fibres from synthetic polymers,[2–5] keratin,[6,7] nucleic acids,[8] and ferromagnetic transition metals.[9] Polymers that can be electrospun into fibres usually have high molecular weights, or require a high molecular weight additive. This is because intermolecular forces are crucial for the formation of smooth fibres instead of spraying small particles. Asphaltenes have low molecular weights compared to commonly electrospun polymers such as polyacrylonitrile and polyvinylpyrrolidone, but Natarajan *et al*. demonstrated that asphaltenes can be electrospun into fibres without any additives. Here, we report the electrospinning and carbonization of asphaltene fibres. Carbonization of electrospun fibres is most commonly performed using polyacrylonitrile (PAN) as a precursor.[3,10,11] In 1996, Chun *et*

al. first demonstrated the electrospinning of polyacrylonitrile nanofibres.[12] Since then, there has been extensive work done on the electrospinning and carbonization of PAN fibres. Electrospun PAN fibres have promising applications in batteries,[10,13] filtration membranes,[14,15] nanocomposites,[16,17] and supercapacitors[18,19] among a wide range of potential uses. Electrospun fibres from various other polymers have also been investigated for analytical devices,[20–22] tissue engineering,[23,24] and photovoltaics.[25,26] Research in electrospinning has grown tremendously in recent years. Electrospinning is a simple, effective, and versatile technique to produce fibres from countless different polymers that can be used across many disciplines.

As mentioned above, polyacrylonitrile is the predominant polymer used for electrospinning and carbonization. This is because polyacrylonitrile can maintain its morphology after oxidative stabilization and pyrolysis. Like polyacrylonitrile, asphaltene can also be electrospun into fibres, but its potential as a precursor for carbon fibres have not been established in literature. Asphaltenes have a high carbon content, which is very important for any carbon precursor. We will explore the carbonization of electrospun asphaltene fibres and probe their electrochemical performance.

3.2 Experimental

3.2.1 Materials

All solutions were prepared using 18.2 megaohm-cm deionized water. No additional treatment or purification was done on any reagent. Reagents that were used include hexaammineruthenium(III) chloride (98%, Sigma-Aldrich), dopamine hydrochloride (Sigma-Aldrich), potassium ferrocyanide (99.0%, AnalaR), toluene (99.9%, Sigma-Aldrich), sulphuric acid

(95.0%-98.0%, Caledon), and potassium chloride (99.0-100.5%, Sigma-Aldrich). Substrates used for electrospinning were P-doped Si squares (2 cm x 2 cm). Glassy carbon (GC-20) was obtained from Tokai Carbon. Pentane-precipitated asphaltenes from Athabasca, Alberta were used. Asphaltenes were washed and filtered with pentane until the solvent only had a light colour.

3.2.2 Elemental Analysis

The elemental composition of asphaltenes was determined using a Thermo Flash 2000 CHNS-O combustion analyzer. To determine the carbon, hydrogen, nitrogen, and sulfur composition, ~1.3 gram of the asphaltene sample was pyrolyzed in the combustion reactor at 1000 ^{o}C in an oxidizing atmosphere. The C, H, N, and S in the sample were converted to CO_2, H_2O, N_2, and SO_2. These gases were separated in a Porapak QS column (4 mm ID, 2 m long) and detected using a thermal-conductivity detector. To determine the oxygen composition, ~4 grams of the asphaltene sample was pyrolyzed at 1060 ^{o}C under helium. The oxygen was converted to CO by a layer of nickel coated carbon and is separated and detected in the same manner as above. The elemental composition of the asphaltene was determined to be C(82.52%), H(8.14%), N(1.18%), S(7.04%), and O(1.13%).

3.2.3 Electrospinning

A glass syringe with a gauge 20 needle was suspended 10 cm above an aluminum plate. Doped Si substrates (2 cm x 2 cm) were placed on the aluminum plate to collect fibres. A power supply was used to apply 10 kV between the tip of the needle and the aluminum plate. Three different solutions were electrospun: 30%, 40%, and 50% (w/w) asphaltene in toluene. The asphaltene solution flows through the needle by gravitational pull, as opposed to using a

syringe pump. Electrospinning was performed for approximately 10 minutes, until the entire silicon substrates were covered.

3.2.4 Pyrolysis of asphaltene fibres

Three silicon substrates with asphaltene fibres were pyrolyzed at 1000 °C for 1.5 h in forming gas (95% argon 5% H_2) without stabilization (20-1000 °C at 5 °C/min, hold at 1000 °C for 1.5 h). Three samples were first stabilized at 250 °C (20-250 °C at 5 °C/min, hold at 250 °C for 1 h) and another three samples were stabilized at 200 °C (20-200 °C at 5 °C/min, hold at 200 °C for 1h) in air, and then pyrolyzed at 1000 °C for 1.5 h in forming gas (250 or 200 to 1000 °C at 5 °C/min, hold at 1000 °C for 1.5 h). All stabilization and pyrolysis were done in a Lindberg three zone tube furnace.

3.2.5 SEM and AFM characterization

A JEOL SEM instrument with a secondary electron detector was used to obtain images before and after pyrolysis. Fibre widths were measured using ImageJ from SEM images. A section profile of a single pyrolyzed fibre was obtained from contact mode AFM using a Veeco multimode SPM instrument. A silicon nitride AFM probe with 2nm tip radius was used (NanoSensors).

3.2.6 Raman spectroscopy

Raman spectroscopy was performed using a Renishaw inVia Raman microscope system with an argon laser operating at 514.5 nm. Three samples without stabilization, and three samples with stabilization at 200 °C were analyzed using Raman. Raman parameters were 514.5 nm laser, 30 mW power, 100s exposure, and a 20x objective lens. The resulting spectra were

baseline subtracted, and the ratio of the D-band to G-band was determined. Spectra for 9 random spots were used to calculate the ratios.

3.2.7 Electrochemistry

Cyclic voltammetry was performed using a typical three electrode cell, with a Pt mesh counter electrode and an Ag/AgCl reference electrode. An O-ring exposes approximately 28 mm^2 of the working electrode to the electrolyte solution. A PINE potentiostat and Aftermath software were used to obtain cyclic voltammograms. Experiments were done on both GC-20 and pyrolyzed asphaltene fibres on doped Si as the working electrode. Redox systems used were 0.1mM $[Ru(NH_3)_6]^{3+/2+}$ in 1M KCl, 0.1mM $[Fe(CN)_6]^{3-/4-}$ in 1M KCl, and 0.1 mM dopamine in 0.1M H_2SO_4. ΔE_p was determined directly from the peak separation without internal resistance correction. The rate constant, $k°$, was calculated from ΔE_p according to Nicholson's method.[27] Three different scan rates (0.1, 0.2, 0.5 V/s) were used to determine $k°$ for each redox system.

Glassy carbon was polished using 1 µm, 0.3 µm, and 0.05 µm alumina on a piece of micro-cloth (Buehler). After polishing, it was sonicated in isopropanol for 15 minutes and rinsed with deionized water prior to cyclic voltammetry. Pyrolyzed asphaltene fibres were also sonicated in isopropanol for 15 minutes and rinsed with deionized water.

3.3 Results and discussion

The electrospinning set up was oriented vertically, in such a way that the asphaltene solution was flowing gravitationally, rather than using a pump. This was found to maintain a steady flow rate due to the high viscosity of the asphaltene solution. Natarajan *et al*. found that the electrospinning of asphaltene fibres depends on the concentration of the solution. In their

study, 20% (w/w) and 30% (w/w) asphaltene in toluene produced beads, whereas 40% (w/w) asphaltene in toluene produced smooth fibres.[1] We also investigated the effect of concentration on fibre formation. Three different concentrations were used for electrospinning: 30% (w/w), 40% (w/w), and 50% (w/w) asphaltene in toluene. Figure 3.1 shows the SEM images after electrospinning from different concentrations. At 30%, broken beads were formed, and these beads are identical in appearance as those found by Natarajan. Fibres were observed for the 40% and 50% solutions. However, at 40%, the results were inconsistent, as sometimes beads would form, and sometimes fibres would form. Asphaltene fibres were consistently obtained for 50% solutions. The fibres range from ~5 to ~15 μm in width and appear to be smooth with no beads, consistent with fibres produced by Natarajan. The formation of beads and beaded-fibres could be the result of incomplete and slow solvent evaporation.[28] The formation of beads from low asphaltene concentration solutions could be due to several factors. A low concentration solution contains a higher percentage of solvent, and this could lead to incomplete solvent evaporation and bead formation. Furthermore, unlike traditional polymers used in electrospinning, such as polyacrylonitrile and polyvinylpyrrolidone with molecular weights in the range of 10,000-40,000, asphaltenes have molecular weights in the range of 500-1,000 daltons.[29] Successful fibre formation requires strong intermolecular interactions and polymer entanglement, and high molecular weight polymers generally produce high quality fibres. In the case of asphaltenes, various intermolecular forces can be operative, including Van der waals forces, hydrogen bonding, electrostatics, and π-π stacking.[30] A high concentration is required to increase the prevalence of these intermolecular interactions to promote fibre formation.

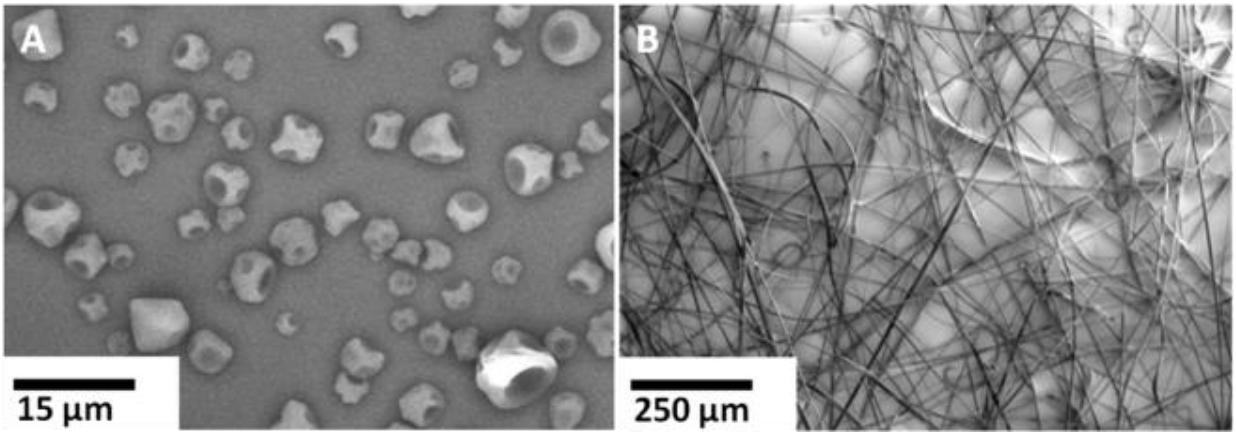

Figure 3.1 SEM images of electrospun product from A) 30% and B) 50% (w/w) asphaltene in toluene.

3.3.1 Pyrolysis and stabilization

The asphaltenes were carbonized by pyrolysis at 1000 °C in forming gas. A pre-heat treatment step referred to as oxidative stabilization is often used for the pyrolysis of polyacrylonitrile fibres. This is done in air at a lower temperature, usually around 200-300 °C. It has been found that oxidative stabilization prior to carbonization preserves the shape of the fibres as well as improving the crystallinity and mechanical properties of the carbonized product.[31,32] Figure 3.2 shows the SEM images of pyrolyzed asphaltene fibres without and with oxidative stabilization at 250 and 200 °C in air. With no stabilization (Figure 3.2A), asphaltene fibres appear to melt into a puddle during pyrolysis (1000 °C for 1.5 hours). Stabilization at 250 °C (Figure 3.2B) improves the preservation of the fibres, but significant melting is still observed. Stabilization at 200 °C (Figure 3.2C) shows further improvement. Carbonized asphaltene fibres are cross-linked and most of the fibre morphology is preserved by first stabilizing at 200 °C. A lower stabilization temperature improves fibre morphology during pyrolysis because the stabilization temperature should be lower than when significant thermal degradation occurs. It is likely that at 250 ^{o}C, thermal degradation of asphaltene molecules are occurring at a significant rate. Figure 3.3 shows that the fibre widths before and after pyrolysis. Even after stabilization at 200 °C, the average widths of fibres slightly increase after pyrolysis, from about 10 to 15 µm. An AFM profile (Figure 3.4) of a single carbonized fibre shows a rounded fibre, but the maximum height is ~120 nm whereas the width is ~10 µm. This suggests stabilization at 200 °C for 1 hour is still not sufficient for completely preserving the morphology of asphaltene fibres.

Preliminary cyclic voltammetry investigation shows that by first stabilizing fibres at a lower temperature, the electrochemical reactivity is improved for the final pyrolyzed product. Table 3.1 lists the ΔE_p from cyclic voltammetry of $[Fe(CN)_6]^{3-/4-}$ for pyrolyzed fibres that were not stabilized, and stabilized at 200 °C. The fibres that were not stabilized exhibited a ΔE_p of 160±40 mV, much larger than 68 mV for polished glassy carbon. However, by stabilizing at 200 °C, ΔE_p is decreased from 160±40 mV to 90±20 mV. A lower ΔE_p translates to a larger electron transfer rate, which means that stabilizing the fibres improved the electrochemical reactivity of the pyrolyzed fibres. The mechanism behind oxidative stabilization is not completely understood, but it is known to involve cross-linking reactions and improves the crystallinity of the carbonized product.[25] We believe that oxidative stabilization acts in a similar manner for asphaltene fibres. Increased cross-linking of asphaltene molecules during stabilization likely improves graphitization during pyrolysis, hence increasing the conductivity and electrochemical reactivity. All further electrochemistry experiments were done on fibres that were first stabilized at 200 °C in air.

	ΔEp (mV) polished GC	ΔEp (mV) pyrolyzed fibres (not stabilized)	ΔEp (mV) pyrolyzed fibres (stabilized at 200 °C)
$[Fe(CN)_6]^{3-/4-}$ (0.2 V/s)	68	160±40	90±20

Table 3.1 Cyclic voltammetry data for non-stabilized and stabilized asphaltene fibres.

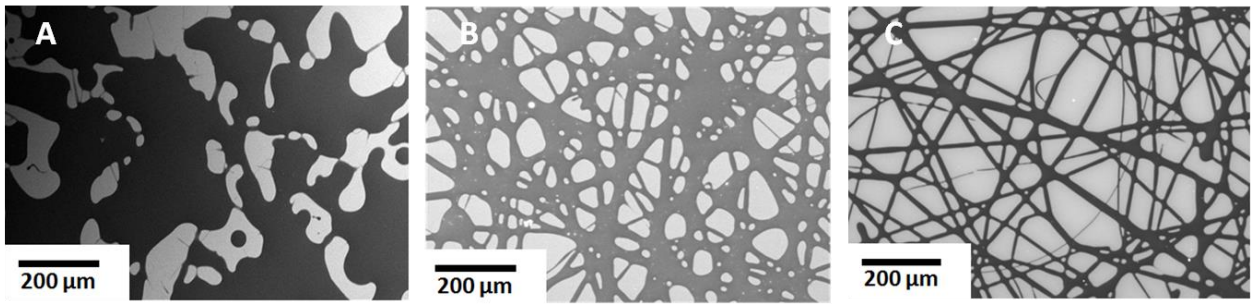

Figure 3.2 SEM images of pyrolyzed asphaltene fibres. A) no stabilization B) stabilization at 250 °C for 1h C) stabilization at 200 °C for 1h.

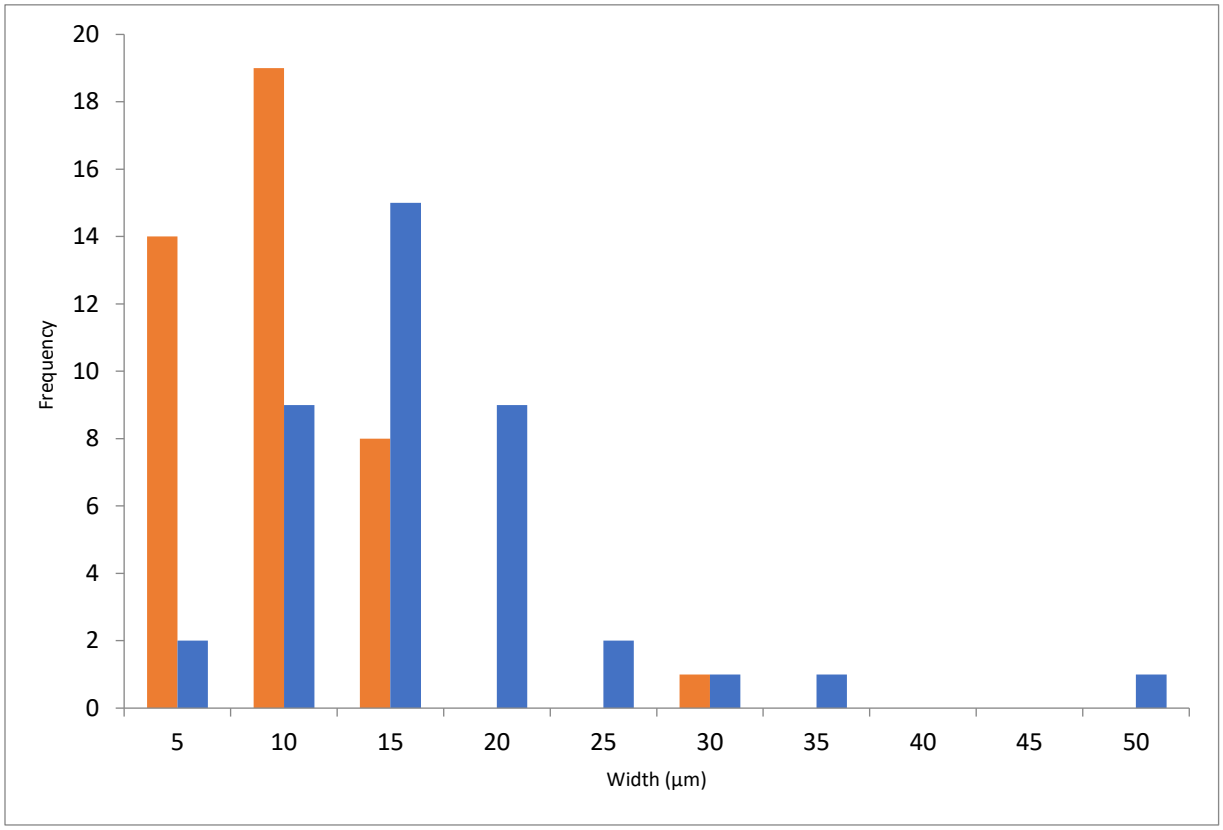

Figure 3.3 Fibre widths measured from SEM. Red: asphaltene fibres before pyrolysis. Blue: asphaltene fibres after stabilization at 200 °C and pyrolysis at 1000 °C.

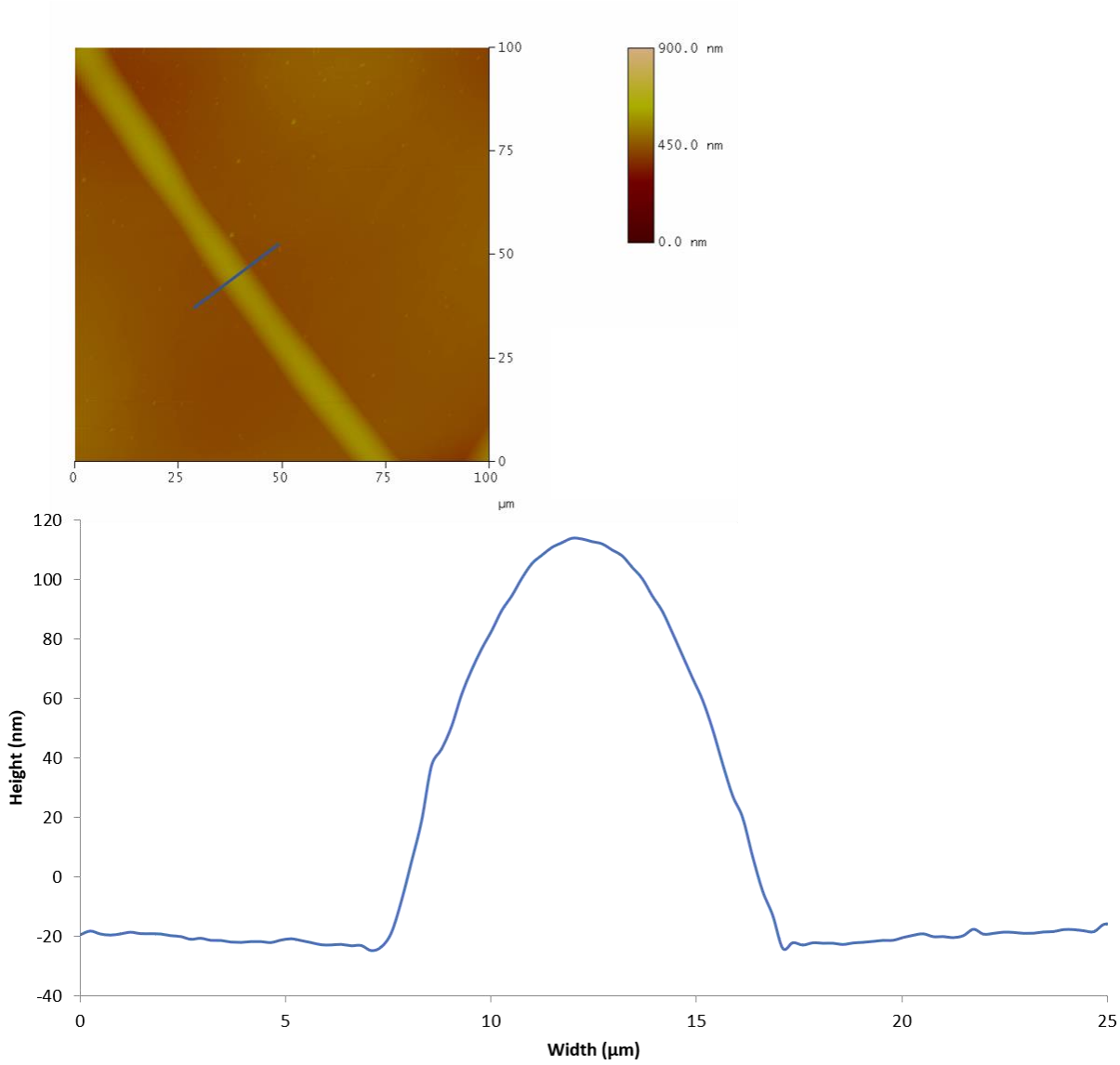

Figure 3.4 AFM section analysis of a single pyrolyzed asphaltene fibre.

3.3.2 Raman spectroscopy

As discussed in Chapter 2, Raman spectroscopy is widely used to characterize graphitic material due to the presence of two distinct bands: the D-band and G-band. Figure 3.5 shows the presence of the D-band and G-band at 1344 cm^{-1} and 1598 cm^{-1}, respectively, for pyrolyzed asphaltene fibres with and without stabilization at 200 °C.

The absence of any fluorescence and the appearance of the G-band indicate that pyrolysis at 1000°C was effective in carbonizing asphaltene fibres. The Raman spectrum of the asphaltene precursor (514 nm excitation) contains a high fluorescent background. After pyrolysis, regardless of stabilization at 200 °C, these fibres are graphitized and hence become conductive, as evidenced by electrochemistry and Raman. The ratio of intensities of the D-band and G-band can be used to estimate the graphite crystalline size. In general, as the number of defects in the graphitic structure increase, the crystalline size decreases and the intensity of the D-band will also increase.[33] In Figure 3.5, where the spectra are normalized using the G-band, the ratio of D-band to G-band is 0.71±0.06 and 0.84±0.06 for fibres that were, and were not first stabilized in air at 200 °C. Using the model proposed by Knight and White,[33] L_a, which is the crystalline size parallel to the plane of graphite, is estimated to be 6.2±0.4 nm and 5.2±0.3 nm for stabilized and non-stabilized fibres, respectively. This suggests, by first stabilizing in air at 200 °C prior to pyrolysis at 1000 °C, the resulting fibres have a slightly larger crystalline size. The increase in L_a from oxidative stabilization is likely due to cross-linking, cyclization, and hydrogen elimination reactions.[34] Infrared spectroscopy and NMR studies on the oxidative stabilization of polyacrylonitrile have shown an increase in C=C bonds, C=CH bonds, and other cyclized conjugated structures.[35,36] The crystalline structure of graphite is composed of planes of sp^2

carbon, so it is very likely that an increase in C=C and C=CH bonds will affect the crystalline size. Recall from Table 3.1 that oxidative stabilization improves the electrochemical behaviour of the graphitized fibres. Therefore, Raman spectroscopy provides further evidence that oxidative stabilization improves the crystallinity and conductivity of the pyrolyzed product.

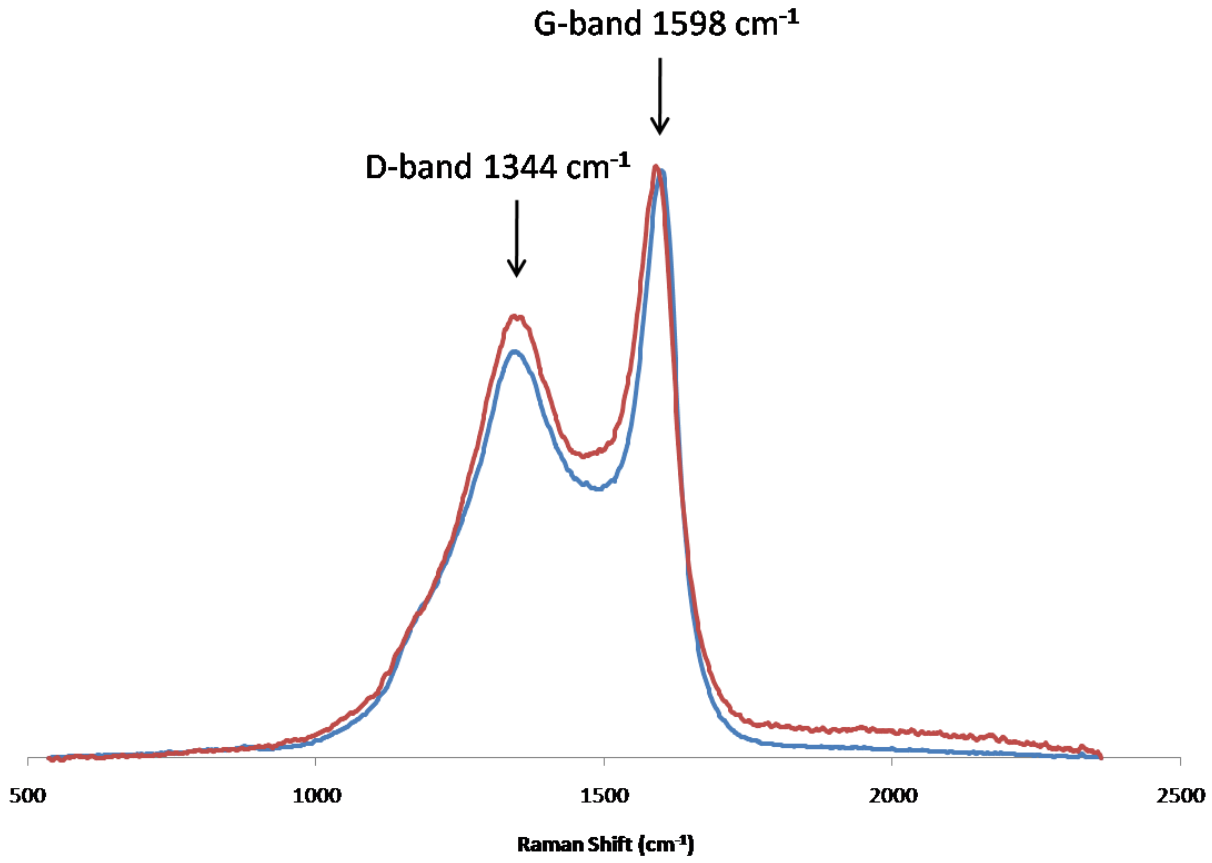

Figure 3.5 Raman spectroscopy after the pyrolysis of asphaltene fibres at 1000 °C in forming gas, with and without oxidative stabilization at 200 °C. Laser parameter: 514.5 nm, 30 mW, 100 seconds. Red: pyrolyzed asphaltene fibres without stabilization. Blue: pyrolyzed asphaltene fibres that were first stabilized at 200 °C.

3.3.3 Electrochemical characterization

Electrode kinetics were determined for the pyrolyzed asphaltene fibres compared to polished glassy carbon (GC). Figure 3.6(A-C) shows the cyclic voltammograms from pyrolyzed fibres overlaid with polished GC. Cyclic voltammetry was performed using three different redox systems: $Ru(NH_3)_6^{3+/2+}$, $Fe(CN)_6^{3-/4-}$, and dopamine. To accurately assess the electrochemical reactivity of an electrode, multiple redox systems should be tested. This is because each redox system behaves differently in regards to electron transfer at the electrode surface. Figure 3.6 (A-C) shows well defined, symmetrical peaks for all systems at pyrolyzed asphaltene fibres and polished GC. However, the peak separations are wider for the fibres than for GC. This suggests electron transfer at the electrode surface is slower at the fibres.

Table 3.2 lists the ΔE_p and the heterogeneous electron transfer rate constant, k^0, for our fibres compared to polished GC for all three redox systems. A plot of ΔE_p as a function of i_p with increasing concentration of dopamine is linear with a slope close to zero, indicating that there is negligible internal resistance. Hence, ΔE_p is not corrected, and is used directly to calculate k^0 using Nicholson's method.[27] For both $[Ru(NH_3)_6]^{3+/2+}$ and $[Fe(CN)_6]^{3-/4-}$, k^0 is smaller for our pyrolyzed asphaltene fibres compared to polished GC. For a typical outer-sphere reaction, $[Ru(NH_3)_6]^{3+/2+}$ is not sensitive to surface functional groups or cleanliness, but rather depends on the conductivity of the electrode. This is consistent with the data that the glassy carbon, made at 2000 °C, exhibits a larger k^0 than the fibres, which were pyrolyzed at 1000 °C. Conductivity of graphitic material increases as the temperature of fabrication increases.[37] For $Fe(CN)_6]^{3-/4-}$, k^0 is largely affected by surface cleanliness. Glassy carbon has the advantage of being able to be polished, and thus exhibits a faster electron transfer rate. The electron transfer rate constant

was not determined for dopamine because dopamine oxidation is a multistep, surface catalyzed reaction. Instead, we can compare the ΔE_p. The rate of dopamine oxidation increases if dopamine can easily adsorb to the surface of the electrode. The ΔE_p for dopamine oxidation is much larger for our fibres than for polished GC. Asphaltene fibres were pyrolyzed in forming gas, and the surface is likely to be hydrogen terminated with low oxygen composition. This could account for poor adsorption of dopamine onto the fibres.

From Table 3.2, it is clear that the fibres exhibit slower electron transfer rates for all three redox systems compared to glassy carbon. However, the fibres exhibit very similar electron transfer kinetics compared to other pyrolytic carbon materials (Table 3.2). For example, pyrolyzed photoresist used as a microelectromechanical device has k^0 of 0.019 cm/s and 0.017 cm/s for $[Fe(CN)_6]^{3-/4-}$ and $[Ru(NH_3)_6]^{3+/2+}$, respectively. Both of these values are very comparable to our fibres. Other pyrolytic carbon from methane and natural gases also show very similar kinetics to our fibres (Table 3.3). The goal of this research was to explore potential uses of asphaltenes, and our data show that by having similar electron transfer behavior, asphaltenes can be used as a cheaper alternative to more expensive pre-cursors such as photoresist.

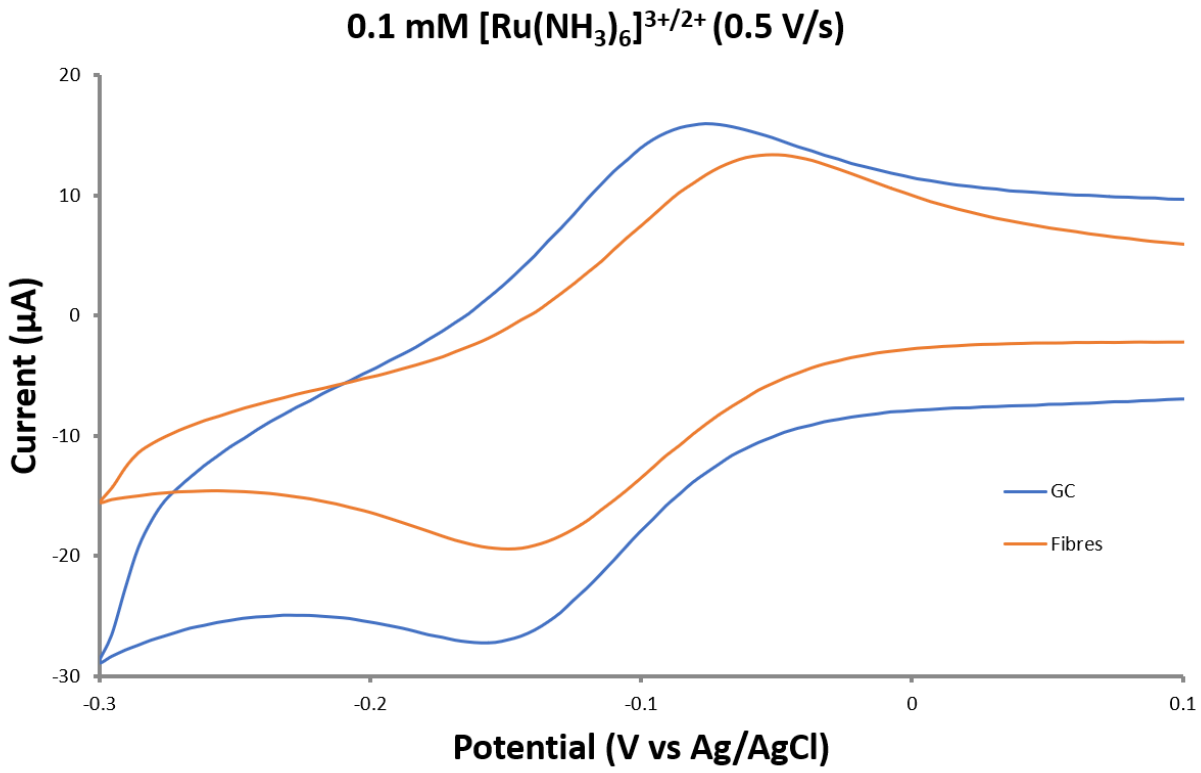

Figure 3.6A. Cyclic voltammogram of $[Ru(NH_3)_6]^{3+/2+}$ comparing polished glassy carbon (blue) to pyrolyzed asphaltene fibres (red)

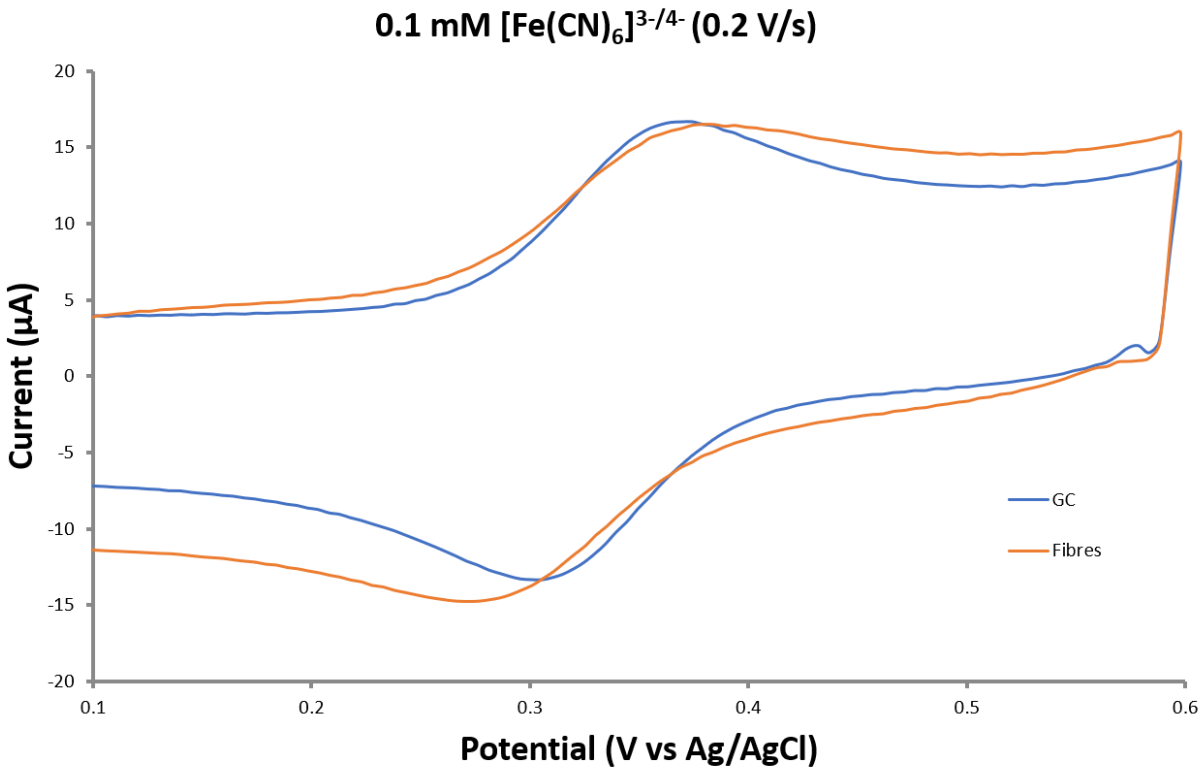

Figure 3.6B Cyclic voltammogram of $[Fe(CN)_6]^{3-/4-}$ comparing polished glassy carbon (blue) to pyrolyzed asphaltene fibres (red)

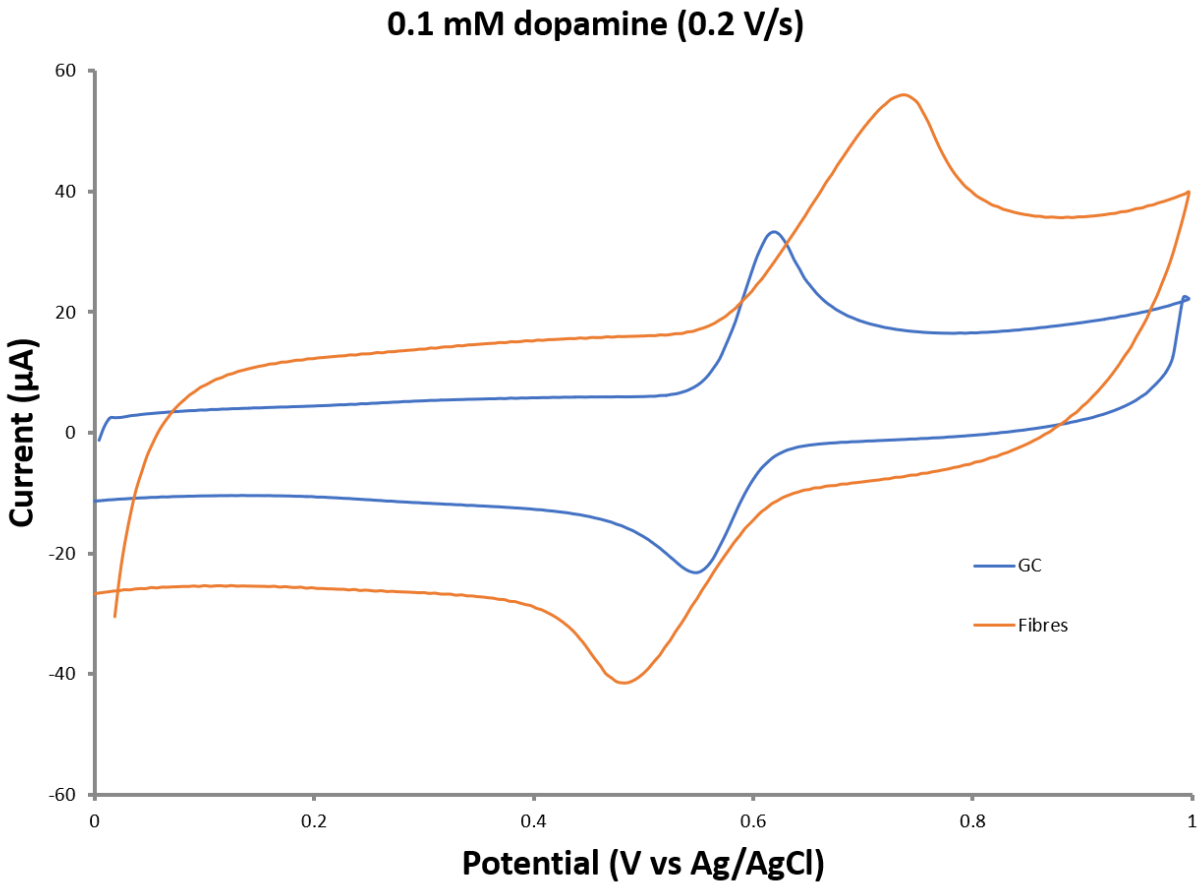

Figure 3.6C Cyclic voltammogram of dopamine comparing polished glassy carbon (blue) to pyrolyzed asphaltene fibres (red)

	ΔEp (mV) Polished GC 0.2 V/s	**ΔEp (mV) pyrolyzed fibres (stabilized) 0.2 V/s**	**k° (cm/s) Polished GC**	**k° (cm/s) pyrolyzed fibres (stabilized)**
$[Fe(CN)_6]^{3-/4-}$	68	90±20	0.030±0.009	0.010±0.002
$[Ru(NH_3)_6]^{3+/2+}$	69	82±3	0.037±0.016	0.016±0.003
Dopamine	69	240±30		

Table 3.2 Summary of electrode kinetics for pyrolyzed asphaltene fibres compared to polished glassy carbon.

	k° (cm/s) pyrolyzed asphaltene fibres (stabilized at 200 °C)	**k° (cm/s) pyrolyzed photoresist[38]**	**k° (cm/s) pyrolytic methane electrode[39]**	**k° (cm/s) pyrolytic natural gas on Macor[37]**
$[Fe(CN)_6]^{3-/4-}$	0.010±0.002	0.019	0.009	0.004-0.015
$[Ru(NH_3)_6]^{3+/2+}$	0.016±0.003	0.017		

Table 3.3 Comparison of k^0 between pyrolyzed asphaltene fibres and other pyrolytic carbon materials.

3.4 Conclusion

Asphaltenes are known as problematic, waste materials from oil production, and very little research is focused on their potential uses. However, we have shown that electrospinning can be used to make asphaltene fibres with widths from 5-15 µm. These fibres can be pyrolyzed to yield conductive carbon fibres. Pyrolyzed asphaltene fibres show normal, symmetrical cyclic voltammograms and electron transfer kinetics from these fibres are very comparable to other pyrolytic carbon materials. This suggests asphaltenes can be used as an inexpensive, suitable alternative for pyrolytic carbon electrodes. Asphaltene fibres may also have potential applications in other areas such as supercapacitors and filtration.

3.5 References

1. Natarajan, A., Mahavadi, S. C., Natarajan, T. S., Masliyah, J. H. & Xu, Z. Preparation of Solid and Hollow Asphaltene Fibers by Single Step Electrospinning. *J. Eng. Fiber. Fabr.* **6,** 1–6 (2011).

2. Ko, F. *et al.* Electrospinning of continuous carbon nanotube-filled nanofiber yarns. *Adv. Mater.* **15,** 1161–1165 (2003).

3. Zussman, E. *et al.* Mechanical and structural characterization of electrospun PAN-derived carbon nanofibers. *Carbon N. Y.* **43,** 2175–2185 (2005).

4. Qin, X. H. Structure and property of electrospinning PAN nanofibers by different preoxidation temperature. *J. Therm. Anal. Calorim.* **99,** 571–575 (2010).

5. Pan, H., Li, L., Hu, L. & Cui, X. Continuous aligned polymer fibers produced by a modified electrospinning method. *Polymer (Guildf).* **47,** 4901–4904 (2006).

6. Aluigi, A. *et al.* Structure and properties of keratin/PEO blend nanofibres. *Eur. Polym. J.* **44,** 2465–2475 (2008).

7. Zoccola, M. *et al.* Study on cast membranes and electrospun nanofibers made from keratin/fibroin blends. *Biomacromolecules* **9,** 2819–2825 (2008).

8. Fang, X. & Reneker, D. H. DNA fibers by electrospinning. *J. Macromol. Sci. Part B* **36,** 169–173 (1997).

9. Wu, H., Zhang, R., Liu, X., Lin, D. & Pan, W. Electrospinning of Fe, Co, and Ni nanofibers: synthesis, assembly, and magnetic properties. *Chemistry of materials* **19,** 3506–3511 (2007).

10. Ji, L., Jung, K.-H., Medford, A. J. & Zhang, X. Electrospun polyacrylonitrile fibers with dispersed Si nanoparticles and their electrochemical behaviors after carbonization. *J. Mater. Chem.* **19,** 4992 (2009).

11. Hou, H. & Reneker, D. H. Carbon Nanotubes on Carbon Nanofibers: A Novel Structure Based on Electrospun Polymer Nanofibers. *Adv. Mater.* **16,** 69–73 (2004).

12. Reneker, D. H. & Chun, I. Nanometer diameter fibers of polymer, produced by electrospinning. *Nanotechnology* **7,** 216–223 (1996).

13. Yu, Y., Yang, Q., Teng, D., Yang, X. & Ryu, S. Reticular Sn nanoparticle-dispersed PAN-based carbon nanofibers for anode material in rechargeable lithium-ion batteries. *Electrochem. commun.* **12,** 1187–1190 (2010).

14. Kampalanonwat, P. & Supaphol, P. Preparation and adsorption behavior of aminated electrospun polyacrylonitrile nanofiber mats for heavy metal ion removal. *ACS Appl. Mater. Interfaces* **2,** 3619–3627 (2010).

15. Wang, M. X., Huang, Z. H., Shimohara, T., Kang, F. & Liang, K. NO removal by electrospun porous carbon nanofibers at room temperature. *Chem. Eng. J.* **170,** 505–511 (2011).

16. Chronakis, I. S. Novel nanocomposites and nanoceramics based on polymer nanofibers using electrospinning process - A review. *J. Mater. Process. Technol.* **167,** 283–293 (2005).

17. Mack, J. J. *et al.* Graphite nanoplatelet reinforcement of electrospun polyacrylonitrile nanofibers. *Adv. Mater.* **17,** 77–80 (2005).

18. Kim, C. *et al.* Self-sustained thin Webs consisting of porous carbon nanofibers for supercapacitors via the electrospinning of polyacrylonitrile solutions containing zinc chloride. *Adv. Mater.* **19,** 2341–2346 (2007).

19. Ra, E. J., Raymundo-Piñero, E., Lee, Y. H. & Béguin, F. High power supercapacitors using polyacrylonitrile-based carbon nanofiber paper. *Carbon N. Y.* **47,** 2984–2992 (2009).

20. Zewe, J. W., Steach, J. K. & Olesik, S. V. Electrospun Fibers for Solid-Phase Microextraction. *Anal. Chem.* **82,** 5341–5348 (2010).

21. Bagheri, H., Akbarinejad, A. & Aghakhani, A. A highly thermal-resistant electrospun-based polyetherimide nanofibers coating for solid-phase microextraction. *Anal. Bioanal. Chem.* **406,** 2141–2149 (2013).

22. Bagheri, H. & Aghakhani, A. Novel nanofiber coatings prepared by electrospinning technique for headspace solid-phase microextraction of chlorobenzenes from environmental samples. *Anal. Methods* **3,** 1284–1289 (2011).

23. Pham, Q. P., Sharma, U. & Mikos, A. G. Electrospinning of Polymeric Nanofibers for Tissue Engineering Applications: A Review. *Tissue Eng.* **0,** 60509065116001 (2006).

24. Sill, T. J. & von Recum, H. A. Electrospinning: Applications in drug delivery and tissue engineering. *Biomaterials* **29,** 1989–2006 (2008).

25. Onozuka, K. *et al.* Electrospinning processed nanofibrous TiO2 membranes for photovoltaic applications. *Nanotechnology* **17,** 1026–1031 (2006).

26. Peining, Z., Nair, A. S., Shengjie, P., Shengyuan, Y. & Ramakrishna, S. Facile Fabrication of TiO2 − Graphene Composite with Enhanced Photovoltaic and Photocatalytic Properties by Electrospinning. *Appl. Mater. Interfaces* **4,** 581–585 (2012).

27. Nicholson, R. S. Theory and Application of Cyclic Voltammetry for Measurement of Electrode Reaction Kinetics. *Anal. Chem.* **37,** 1351–1355 (1965).

28. Tripatanasuwan, S., Zhong, Z. & Reneker, D. H. Effect of evaporation and solidification of the charged jet in electrospinning of poly(ethylene oxide) aqueous solution. *Polymer (Guildf).* **48,** 5742–5746 (2007).

29. Groenzin, H. & Mullins, O. C. Petroleum asphaltene molecular size and structure. *ACS Div. Fuel Chem. Prepr.* **44,** 728–732 (1999).

30. Gray, M. R., Tykwinski, R. R., Stryker, J. M. & Tan, X. Supramolecular assembly model for aggregation of petroleum asphaltenes. *Energy and Fuels* **25,** 3125–3134 (2011).

31. Zhang, W. X., Wang, Y. Z. & Sun, C. F. Characterization on oxidative stabilization of polyacrylonitrile nanofibers prepared by electrospinning. *J. Polym. Res.* **14,** 467–474 (2007).

32. Wu, M., Wang, Q., Li, K., Wu, Y. & Liu, H. Optimization of stabilization conditions for electrospun polyacrylonitrile nanofibers. *Polym. Degrad. Stab.* **97,** 1511–1519 (2012).

33. Knight, D. S. & White, W. B. Characterization of diamond films by Raman spectroscopy. *J. Mater. Res.* **4,** 385–393 (1989).

34. Bashir, Z. A critical review of the stabilisation of polyacrylonitrile. *Carbon N. Y.* **29,** 1081–1090 (1991).

35. Conley, R. T. & Bieron, J. F. Examination of the oxidative degradation of polyacrylonitrile using infrared spectroscopy. *J. Appl. Polym. Sci.* **7,** 1757–1773 (1963).

36. Fochler, H. S., Mooney, J. R., Ball, L. E., Boyer, R. D. & Grasselli, J. G. Infrared and NMR spectroscopic studies of the thermal degradation of polyacrylonitrile. *Spectrochim. Acta Part A Mol. Spectrosc.* **41,** 271–278 (1985).

37. McFadden, C. F., Russell, L. L., Melaragno, P. R. & Davis, J. A. Low-Temperature Pyrolytic Carbon Films: Electrochemical Performance and Surface Morphology as a Function of Pyrolysis Time, Temperature, and Substrate. *Anal. Chem.* **64,** 1521–1527 (1992).

38. Singh, A., Jayaram, J., Madou, M. & Akbar, S. Pyrolysis of Negative Photoresists to Fabricate Carbon Structures for Microelectromechanical Systems and Electrochemical Applications. *J. Electrochem. Soc.* **149,** E78 (2002).

39. Beilby, A. L. & Carlsson, A. A pyrolytic carbon film electrode for voltammetry. *J. Electroanal. Chem. Interfacial Electrochem.* **248,** 283–304 (1988).

Chapter 4

Electrospinning of Asphaltene Composite Fibres

4.1 Introduction

Electrospinning of asphaltene fibres have been successfully demonstrated. However, the electrospinning process is not ideal. Asphaltenes have a low molecular weight, so a high concentration is required to form smooth fibres. This high concentration results in a viscous solution that is prone to clogging during electrospinning. Furthermore, toluene is one of few solvents that can dissolve asphaltenes in such a high concentration. The volatility of toluene further complicates the clogging issue during electrospinning. To overcome these issues, a lower concentration of asphaltenes must be used.

One method of improving various aspects of electrospun fibres is by the addition of a polymer additive. The presence of an additive can change properties such as fibre integrity, fibre size, thermal stability, and mechanical strength. For example, carbon nanotubes have been used as a filler material during electrospinning to improve different properties of composite nanofibres. Ge *et al.* electrospun composite MWCNT/polyacrylonitrile nanofibres, which showed improved thermal, electrical, and mechanical properties.[1] Sen *et al.* used SWCNTs to electrospin polyurethane composite nanofibres, which showed over 100% enhancement in tensile strength compared to pure electrospin polyurethane.[2] Other materials used as additives include graphene,[3,4] Ag/Au nanoparticles,[5,6] Nylon,[7] polyethylene oxide,[8] among others. Additives such as polyethylene oxide are high molecular weight polymers. These high molecular weight polymers are used to increase intermolecular interactions to improve the quality of electrospinning.

The electrospinning of asphaltenes can be improved by the addition of a small amount of high molecular weight polymers. This chapter will explore the formation of asphaltene

composite nanofibres with polyethylene oxide (PEO), polyvinylpyrrolidone (PVP), and polyacrylonitrile (PAN). These polymers range from 150 kDa to 1,300 kDa, compared to ~500-1000 Daltons for asphaltenes. By acting as a binder, less asphaltenes will be required for electrospinning.

4.2 Experimental

4.2.1 Materials

Polyethylene oxide (2000 kDa and 5000 kDa), polyvinylpyrrolidone (1300 kDa), and polyacrylonitrile (150 kDa) were purchased from Sigma-Aldrich. Pentane-precipitated asphaltenes from Athabasca, Alberta were used. Asphaltenes were washed and filtered with pentane until the solvent only had a light colour. For solution preparation, toluene (99.9%, Sigma-Aldrich) and N,N-dimethylformamide (99.8%, Sigma-Aldrich) were used.

For SPME experiments using electrospun fibres, solutions of naphthalene (99%, Sigma-Aldrich), biphenyl (≥99%, Sigma-Aldrich), pyrene (98%, Sigma-Aldrich), and anthracene (97%, Sigma-Aldrich) were made using acetonitrile (≥99.9%, Sigma-Aldrich) and 18.2 megaohm-cm deionized water. The stainless-steel wire (0.010 inch) was purchased from Malin Co.. SPME experiments were performed using 20 mL crimp top vials with a PTFE/butyl rubber tin plate seal (Chromatographic Specialities Inc.).

4.2.2 Electrospinning

Electrospinning was performed using a KD Scientific syringe pump, a high voltage power supply (Gamma High Voltage Research), 1 mL plastic Luer-Lok syringe (Becton Dickinson), 20-

gauge stainless steel needle with flattened tip, and aluminum foil on a metal plate as the collector. For SPME experiments, a stainless-steel wire was used as the collector instead.

4.2.3 Thermal stabilization and carbonization

All thermal treatment was performed using a Lindberg three-zone tube furnace, with samples in a quartz boat. For thermal stabilization, heat treatment was done in ambient atmosphere, with no additional gas supply. For carbonization, the tube furnace was connected by gas line to forming gas (95% Ar, 5% H_2).

4.2.4 Scanning electron microscopy

Samples were imaged using a JEOL instrument with a secondary electron detector. Fibre widths were measured using ImageJ from SEM images.

4.2.5 Raman spectroscopy

Raman spectroscopy for carbonized fibres were analyzed using a Renishaw Raman microscope system with a 785 nm laser. Spectra was obtained using the 50x objective lens with 5 seconds of exposure and 10 accumulations. Spectra analysis and peak fitting was done using OriginPro.

4.2.6 Head-space SPME detection of polycyclic aromatic hydrocarbons

Stock 2 g/L solutions of naphthalene, biphenyl, pyrene, and anthracene were prepared in acetonitrile. Nanopure 18.2 megaohm-cm deionized water was used to dilute stock solutions to a 1 mg/L mixture of all four PAHs.

A ~15 cm 0.010 inch stainless wire was inserted into a metal sheath from a Supelco SPME fibre. Approximately 1.7 cm of the stainless wire was exposed and the end of the wire was attached to the negative terminal of the power supply using an alligator clip. To prepare polymer solutions for electrospinning, solutions of PAN and/or asphaltene was dissolved in DMF and left to heat (80 ^{o}C) with magnetic stirring overnight. Using an 1 mL plastic Luer-Lok syringe (Becton Dickinson) and a 20-gauge stainless steel needle with flattened tip, the polymer solution was electrospun onto the exposed stainless wire for 30 seconds at 15 kV, 15 cm (distance from needle to wire), and 2 μL/min. After electrospinning, the coated-stainless wire was conditioned in ambient atmosphere at 250 ^{o}C for 20 minutes.

Head-space SPME was done by adding 5 mL of the 1 mg/L PAH mixture in a 20 mL crimp top vials with a PTFE/butyl rubber tin plate seal. The solution was maintained at 60 ^{o}C with magnetic stirring during head-space sampling for 15 min. After extract, the SPME wire was immediately inserted into the GC instrument for desorption. The GC column was a fused silica capillary column (Supelco SLB-5ms) with dimensions of 30 m x 0.25 mm x 0.25 μm film thickness. Thermal desorption was performed for 3 minutes at 250 ^{o}C. After desorption, temperature of the column was increased from 50 ^{o}C to 240 ^{o}C at 10 ^{o}C/min and then maintained at 240 ^{o}C for 10 minutes. Detection of eluted analytes was done using an FID.

4.3 Results and discussion

4.3.1 Polyethylene oxide/Asphaltene composite fibres

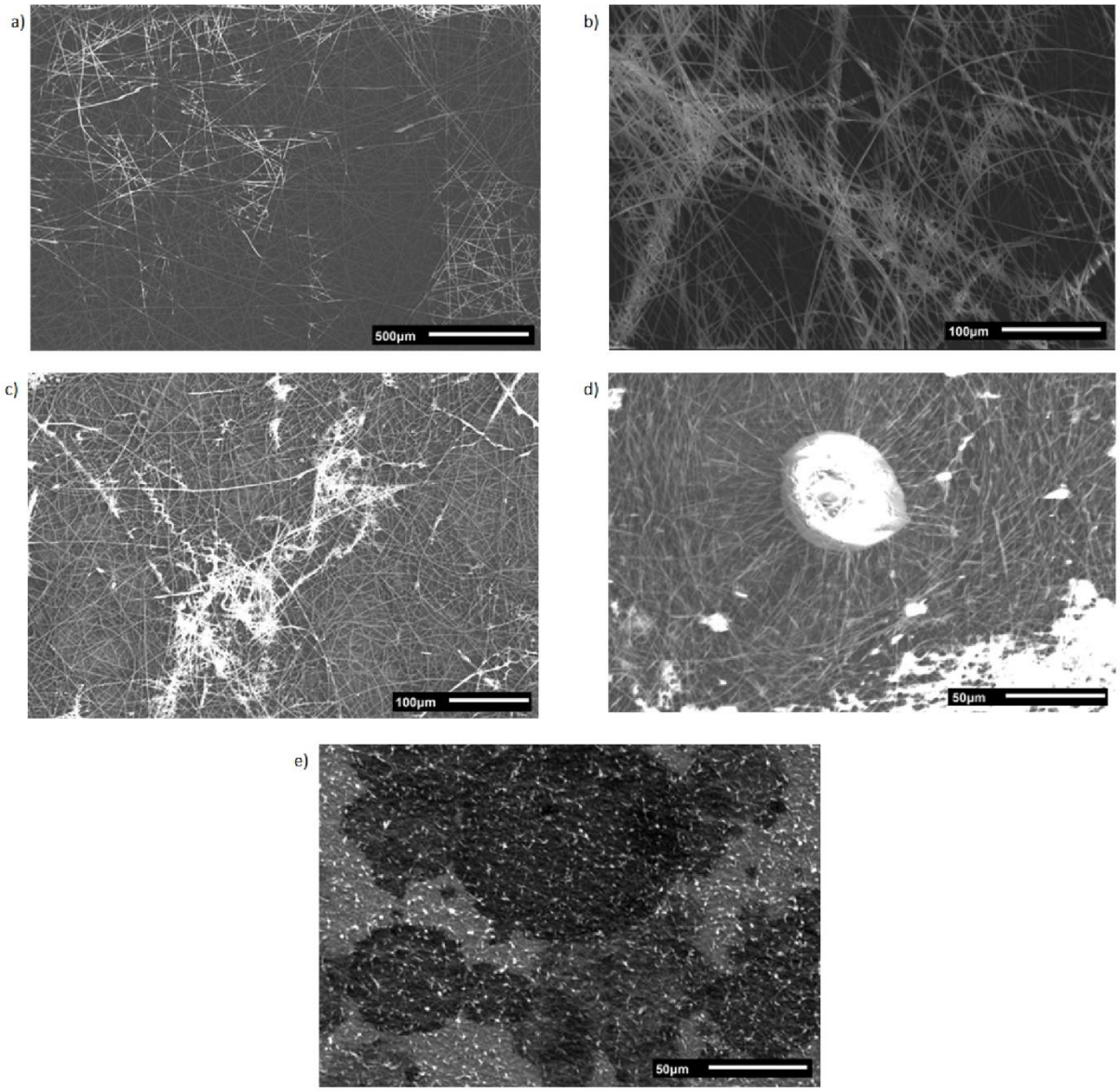

Figure 4.1 Electrospun fibres from 1% (w/w) PEO in toluene/DMF (50%/50%) and a) 30% asphaltene (w/w) b) 20% asphaltene (w/w) c) 15% asphaltene (w/w) d) 10% asphaltene (w/w) e) 0% asphaltene.

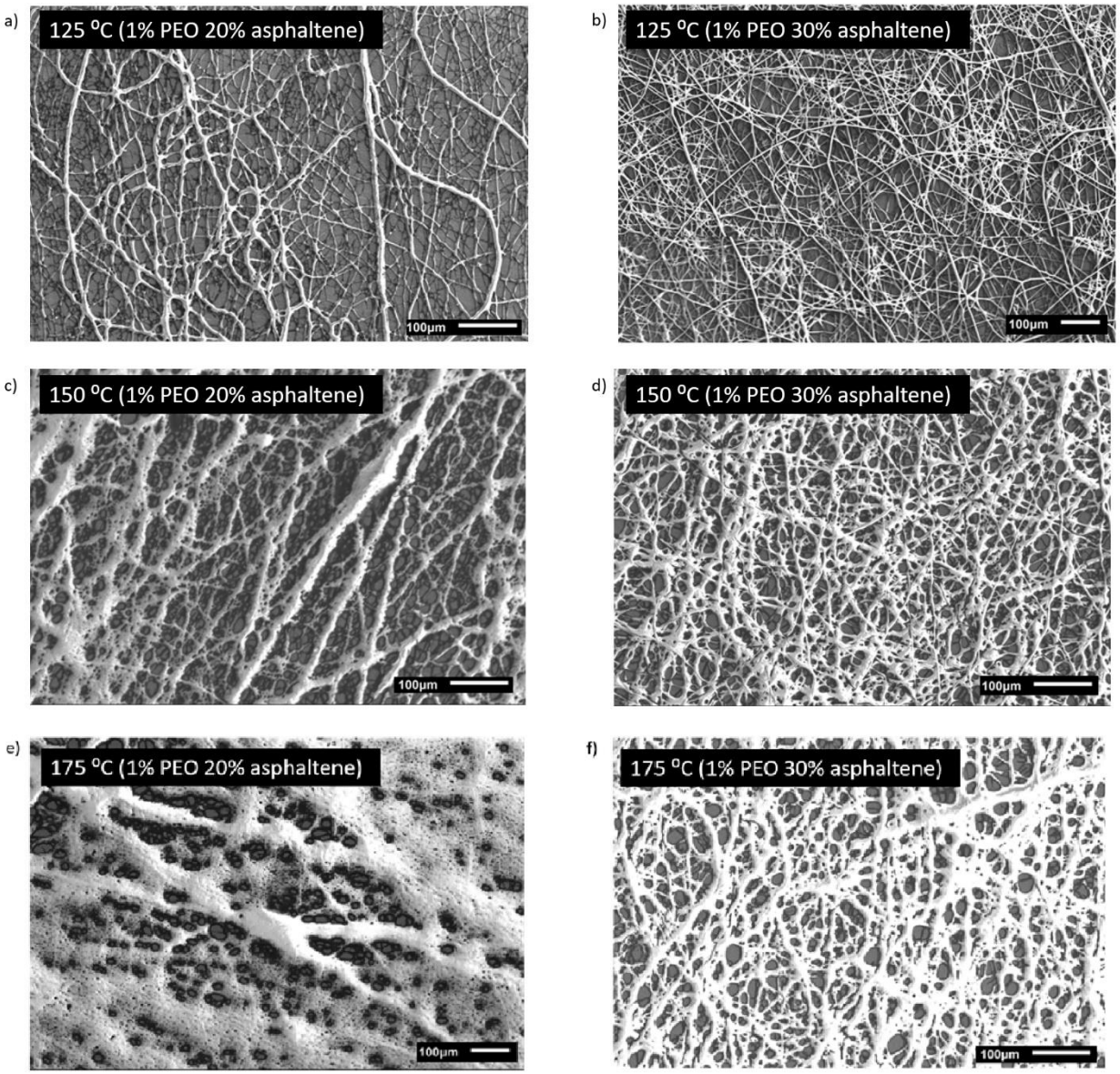

Figure 4.2 SEM images after thermal stabilization of PEO/asphaltene composite fibres.

Two polyethylene oxide (PEO) polymers with molecular weights of 2000 and 5000 kDa were used. A 1% (w/w) 2000 kDa PEO and 40% (w/w) asphaltene solution was made in toluene. The solution was left to heat with magnetic stirring overnight, but the resulting solution was viscous and inhomogeneous. The addition of PEO altered interfacial interactions between the solute and toluene. A 30% (w/w) asphaltene solution was also made with 1% (w/w) 2000 and 5000 kDa PEO, but the same phenomenon occurred. Toluene is not a suitable solvent for PEO and asphaltenes.

To increase the solubility of a PEO/asphaltene mixture, a toluene/DMF (50%/50%) solution was used. A 1% (w/w) 2000 kDa PEO solution was added to 30%, 20%, 15%, 10%, and 0% (w/w) asphaltenes and was left to heat with magnetic stirring overnight. All solutions were dissolved and homogeneous. Solutions were electrospun at 10 kV, 15 cm (distance from syringe to collector), and 5 μL/min. Figure 4.1 shows the SEM images of electrospun PEO/asphaltene composite fibres. A 1% (w/w) PEO solution with no asphaltenes could not be electrospun into smooth fibres. The SEM image shows large, interconnected beads, suggesting that 1% PEO does not have sufficient intermolecular interactions to form fibres. At 10% and 15% (w/w) asphaltenes, electrospun fibres were mostly smooth, with a small number of beads. The presence of beads could also indicate incomplete solvent evaporation. At low asphaltene concentrations, there is a higher fraction of solvent, which can lead to this effect. With higher asphaltene concentrations (20% and 30%), electrospun fibres are smooth, showing no irregularities or beads. Electrospinning was also tried with 5000 kDa PEO. Solutions with 0.5-1% 5000 kDa PEO were dissolved with 20-30% asphaltenes in a toluene/DMF mixture. However,

the polymer was not homogeneously dissolved in solution in all cases. The 5000 kDa PEO and asphaltenes precipitated out of solution and were not able to be electrospun.

The diameter for 2000 kDa PEO/asphaltene composite fibres are listed in Table 4.1. The fibre diameters range from 0.4±0.1 μm to 2.3±0.4 μm as the asphaltene concentration increases from 10% to 30%. This is expected as an increase in polymer concentration will lead to larger electrospun fibres. From the previous chapter, pure electrospun asphaltene fibres have diameters in the range of 10 μm. By adding a small amount of PEO and decreasing the asphaltene concentration, nano-sized fibres were able to be formed.

Electrospun fibres from 1% 2000 kDa PEO/20-30% asphaltene (w/w) solutions were heat treated to test their thermal stability. Figure 4.2 shows the result after heat treatment at 125 ^{o}C, 150 ^{o}C, and 175 ^{o}C in air for one hour. After heat treatment at 125 ^{o}C, fibres from the 20% asphaltene sample still maintain most of their morphology, but the fibre junctions are all interconnected due to thermal decomposition. For the 30% sample, there is little or no change to fibre shape or morphology. The 30% asphaltene sample is more thermally stable than 20% because asphaltenes are stable up to approximately 300-350 ^{o}C, and fibres from the 30% sample have a higher fraction of asphaltenes. However, after heat treatment at 150 ^{o}C and 175 ^{o}C, fibres from both of the 20% and 30% samples are mostly decomposed with a large degree of melting. These results suggest that PEO/asphaltene composite fibres are not thermally stable above 100 ^{o}C, but the stability can be slightly improved by increasing the amount of asphaltenes. Thermal stabilization was also conducted in forming gas (95% Ar 5% H_2). Figure 4.3 shows the comparison of thermal stabilization at 175 ^{o}C in air and in forming gas. In both cases,

thermal degradation is present. A reducing atmosphere does not seem to help with maintaining fibre morphology.

	30% asphaltene	20% asphaltene	15% asphaltene	10% asphaltene
Fibre diameter (μm) (n=20)	2.3±0.4	1.7±0.4	0.8±0.3	0.4±0.1

Table 4.1 Fibre diameter for 1% 2000kDa PEO/asphaltene composite fibres.

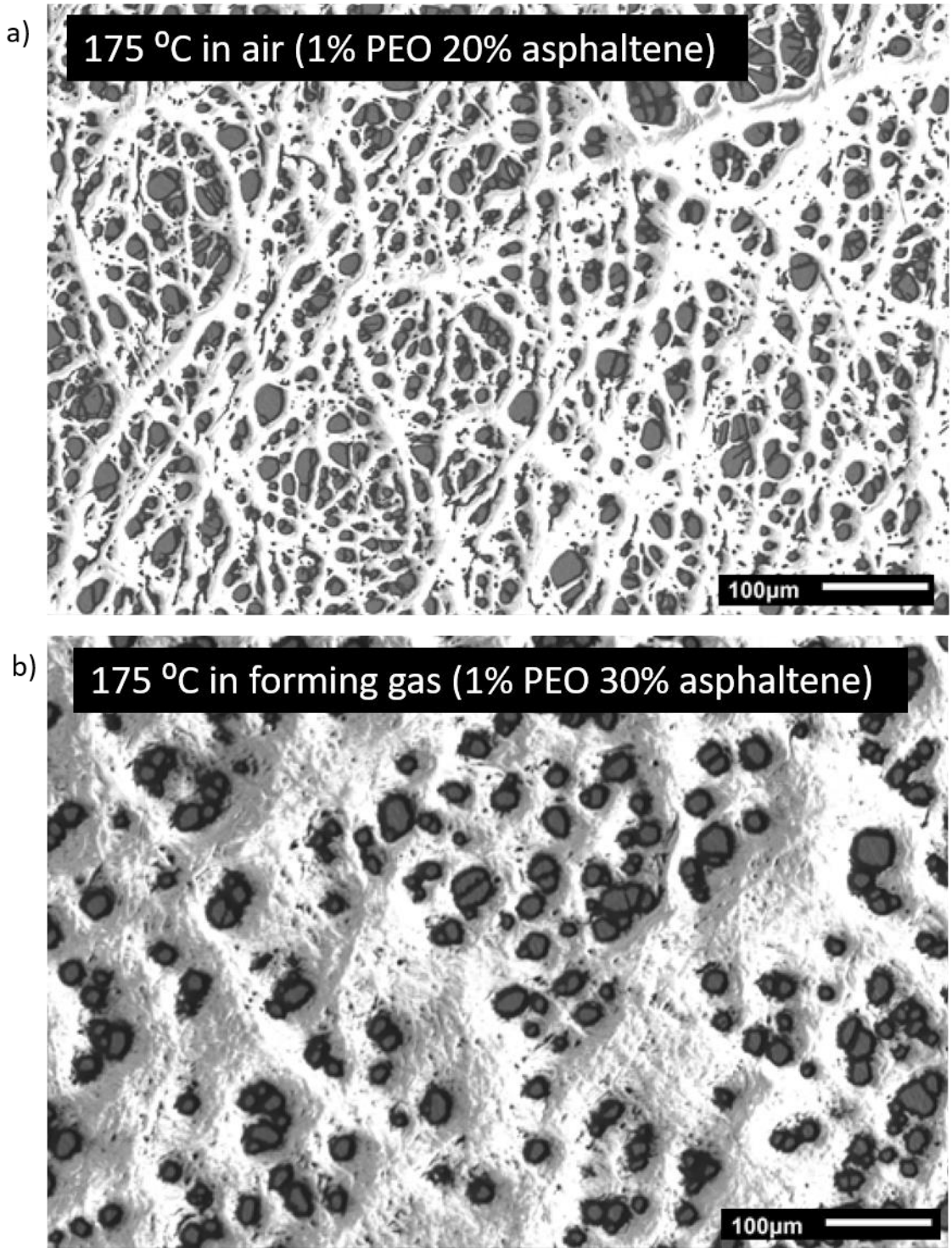

Figure 4.3 Thermal stabilization of PEO/asphaltene composite fibre in a) air b) forming gas.

4.3.2 Polyvinylpyrrolidone/asphaltene composite fibres

Polyvinylpyrrolidone (PVP) electrospun fibres are widely used for biomedicine applications because of their water solubility. There have been examples of electrospun PVP fibre mats being loaded with drugs such as ibuprofen to form oral fast-dissolving membranes for drug delivery.[9,10] Composite PVP electrospun fibres have been demonstrated with carbon nanotubes,[11] silica nanoparticles,[12] hydroxyapatite.[13] Pure electrospun PVP fibres have also been carbonized into carbon nanofibres at 800 ^{o}C after ambient stabilization.[14] The electrospinnabiilty of composite PVP and asphaltene solutions will be explored in this section.

A 10% (w/w) asphaltene solution with 15-20% (w/w) PVP was made in N,N-dimethylformamide (DMF). After heating overnight with magnetic stirring, the solution was not completely homogeneous. However, electrospinning was attempted using the polymer solution at 10 kV, 15 cm, 10 μL/min. Figure 4.4 shows the SEM images of the electrospun material. For both solutions, even though there is the formation of smooth fibres, there are also many large clusters of material. This is likely due to electrospraying. The solution of PVP and asphaltenes is not homogeneous, because asphaltenes are not as soluble in DMF compared to toluene. During electrospinning, PVP is well dissolved and can be successfully spun into fibres. However, at the same time, undissolved asphaltenes will be electrosprayed onto the collector as large droplets of material. To improve the solubility of the polymer mixture, 20% (w/w) PVP was dissolved with only 2% (w/w) asphaltene in DMF and was electrospun under the same conditions. Nanofibres were successfully formed during electrospinning, but similar to before, asphaltenes were not very dissolved and formed large beads. These results show that by using only DMF as

solvent, only a very small amount of asphaltenes can be added to PVP. Even at 2% asphaltenes, DMF cannot fully solvate the PVP/asphaltene mixture.

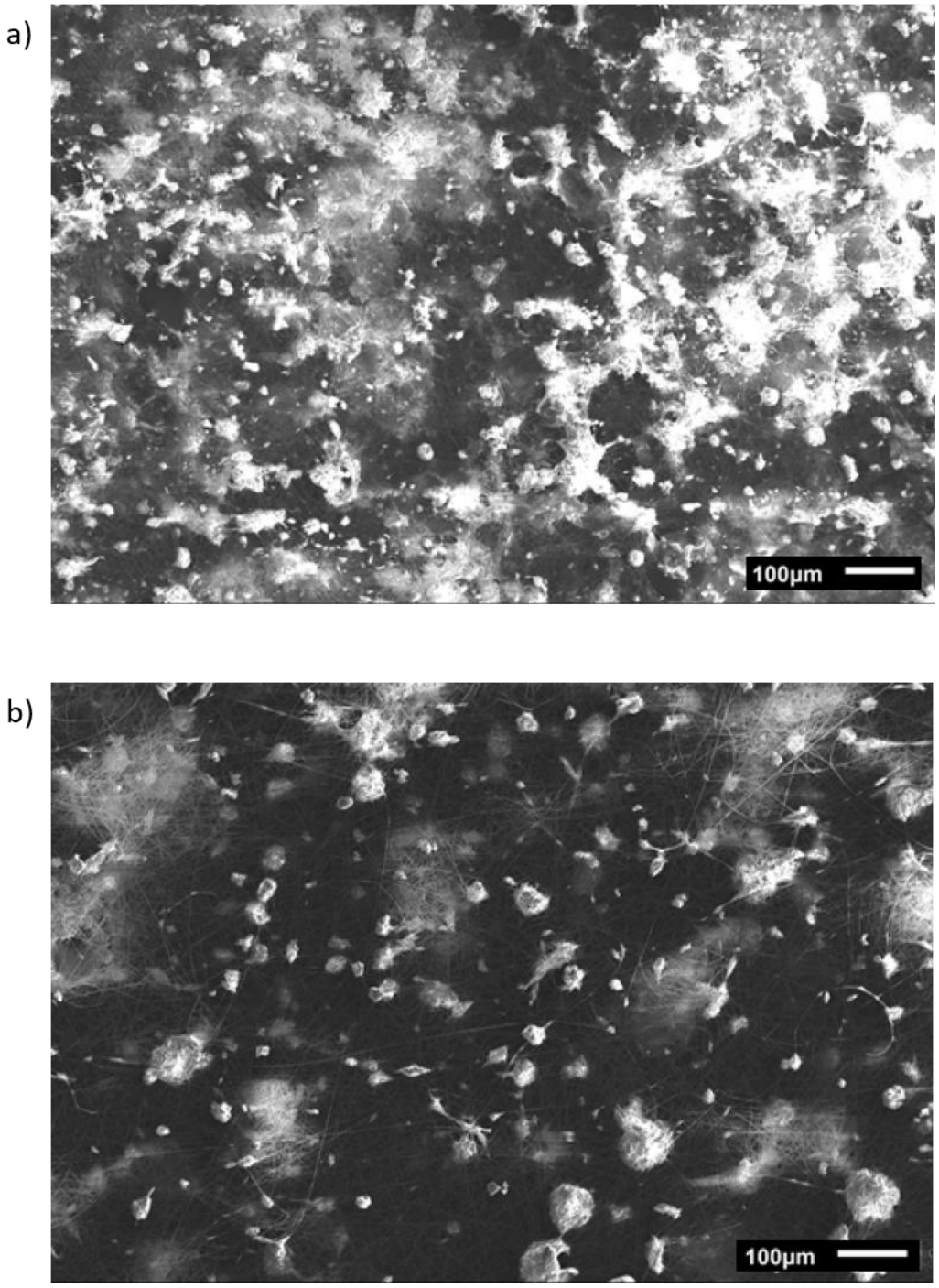

Figure 4.4 Electrospun material from PVP and asphaltene solution in DMF a) 15% PVP, 10% asphaltene b) 20% PVP, 10% asphaltene.

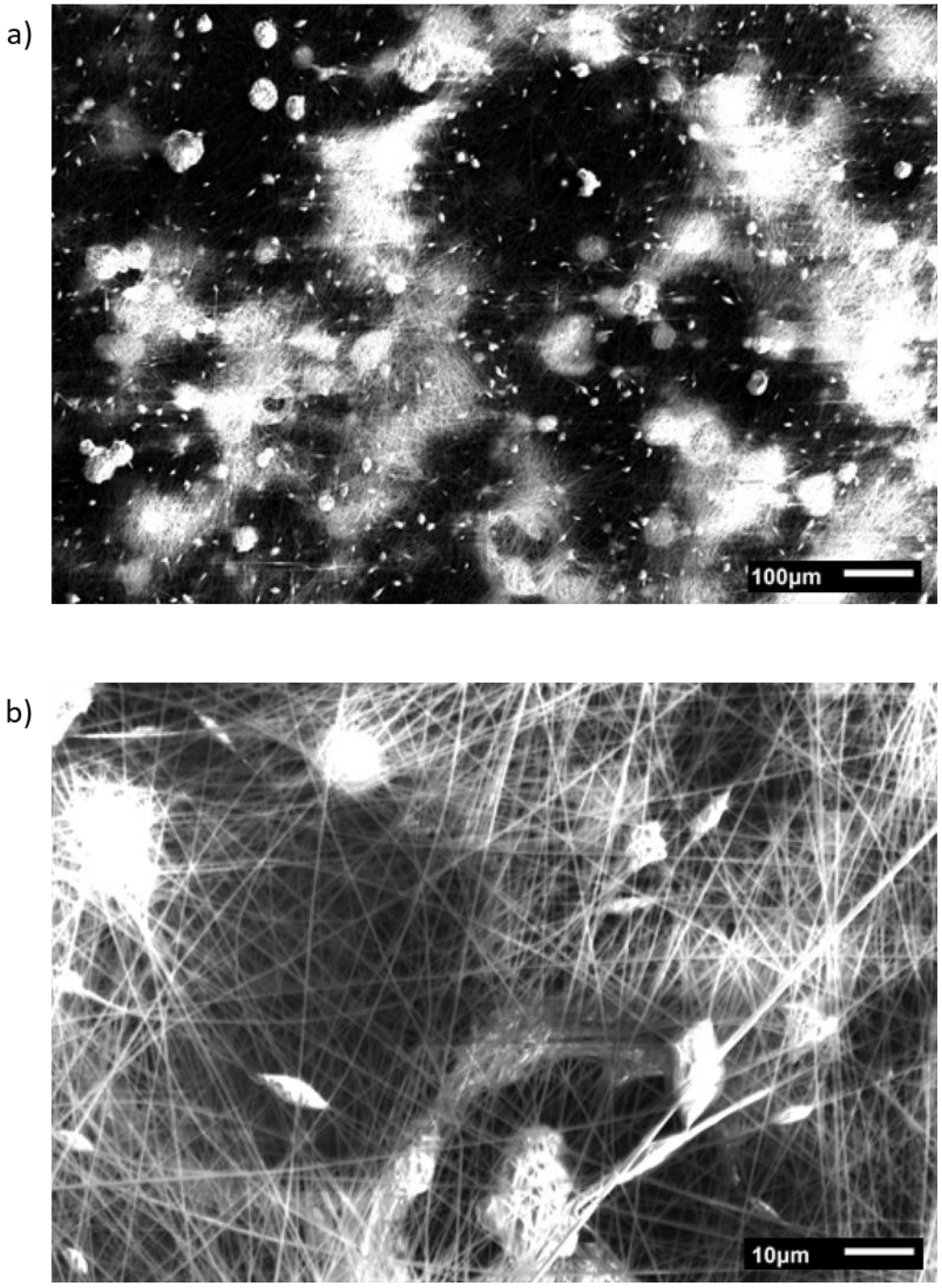

Figure 4.5 Electrospun materials from 20% PVP, 2% asphaltene in DMF a) 100x magnification b) 1000x magnification.

Instead of DMF, a 2:1 ratio of DMF to toluene was used to dissolve 15% (w/w) PVP with 5% (w/w), 10% (w/w), and 15% (w/w) asphaltenes. After heating overnight with magnetic stirring, the solutions were well dissolved with no phase separation. The polymer solutions were electrospun at 10 kV, 15 cm, 10 μL/min and imaged with SEM. The electrospun nanofibres under 3000 times magnification are shown in Figure 4.6. Contrary to earlier, the nanofibres spun from a DMF/toluene mixed solvent show smooth fibres with no beads or clusters of solid material. This is because the DMF/toluene mixed solvent can fully dissolve both PVP and asphaltenes. At 5% asphaltenes, the composite fibres are the smallest, with the fibre diameter at 0.5±0.1 μm (Table 4.2). At 10% and 15% asphaltenes, the fibre diameters increase slightly to approximately 0.7-0.8 μm, though the difference in diameter between all samples are small enough to be within margins of error. There is no significant difference in size between electrospun PVP fibres with 5%, 10%, and 15% asphaltenes. Appearance-wise, the fibre mat from 5% asphaltenes is light in colour whereas fibre mats from 10% and 15% asphaltenes are both darker brown, indicating a higher amount of asphaltenes. However, there is no significant difference in colour or fibre size between 10% and 15% asphaltenes, suggesting that the solution is being saturated with asphaltenes around 15%; any more than that, the extra asphaltenes will begin to precipitate.

The thermal stability of PVP/asphaltene composite fibres were first examined similarly to PEO/asphaltene composite fibres. Fibres that are shown in Figure 4.6 were heat treated at 150 ^{o}C and 200 ^{o}C in air for one hour (0.5 ^{o}C/min). Contrary to PEO/asphaltene composite fibres, the PVP/asphaltene fibres are thermally stable at these temperatures. There is no change in physical appearance, nor fibre morphology under SEM. Figure 4.7 shows the SEM

images after heat treatment at 200 ^{o}C (150 ^{o}C is not shown because there is no difference). After heat treatment, the fibres maintain their round morphology, their diameter, and there appears to be no melting or crosslinking of fibre junctions. After heat treatment in air, PVP/asphaltene composite fibres were carbonized at 800 ^{o}C in forming gas (95% Ar/5% H_2). However, the electrospun fibres were completely decomposed. The carbonized product was a graphitized film instead of individual fibres. The decomposition of fibres is the result of insufficient stabilization. Oxidative stabilization is a critical step to preserve fibre morphology at higher temperatures. Wang *et al*. carbonized electrospun PVP fibres by using a two-step stabilization process.[14] The fibres were first stabilized at 150 ^{o}C in air for 24 hours, followed by another stabilization step above 300 ^{o}C for 4 hours. Similar to Wang *et al.*, composite PVP/asphaltene fibres were stabilized at 150 ^{o}C (0.5 ^{o}C/min) in air for 24 hours, then at 350 ^{o}C (0.5 ^{o}C/min) in air for 4 hours, and finally carbonized at 800 ^{o}C (5 ^{o}C/min) in forming gas (95% Ar/5% H_2) for 1 hour. The carbonized fibres are shown in Figure 4.8. The composite fibres were successfully transformed into carbon fibres. Carbonized fibres maintain excellent morphology, with no breaks or cracks among fibres. The carbonization process is confirmed by Raman spectroscopy shown in Figure 4.9. There are two diagnostic peaks, at 1320 cm^{-1} and 1580 cm^{-1}, which are the D and G bands, respectively. The D band originates from defects in the graphite crystalline structure and the G band is the Raman-allowed in-plane vibration. The presence of these two characteristic Raman bands indicate microcrystalline graphite. There is also a small peak on the shoulder of the D band, around 1160-1170 cm^{-1}. This feature has been seen in the Raman spectra of diamond-like carbon films, suggestive of sp^3 carbon vibrations.[15,16] The Raman spectra for carbonized fibres from 0-15% asphaltene precursor samples are near

identical, as seen in Figure 4.9. The ratio of intensities of the D and G bands can be used to estimate L_A, the size of the graphite crystal parallel to the plane of the graphite.[17] However, there is no significant change in the ratio of intensities nor peak positions. The amount of asphaltenes added to PVP does not affect the degree of carbonization or the molecular structure. This is not surprising since the degree of graphitization and the crystallinity mostly depends on the temperature during pyrolysis.

After carbonization, the fibre diameters are reduced by up to 60%. Table 4.3 shows the change in fibre diameter, including electrospun PVP fibres (15% (w/w)) without any asphaltenes. The sizes of carbonized fibres for all samples are quite similar, between ~0.25 and ~0.4 μm in diameter. However, it is more interesting to look at the percent decrease in fibre diameter. For electrospun PVP fibres with no asphaltene, there was a 60±15% decrease in fibre diameter after carbonization. As the amount of asphaltenes increase from 5% to 15%, the percent decrease in fibre diameter also decreases from 50±17% and 41±14%. This suggests that as the amount of asphaltenes in the composite fibre increases, there is less change in fibre size after carbonization. However, the uncertainty in fibre diameter and the % decrease are both considerable. The relative uncertainty in % decrease ranges from 25 to 50%. Even though the average value of the % decrease of fibre diameter suggests the carbon yield is increasing as the amount of asphaltene increases, more investigation is needed due to the high uncertainty.

	15% PVP 15% asphaltene	15% PVP 10% asphaltene	15% PVP 5% asphaltene
Fibre diameter (μm) (n=20)	0.70±0.12	0.8±0.3	0.50±0.13

Table 4.2 Fibre diameter for composite PVP/asphaltene fibres.

	15% PVP 15% asphaltene	15% PVP 10% asphaltene	15% PVP 5% asphaltene	15% PVP 0% asphaltene
Fibre diameter after carbonization (μm) (n=20)	0.41±0.07	0.43±0.10	0.25±0.06	0.35±0.09
Percent decrease in fibre diameter	41±14%	44±27%	50±17%	60±15%

Table 4.3 Change in diameter after carbonization for composite PVP/asphaltene fibres.

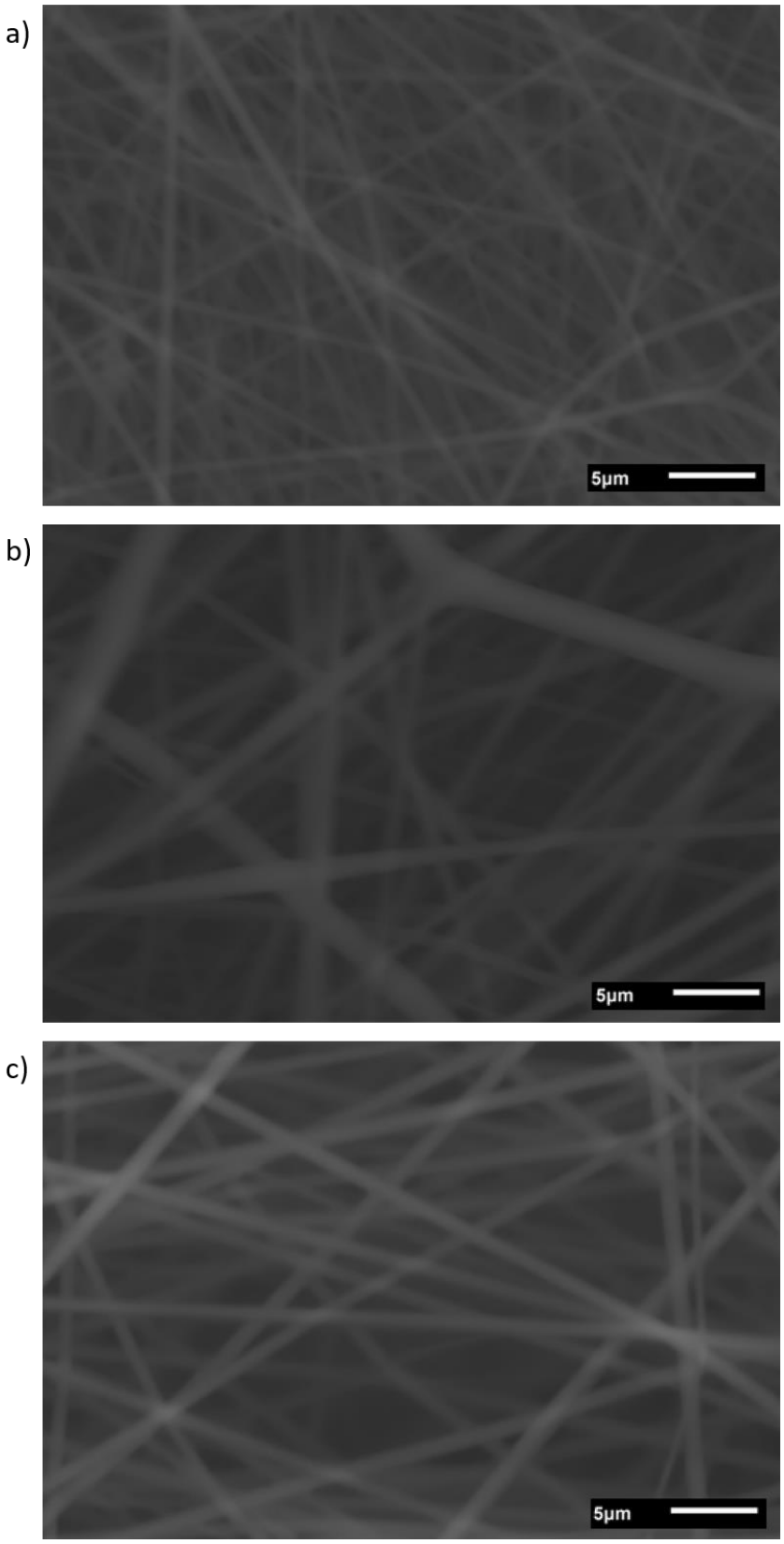

Figure 4.6 Electrospun composite fibres with 15% PVP and a) 5% asphaltene b) 10% asphaltene c) 15% asphaltene.

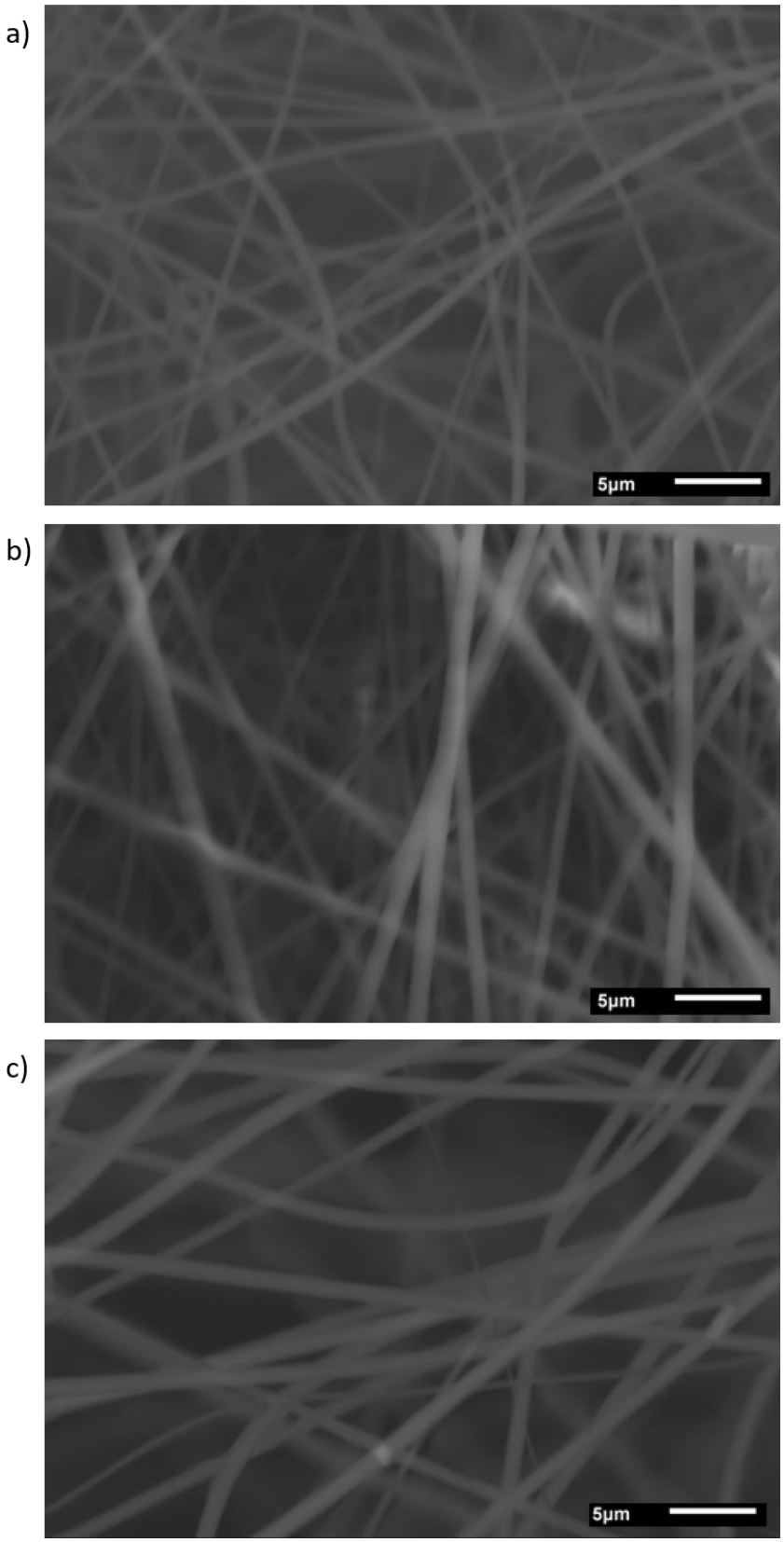

Figure 4.7 Electrospun composite fibres after heat treatment at 200 ^{o}C in air with 15% PVP and a) 5% asphaltene b) 10% asphaltene c) 15% asphaltene.

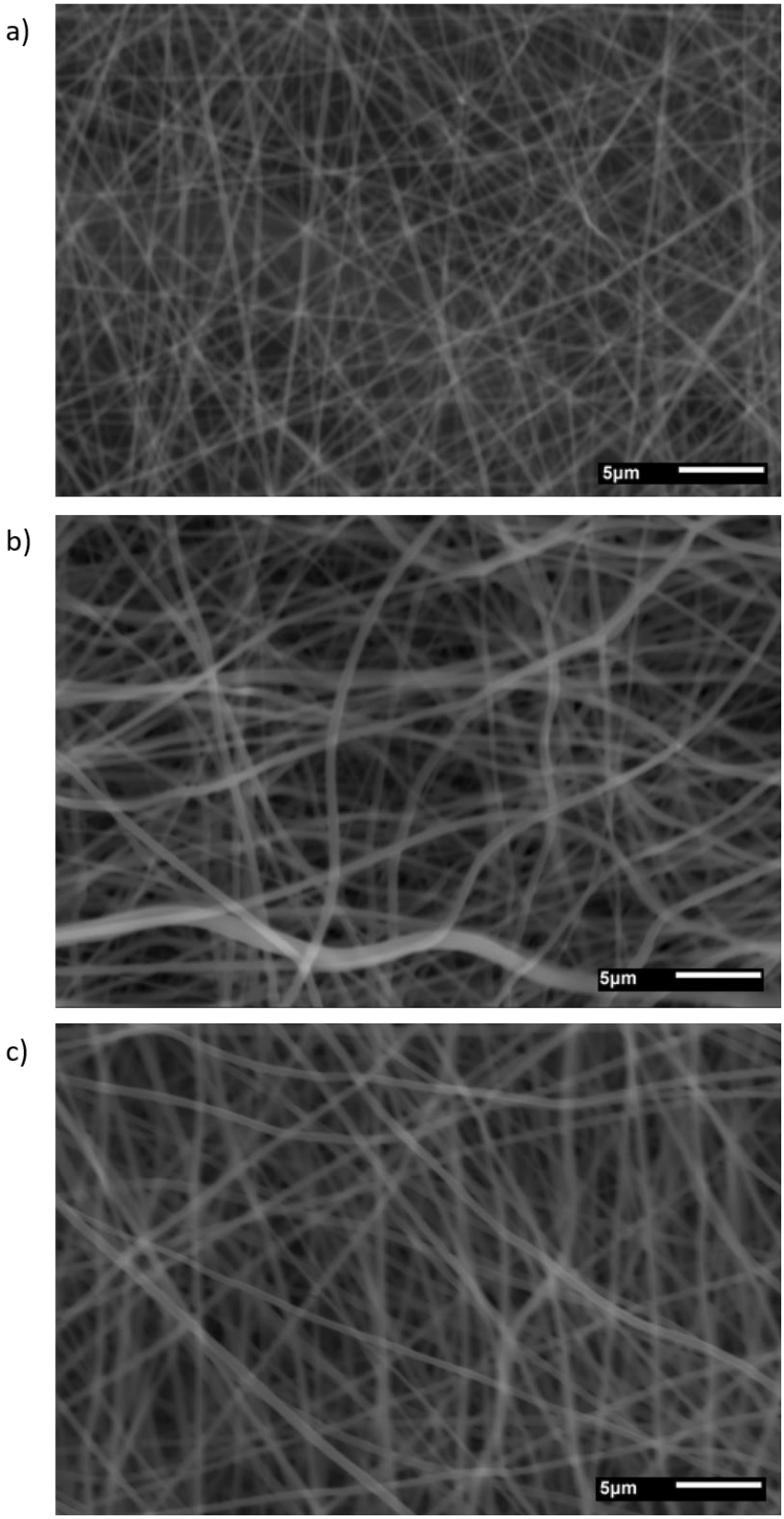

Figure 4.8 Electrospun composite fibres carbonized at 800 ^{o}C with 15% PVP and a) 5% asphaltene b) 10% asphaltene c) 15% asphaltene.

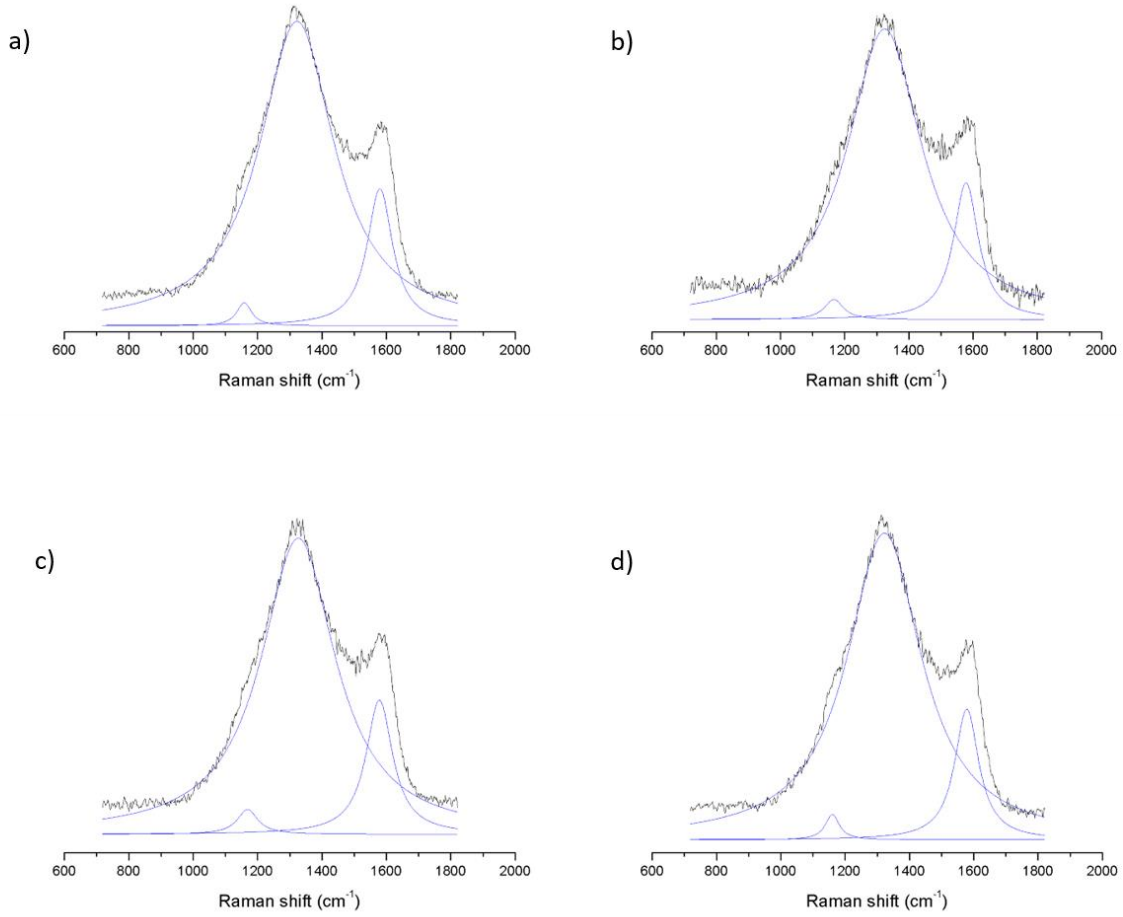

Figure 4.9 Raman spectroscopy for carbonized PVP/asphaltene fibres. a) 15% PVP b) 15% PVP + 5% asphaltene c) 15% PVP + 10% asphaltene d) 15% PVP + 15% asphaltene.

To see the effect of asphaltenes on carbon yield, it is best to compare the percent decrease in fibre diameter for electrospun PVP fibres with and without asphaltenes. Solutions of 10% PVP and 12.5% PVP with 0% and 10% asphaltenes were electrospun and carbonized under the same conditions as previously mentioned. Table 4.4 lists the fibre diameters, with also data for 15% PVP included. For 10%, 12.5%, and 15% PVP, the percent decrease in fibre diameter is smaller for fibres with asphaltenes than without. Again, this suggests that asphaltenes can increase the carbon yield during carbonization compared to PVP. However, due to the wide distribution of fibre diameters, the percent decrease includes large uncertainties. For example, for 10% PVP, the percent decrease in fibre diameter is 30±30% and 50±20% for with and without asphaltenes, respectively. To determine if the differences in percent decrease are significant, a *t*-test is required. For all three concentrations of PVP, the differences in percent decrease for fibres with and without asphaltenes are all significant at $\alpha = 0.1$. At $\alpha = 0.01$, the differences in percent decrease are significant for 10% and 12.5% PVP fibres. This is strong evidence that asphaltenes can have a significant effect on carbon yield after carbonization.

	10% PVP 0% asphaltene	10% PVP 10% asphaltene	12.5% PVP 0% asphaltene	12.5% PVP 10% asphaltene	15% PVP 0% asphaltene	15% PVP 10% asphaltene
Fibre diameter before carbonization (μm) (n=20)	0.7±0.2	0.63±0.17	0.9±0.2	0.93±0.13	0.9±0.2	0.8±0.3
Fibre diameter after carbonization (μm) (n=20)	0.35±0.08	0.45±0.12	0.20±0.04	0.38±0.08	0.35±0.09	0.43±0.10
Percent decrease in fibre diameter	50±20%	30±30%	76±8%	58±11%	60±15%	44±27%
t-test (*p*-value)	0.000481		0.00000254		0.0707	

Table 4.4 Effect of asphaltenes on fibre diameter and carbon yield for PVP/asphaltene fibres.

4.3.3 Polyacrylonitrile/asphaltene composite fibres

Polyacrylonitrile (PAN) is perhaps the most commonly used precursor for the electrospinning of carbon fibres. Polyacrylonitrile has great "spinnability", meaning that it can easily be electrospun into smooth fibres. The electrospinning and oxidative stabilization of PAN also have a long and detailed history in literature. The electrospinning of PAN fibres and the carbonization of PAN filaments were patented during the 1970s.[18,19] Since then, PAN fibres have been used in a wide array of applications, such as energy storage,[20,21] supercapacitors,[22] filtrations,[23,24] and high-strength carbon fibres.[25,26] This section will explore the electrospinning of polyacrylonitrile and asphaltene composite fibres.

In the previous sections, asphaltenes and polyethylene oxide/polyvinylpyrrolidone were dissolved in a toluene/DMF solvent mixture to improve solubility for electrospinning. However, polyacrylonitrile is not soluble in toluene. Even a small amount of toluene will cause phase separation. Hence, PAN and asphaltenes are dissolved solely in N,N-dimethylformamide. Solutions of 10% (w/w) PAN with 0%, 2.5%, and 5% (w/w) asphaltenes were dissolved in DMF and left to heat with magnetic stirring overnight. Because no toluene is used, only a relatively low amount of asphaltenes can be dissolved in DMF. Asphaltenes, up to 5% (w/w), were well dispersed in DMF, with only small particulates of solid material on the edges of the vial.

Figure 4.10 shows the SEM images of electrospun PAN/asphaltene composite fibres. All samples were electrospun at 15 kV, 15 cm (distance from needle to collector), and 10 μL/min. With no asphaltenes added (Figure 4.10a), electrospun PAN fibres are not smooth, with a large number of beads. This is indicative of low polymer concentration and insufficient solvent evaporation during electrospinning. At 2.5% and 5% asphaltenes, the fibres become noticeably

smoother, but there are small amounts of round particulates. It is likely that because asphaltenes are not perfectly dispersed in DMF, electrospraying of undissolved material result in these small particulates.

Electrospun fibres were carbonized by oxidative stabilization in air at 280 ^{o}C (0.5 ^{o}C/min) for one hour, followed by carbonization in forming gas at 800 ^{o}C (5 ^{o}C/min) for one hour. Figure 4.11 shows the SEM images after carbonization and Table 4.5 lists the fibre diameters before and after carbonization. Before carbonization, fibre diameters are 0.26±0.5 μm, 0.31±0.04 μm, and 0.34±0.06 μm for 0% asphaltene, 2.5% asphaltene, and 5% asphaltene, respectively. The fibre diameter increases as the amount of asphaltene in the precursor solution increases, which is not surprising. After carbonization, fibre diameters decrease to 0.13±0.05 μm, 0.31±0.04 μm, and 0.34±0.06 μm. Fibres from the 0% asphaltene sample suffer the greatest decrease in diameter, at 50±20%. At 2.5% and 5% asphaltenes, fibre diameters only decrease by approximately 20-25% after carbonization. Again, similar to PVP/asphaltene composite fibres, the addition of asphaltenes to PAN can increase the carbon yield. A *t*-test analysis shows that the effect of asphaltenes on carbon yield is statistically significant, even more so than PVP/asphaltene fibres.

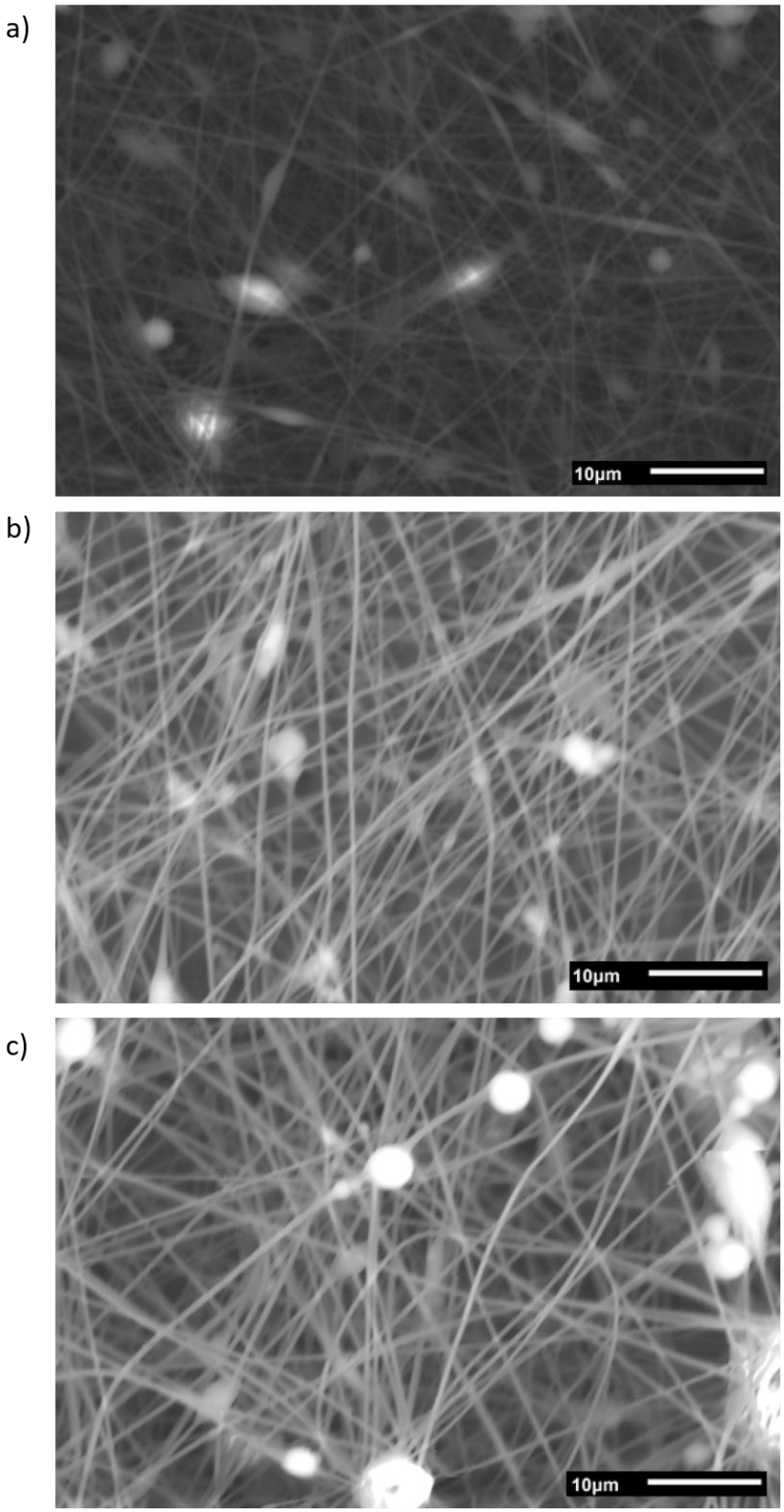

Figure 4.10 Electrospun composite fibres with 10% PAN and a) 0% asphaltene b) 2.5% asphaltene c) 5% asphaltene.

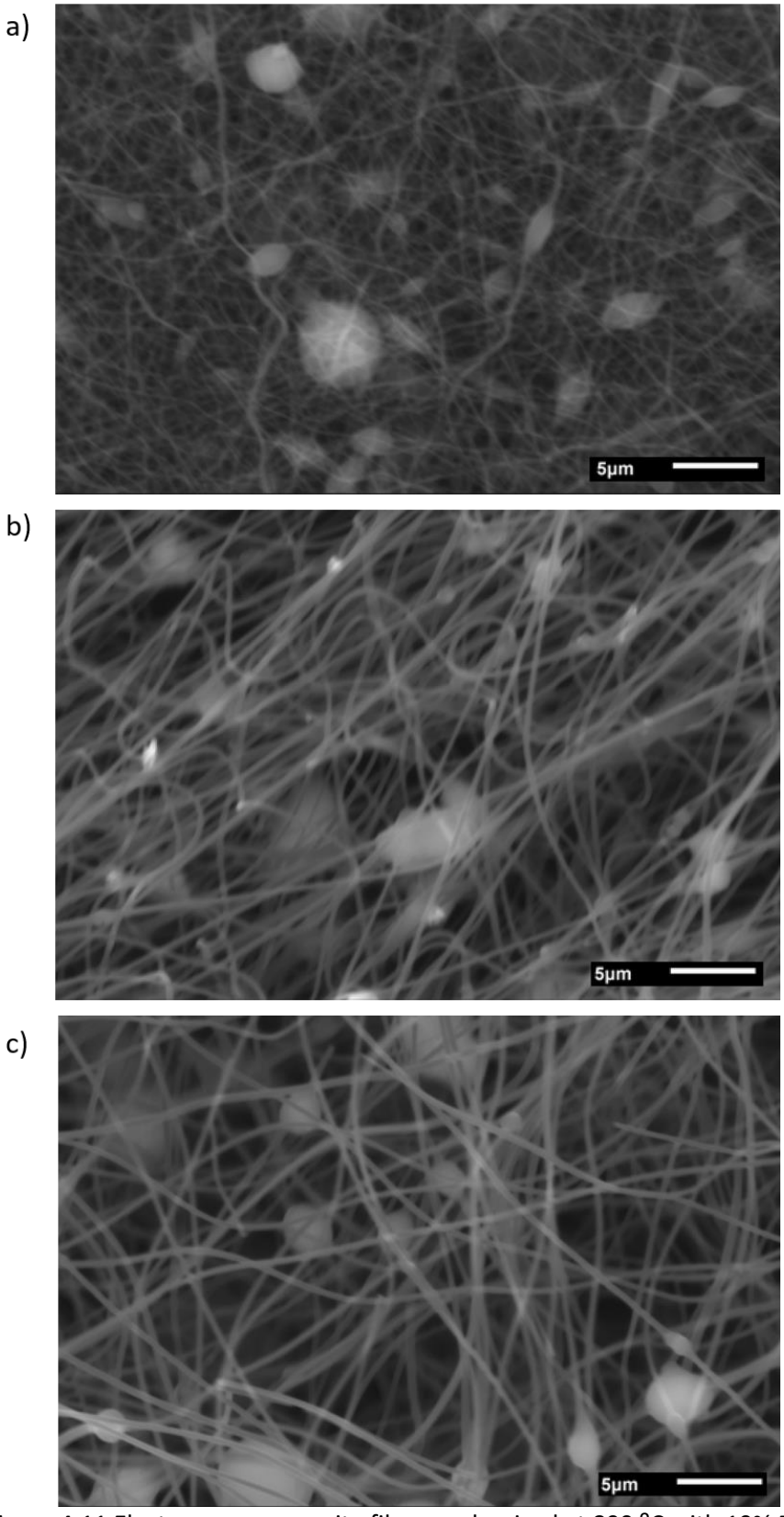

Figure 4.11 Electrospun composite fibres carbonized at 800 ^{o}C with 10% PAN and a) 0% asphaltene b) 2.5% asphaltene c) 5% asphaltene.

	10% PAN 0% asphaltene	10% PAN 2.5% asphaltene	10% PAN 5% asphaltene
Fibre diameter before carbonization (μm) (n=20)	0.26±0.5	0.39±0.04	0.45±0.08
Fibre diameter after carbonization (μm) (n=20)	0.13±0.05	0.31±0.04	0.34±0.06
Percent decrease in fibre diameter	50±20%	21±13%	24±19%
t-test (compare 0% asphaltene to *n*% asphaltene) (*p*-value)	N/A	5.88×10^{-8}	3.40×10^{-7}

Table 4.5 Fibre diameters for PAN/asphaltene composite fibres.

4.3.4 Polyacrylonitrile/asphaltene composite fibres for SPME detection of polycyclic aromatic hydrocarbons

The structure of asphaltenes is composed of carbon aromatic rings and aliphatic side chains. This is very similar to the structure of polycyclic aromatic hydrocarbons (PAHs). The similarity in structure could potentially mean that asphaltenes can be used to adsorb and extract PAHs. Electrospinning is a promising method of manufacturing phases for solid-phase microextraction (SPME). Electrospun nanofibres have the benefit of high surface area, which increases extraction efficiency. Electrospinning is also a simple, cost-effective, and versatile method of manufacturing phases with different chemistry and specificity. The effectiveness of asphaltenes for the extraction of PAHs will be explored.

Previous sections showed that asphaltenes can be added to polyethylene oxide, polyvinylpyrrolidone, and polyacrylonitrile during electrospinning. However, not all of them are applicable for SPME. Composite PEO/asphaltene fibres are not thermally stable, and the electrospinning process is difficult due to frequent clogging and other inconsistencies. Composite PVP/asphaltene fibres have smooth morphology, are thermally stable, and can be electrospun in a consistent basis. However, PVP is water soluble and may not be suitable for aqueous extraction. Composite PAN/asphaltene fibres have high surface area, are thermally stable, are water insoluble, and can be electrospun easily and consistently. Hence, composite PAN/asphaltene fibres will be used for SPME.

The SPME device is easily constructed by using a 0.010 stainless wire in a metal sheath from a previously-used SPME device from Supelco. Composite PAN/asphaltene fibres are directly electrospun onto the stainless wire. Figure 4.12 shows the SEM image of electrospun

PAN/asphaltene fibres on a stainless steel wire. The fibre morphology and size are the same as the fibres shown in Figure 4.10. The fibres are mostly smooth, with small particulates of solid material that come from undissolved asphaltenes in solution. As a proof of concept, a 1 mg/L mixture of PAH in water was used for head-space SPME. Two different coatings were used: electrospun fibres from a 10% PAN solution and from a 10% PAN/5% asphaltene solution. If asphaltenes exhibit high affinity for PAH adsorption, then the extraction efficiency from the 10% PAN/5% asphaltene coating would be higher. Figure 4.13 shows the extraction results for both coatings. For all four PAH tested, the PAN/asphaltene coating show 4-5 times superior extraction than the coating with only PAN. The difference in extraction efficiencies originate from differences in their chemical structure. PAN is a polymer composed of a carbon backbone with nitrile functional groups whereas asphaltenes are composed of aromatic rings. Asphaltenes are very similar in structure to PAHs and Figure 4.13 shows that the addition of asphaltene in the SPME coating results in better extraction. However, at 1 mg/L, the extraction efficiencies are relatively quite low. It is likely that even though asphaltenes show superior affinity for PAH, the total amount of asphaltenes in the coating is low. Unlike PVP, PAN/asphaltene cannot be dissolved in toluene, so a high asphaltene concentration cannot be used for electrospinning. To increase the extraction efficiency, the total amount of asphaltenes in the SPME coating need to be increased. In the next chapter, SPME detection of PAHs for an 100% asphaltene coating will be explored.

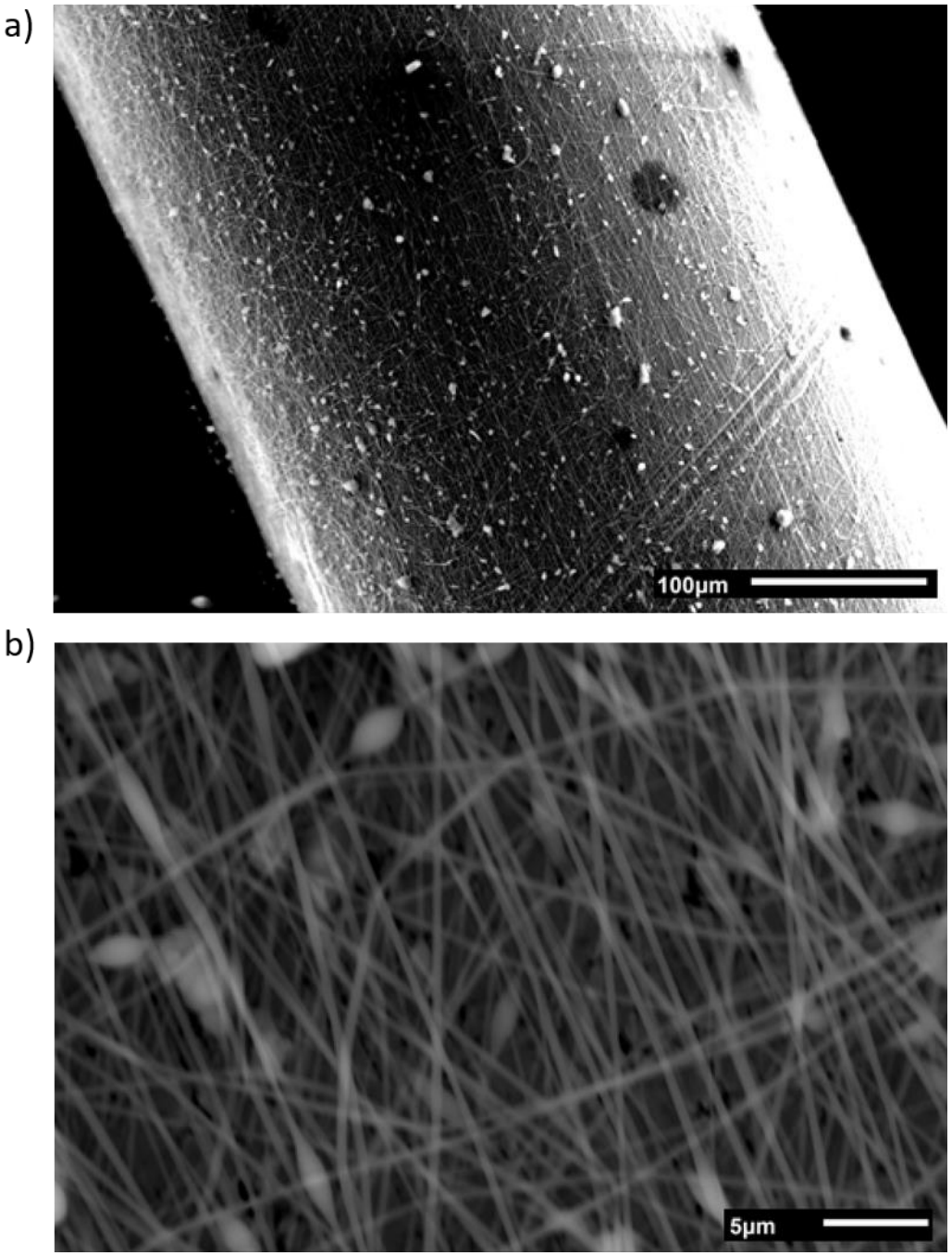

Figure 4.12 Electrospun PAN/asphaltene composite fibres on stainless steel wire for SPME. a) 250x mag b) 3000x mag

.

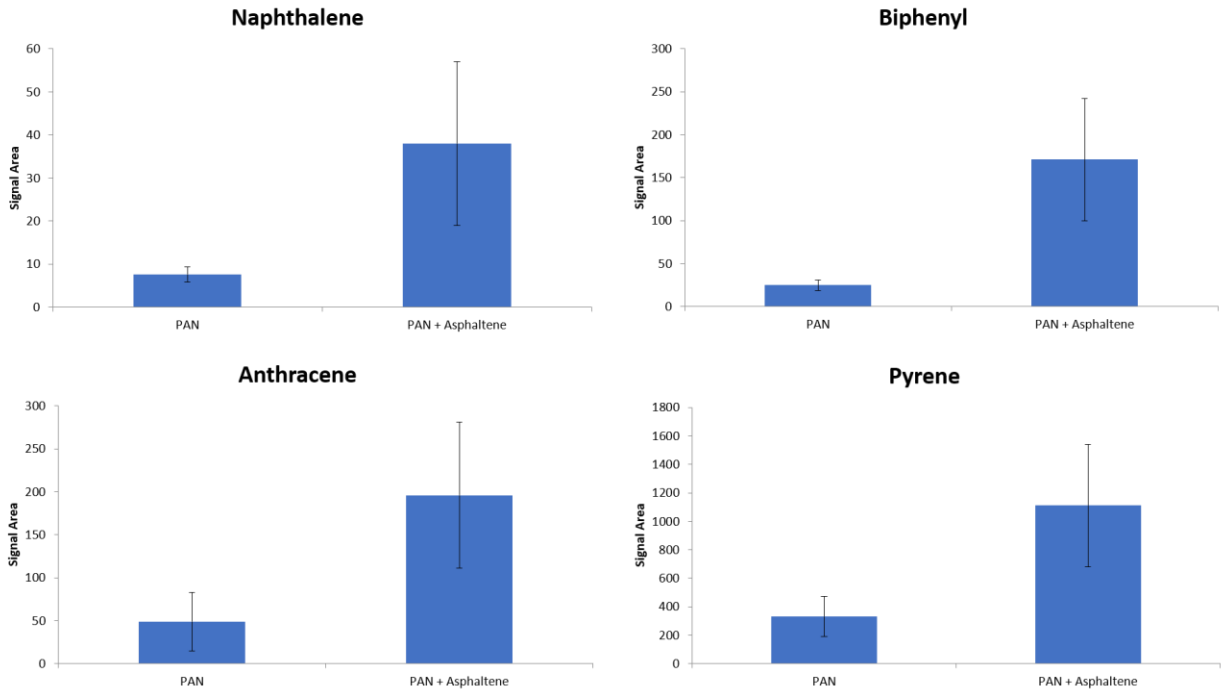

Figure 4.13 Extraction efficiency of 1 mg/L PAH mixture for electrospun PAN fibres and PAN/asphaltene composite fibres. n=3.

4.4 Conclusion

Nanofibres were successfully electrospun using asphaltenes and three different polymers: polyethylene oxide, polyvinylpyrrolidone, and polyacrylonitrile. For polyvinylpyrrolidone and polyacrylonitrile composite fibres, asphaltenes can have a significant effect on the fibre size and yield after carbonization. When asphaltenes are added to the precursor solution, composite fibres exhibit less thermal degradation after carbonization. Asphaltenes were also found to have high affinity for PAHs when composite PAN/asphaltene fibres were used as an extraction phase for SPME. However, the amount of asphaltenes in these composite fibres are relatively low. The extraction and detection of PAHs using asphaltenes will be explored more in detail in the next chapter.

4.5 References

1. Ge, J. J. *et al.* Assembly of well-aligned multiwalled carbon nanotubes in confined polyacrylonitrile environments: Electrospun composite nanofibre sheets. *J. Am. Chem. Soc.* **126,** 15754–15761 (2004).

2. Sen, R. *et al.* Preparation of single-walled carbon nanotube reinforced polystyrene and polyurethane nanofibres and membranes by electrospinning. *Nano Lett.* **4,** 459–464 (2004).

3. Dong, Q. *et al.* Ultrasound-assisted preparation of electrospun carbon nanofibre/graphene composite electrode for supercapacitors. *J. Power Sources* **243,** 350–353 (2013).

4. Wang, C., Li, Y., Ding, G., Xie, X. & Jiang, M. Preparation and characterization of graphene oxide/poly(vinyl alcohol) composite nanofibres via electrospinning. *J. Appl. Polym. Sci.* **127,** 3026–3032 (2013).

5. Nam, S. H. *et al.* Ag or Au nanoparticle-embedded one-dimensional composite TiO2nanofibres prepared via electrospinning for use in lithium-ion batteries. *ACS Appl. Mater. Interfaces* **2,** 2046–2052 (2010).

6. Xu, X. *et al.* Biodegradable electrospun poly(l-lactide) fibres containing antibacterial silver nanoparticles. *Eur. Polym. J.* **42,** 2081–2087 (2006).

7. Bergshoef, M. M. & Vancso, G. J. Transparent nanocomposites with ultrathin, electrospun nylon-4,6 fibre reinforcement. *Adv. Mater.* **11,** 1362–1365 (1999).

8. Aliabadi, M., Irani, M., Ismaeili, J., Piri, H. & Parnian, M. J. Electrospun nanofibre membrane of PEO/Chitosan for the adsorption of nickel, cadmium, lead and copper ions from aqueous solution. *Chem. Eng. J.* **220,** 237–243 (2013).

9. Yu, D. G., Zhang, X. F., Shen, X. X., Brandford-White, C. & Zhu, L. M. Ultrafine ibuprofen-loaded polyvinylpyrrolidone fibre mats using electrospinning. *Polym. Int.* **58,** 1010–1013 (2009).

10. Yu, D. G. *et al.* Oral fast-dissolving drug delivery membranes prepared from electrospun polyvinylpyrrolidone ultrafine fibres. *Nanotechnology* **20,** (2009).

11. Zhang, K., Choi, H. J. & Kim, J. H. Preparation and Characteristics of Electrospun Multiwalled Carbon Nanotube/Polyvinylpyrrolidone Nanocomposite Nanofibre. *J. Nanosci. Nanotechnol.* **11,** 5446–5449 (2011).

12. Newsome, T. E. & Olesik, S. V. Electrospinning silica/polyvinylpyrrolidone composite nanofibres. *J. Appl. Polym. Sci.* **131,** 1–9 (2014).

13. Bishop, A., Balázsi, C., Yang, J. H. & Gouma, P. I. Biopolymer-hydroxyapatite composite coatings prepared by electrospinning. *Polym. Adv. Technol.* **17,** 395–418 (2006).

14. Wang, P. *et al.* Mesoporous carbon nanofibres with a high surface area electrospun from thermoplastic polyvinylpyrrolidone. *Nanoscale* **4,** 7199–7204 (2012).

15. Schwan, J., Ulrich, S., Batori, V., Ehrhardt, H. & Silva, S. R. P. Raman spectroscopy on amorphous carbon films. *J. Appl. Phys.* **80,** 440–447 (1996).

16. Nemanich, R. J., Glass, J. T., Lucovsky, G. & Shroder, R. E. Raman scattering characterization of carbon bonding in diamond and diamondlike thin films. *J. Vac. Sci. Technol. A Vacuum, Surfaces, Film.* **6,** 1783–1787 (1988).

17. Knight, D. S. & White, W. B. Characterization of diamond films by Raman spectroscopy. *J. Mater. Res.* **4,** 385–393 (1989).

18. Tatchell, J. J. Manufacture of carbon filaments. *U.S. Patent No. 3,663,170* (1972). doi:10.1016/j.(73)

19. Simm, W. Apparatus for the production of filters by electrostatic fibre spinning. (1976).

20. Ji, L., Jung, K.-H., Medford, A. J. & Zhang, X. Electrospun polyacrylonitrile fibres with dispersed Si nanoparticles and their electrochemical behaviors after carbonization. *J. Mater. Chem.* **19,** 4992 (2009).

21. Yu, Y., Yang, Q., Teng, D., Yang, X. & Ryu, S. Reticular Sn nanoparticle-dispersed PAN-based carbon nanofibres for anode material in rechargeable lithium-ion batteries. *Electrochem. commun.* **12,** 1187–1190 (2010).

22. Ra, E. J., Raymundo-Piñero, E., Lee, Y. H. & Béguin, F. High power supercapacitors using polyacrylonitrile-based carbon nanofibre paper. *Carbon N. Y.* **47,** 2984–2992 (2009).

23. Wang, M. X., Huang, Z. H., Shimohara, T., Kang, F. & Liang, K. NO removal by electrospun porous carbon nanofibres at room temperature. *Chem. Eng. J.* **170,** 505–511 (2011).

24. Kampalanonwat, P. & Supaphol, P. Preparation and adsorption behavior of aminated electrospun polyacrylonitrile nanofibre mats for heavy metal ion removal. *ACS Appl. Mater. Interfaces* **2,** 3619–3627 (2010).

25. Hou, H. & Reneker, D. H. Carbon Nanotubes on Carbon Nanofibres: A Novel Structure Based on Electrospun Polymer Nanofibres. *Adv. Mater.* **16,** 69–73 (2004).

26. Zussman, E. *et al.* Mechanical and structural characterization of electrospun PAN-derived carbon nanofibres. *Carbon N. Y.* **43,** 2175–2185 (2005).

Chapter 5

Asphaltene-Based SPME Coating for the Detection of Polycyclic Aromatic Hydrocarbons

5.1 Introduction

Polycyclic aromatic hydrocarbons (PAHs) are molecules that are known to have toxic and carcinogenic properties. It is known that PAHs can undergo metabolic activation and form adducts with DNA, causing DNA mutation.[1] PAHs are ubiquitous, and can be detected almost anywhere, but elevated levels are produced from sources such as the combustion of fossil fuels,[2] many industrial processes,[3] and even processed and cooked foods.[4] Hence, the monitoring of PAHs in the environment is necessary to minimize its risk to humans and wildlife. For example, PAHs are a natural fraction of oil sands in Alberta, and the development of the oil industry has contributed to elevated levels of PAHs in the Athabasca river and its tributaries.[5] Constant monitoring and detection of the water supply is crucial for the prevention of related health risks.

Common techniques used for the extraction and detection of PAHs are liquid-liquid extraction (LLE) and solid-phase extraction (SPE). Both of the Canadian Council of Ministers of the Environment and the US Environmental Protection Agency use LLE for the extraction of PAHs.[6,7] Both extraction techniques (LLE and SPE) require additional solvent for extraction and elution. This adds complexity and cost compared to solid-phase microextraction (SPME), which uses a polymer coating to directly extract analytes from the matrix. SPME is a relatively recent technique, being first developed by Pawliszyn in 1990.[8] However, since its inception, this technique has gained tremendous popularity due to its simplicity, its versatility, and its low limit of detection. It has been applied for the detection of a multitude of analytes, such as herbicides,[9] narcotics,[10] DNA,[11] and countless other volatile compounds from environmental or

biological sources. Solid-phase microextraction is a powerful technique and it has immense potential.

The extraction and detection of PAHs using SPME offers several advantages compared to other extraction methods, as mentioned previously. Because PAHs are volatile or semi-volatile compounds, headspace-SPME (HS-SPME) is generally chosen over direct-SPME extraction. In HS-SPME, the fibre is not immersed in the sample matrix, which avoids fibre swelling and damage, and increases the stability and longevity of the fibre. Equation 5.1 describes the theory of headspace-SPME, where the amount of analyte extracted, *n*, depends on the volumes of the coating, sample, and headspace (V_c, V_s, V_h), the initial concentration of the analyte in solution, C_0, and two partition coefficients (K_1, K_2).

$$n = \frac{C_0 V_c V_s K_1 K_2}{V_c K_1 K_2 + V_h K_2 + V_s} \qquad (5.1)$$

During HS-SPME, the extraction efficiency depends on two partition coefficients, the partition of the analyte between the headspace and the fibre coating (K_1), and the partition of the analyte between the matrix and the headspace (K_2). Hence, the fibre coating is an important factor for method development since the chemistry of the coating has a significant impact on the partition coefficient. There are several different coatings that have been used for the extraction of PAHs, such as polyaniline,[12] polyetherimide,[13] graphene oxide based composites,[14,15] carbon nanotube-based composites.[16,17] Extraction efficiency can also be increased by using microwave-assisted heating[18] or cold-fibre extraction.[19] These techniques can enhance the efficiency by altering the partition coefficients between the matrix and the

headspace, or between the headspace and the fibre coating. Generally, these novel SPME coatings have a detection limit of lower than 1 μg/L for common PAHs, but they all require complex, time-consuming, or costly processes. For example, cold-fibre extraction requires liquid CO_2 and nanomaterial coatings such as graphene and CNTs have complex synthetic processes. Here we demonstrate the simple construction of an asphaltene SPME coating for PAH extraction. Asphaltenes are a class of hydrophobic, carbon-based molecules that are derived from crude oils. The structure of asphaltene molecules is widely accepted to be composed of aromatic rings with aliphatic side chains.[20] In fact, the structures of asphaltenes and PAHs are quite similar. This chapter will show that a simple, cost-effective asphaltene coating can be used for the extraction of PAHs using HS-SPME.

5.2 Experimental

5.2.1 Materials

Four different PAHs were used: fluorene (98%, Sigma-Aldrich), fluoranthene (98%, Sigma-Aldrich), pyrene (98%, Sigma-Aldrich), and benz[a]anthracene (99%, Sigma-Aldrich). Solvents that were used are acetonitrile (≥99.9%, Sigma-Aldrich), toluene (99.9%, Sigma-Aldrich) and 18.2 megaohm-cm deionized water. Source of asphaltenes is the Athabasca oil sands in Alberta, Canada. Asphaltenes were precipitated and washed with pentane until the solvent only had a light colour. The stainless-steel wire (0.010 inch) was purchased from Malin Co.. SPME experiments were performed using 20 mL crimp top vials with a PTFE/butyl rubber tin plate seal (Chromatographic Specialities Inc.).

5.2.2 Preparation of asphaltene-coated SPME device

The fibre for a previously used Supelco SPME device was discarded, leaving only the barrel and septum. A new stainless-steel wire (0.010 inch diameter) was inserted into the barrel to prepare the new coating. A 30% (w/w) asphaltene solution in toluene was prepared by heating on a magnetic hot plate overnight. The SPME coating was prepared by immersing ~1.5 cm of the stainless-steel wire into the asphaltene solution for 2 s. After removing the wire from the solution, it was put into a 200 ^{o}C oven for 2 min to evaporate any remaining solvent.

5.2.3 HS-SPME-GC method development

A 2 g/L stock solution of each PAH was prepared in acetonitrile. Solutions used for SPME experiments were diluted from the stock solution using 18.2 megaohm-cm deionized water. For optimization experiments, a PAH mixture was made where each PAH was at 100 μg/L. A Hewlett Packard 6890 GC system with a flame-ionization detector was used. For all GC separations, a Supelco SLB-5MS fused silica capillary column (30 m x 0.25 mm x 0.25 μm) was used. Thermal desorption at the GC inlet was performed at 250 ^{o}C for 3 min. GC separation was performed using a temperature ramp from 50 ^{o}C to 240 ^{o}C at 10 ^{o}C/min and then maintained at 240 ^{o}C for 10 min. Helium gas flow was maintained at 3 mL/min.

5.2.4 Scanning electron microscopy

The asphaltene coated SPME fibre was imaged using SEM (Hitachi S-4800 field emission scanning electron microscope). From cross-sectional imaging, the SPME fibre was cut using a wire cutter and placed in a special cross-section sample holder so the top of the wire could be imaged.

5.3 Results and Discussion

5.3.1 Optimization of temperature

The temperature of the sample matrix during extraction can affect the extraction efficiency in several ways. In HS-SPME, the analytes must partition from the matrix into the headspace. An increase in temperature will increase the volatility of analytes, resulting in higher vapour pressure and an increase in extraction. This is especially significant for higher molecular weight, semi-volatile molecules that have a relatively low vapour pressure. However, the extraction efficiency during HS-SPME also depends on the partition of the analyte from the headspace into the fibre coating. This is an exothermic process and higher temperatures will decrease the amount of adsorption. This means that increasing the temperature will not always result in greater extraction, since temperature has opposite effects on the two partition processes.

Figure 5.1 shows the chromatogram for a 100 μg/L PAH mixture, where fluorene, fluoranthene, pyrene, and benz[a]anthracene elutes at 15.46 min, 20.45 min, 20.49 min, and 24.21 min, respectively. There is also a small peak at 1.5 minutes, which is the acetonitrile peak from the stock solution. The structures of these molecules are shown in Figure 5.2. As shown, these are medium-sized 3 to 4 ring PAHs, which fluorene being the smallest and least non-polar. Figure 5.3 shows the affect of temperature on the extraction of PAHs from a 100 μg/L mixture. The extraction was performed for 5 hours, with constant agitation with a magnetic stir bar, from 40 ^{o}C to 90 ^{o}C. The extraction efficiency generally increases for all four PAHs from 40 ^{o}C to 90 ^{o}C. For fluorene, the best extraction occurs at 70 ^{o}C, and decreases slightly at higher temperatures. Fluorene is a relatively low molecular weight PAH and has a higher vapour

pressure. Increasing the temperature does not increase the vapour pressure of fluorene as dramatically as the other PAHs. For fluoranthene, the extraction plateaus around 80 ^{o}C. It is interesting that for pyrene and benz[a]anthracene, the extraction increases steadily up to 90 ^{o}C. For benz[a]anthracene, temperature has the largest effect on extraction as the signal area increases almost 8-fold from 40 ^{o}C to 90 ^{o}C. The detrimental effect of high temperatures on adsorption is not generally seen for this asphaltene coating. A poly(3,4-ethylenedioxythiophene)/graphene oxide SPME coating used by Banitaba *et al.* has maximum extraction for pyrene and benz[a]anthracene at 65 ^{o}C.[15] A carbon nanotube coating made by Maghsoudi and Noroozian shows maximum extraction for fluorene and fluoranthene at 50-60 ^{o}C.[17] Results from Figure 5.3 suggests that the asphaltene coating seems to tolerate extraction at higher temperatures. This could be due to strong interactions between the coating and PAHs. Even though the extraction efficiency decreases for fluorene after 70 ^{o}C, 90 ^{o}C is chosen as the optimum extraction temperature. At 90 ^{o}C, some extraction efficiency for fluorene is being sacrificed for increased efficiencies of the other three analytes.

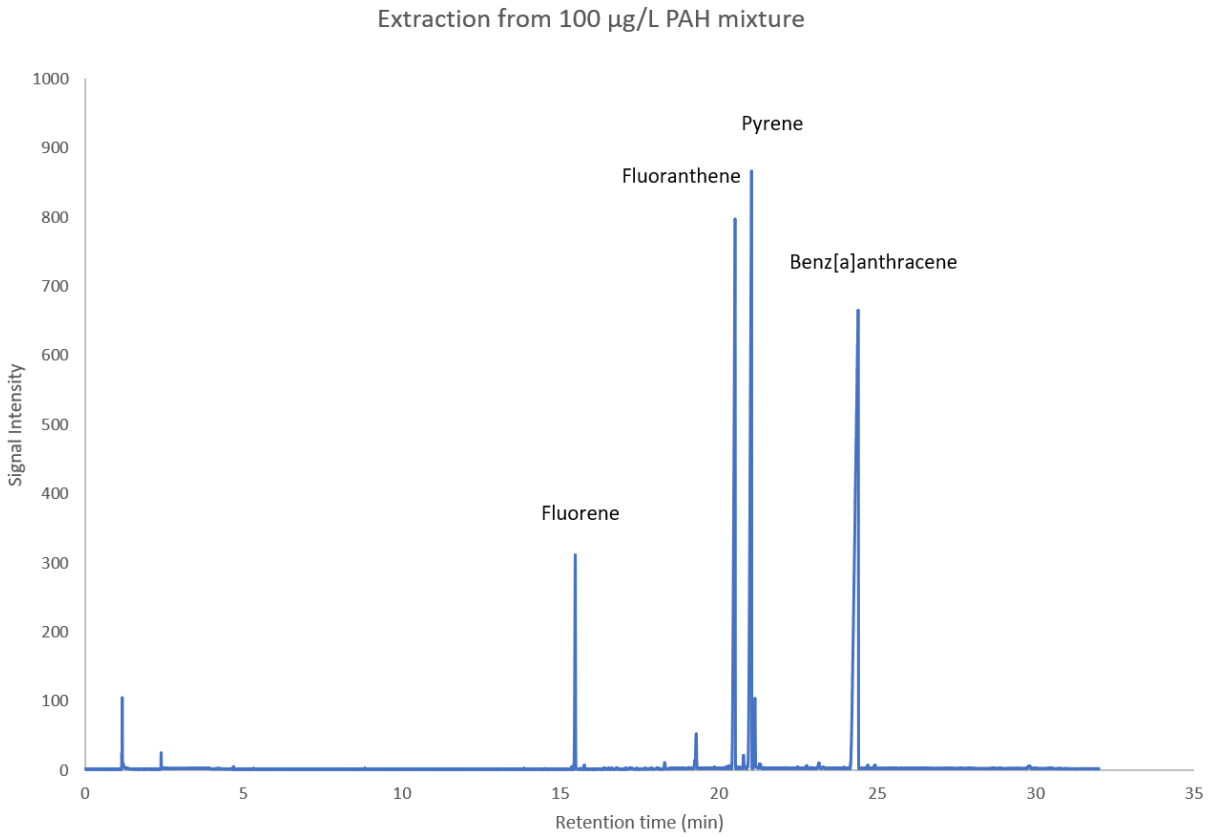

Figure 5.1 GC chromatogram for HS-SPME of 100 µg/L PAH mixture.

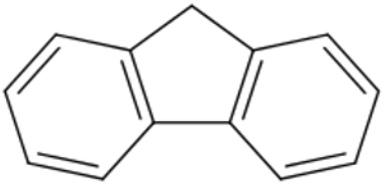

Fluorene

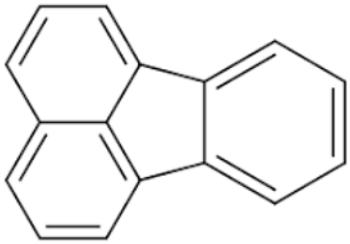

Fluoranthene

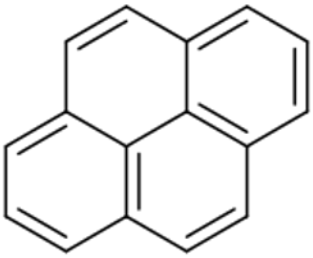

Pyrene

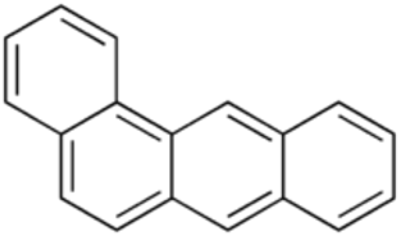

Benz[a]anthracene

Figure 5.2 Chemical structures of fluorene, fluoranthene, pyrene, and benz[a]anthracene.

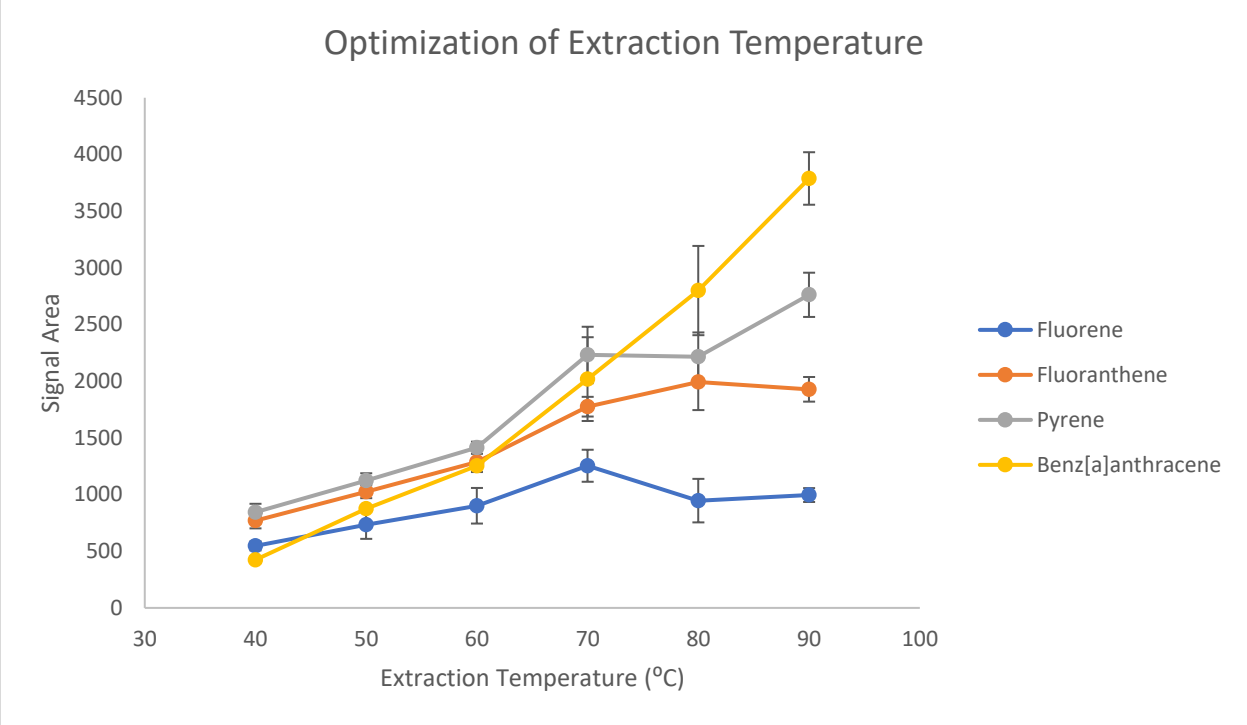

Figure 5.3 Optimization of temperature using 100 µg/L PAH mixture, 5 hours. Error bars are the standard deviations of the signal area from three trials. Signal area is the integrated peak area from the chromatogram.

5.3.2 Optimization of sample volume

The sample volume, or more accurately the ratio of headspace volume to sample volume, is another important factor to consider. Theoretically, the most efficient extraction occurs when the ratio of headspace volume to sample volume is zero, assuming the total volume of the system is constant.[21] At a non-zero ratio, as in HS-SPME, the extraction will always be less than ideal. However, extraction can be improved by using a smaller ratio, meaning more sample volume and less headspace volume.

Extraction of the PAH mixture was performed using a 20 mL vial, with either 3, 5, 7, or 9 mL of sample volume. Figure 5.4 shows the integrated signal areas as a function of sample volume. For all four analytes, the amount extracted increases with respect to increasing sample volume. This is consistent with theoretical considerations. Sample volumes larger than 9 mL were not tested in order to leave enough room in the headspace for the SPME fibre. All subsequent experiments were done using 9 mL of sample volume.

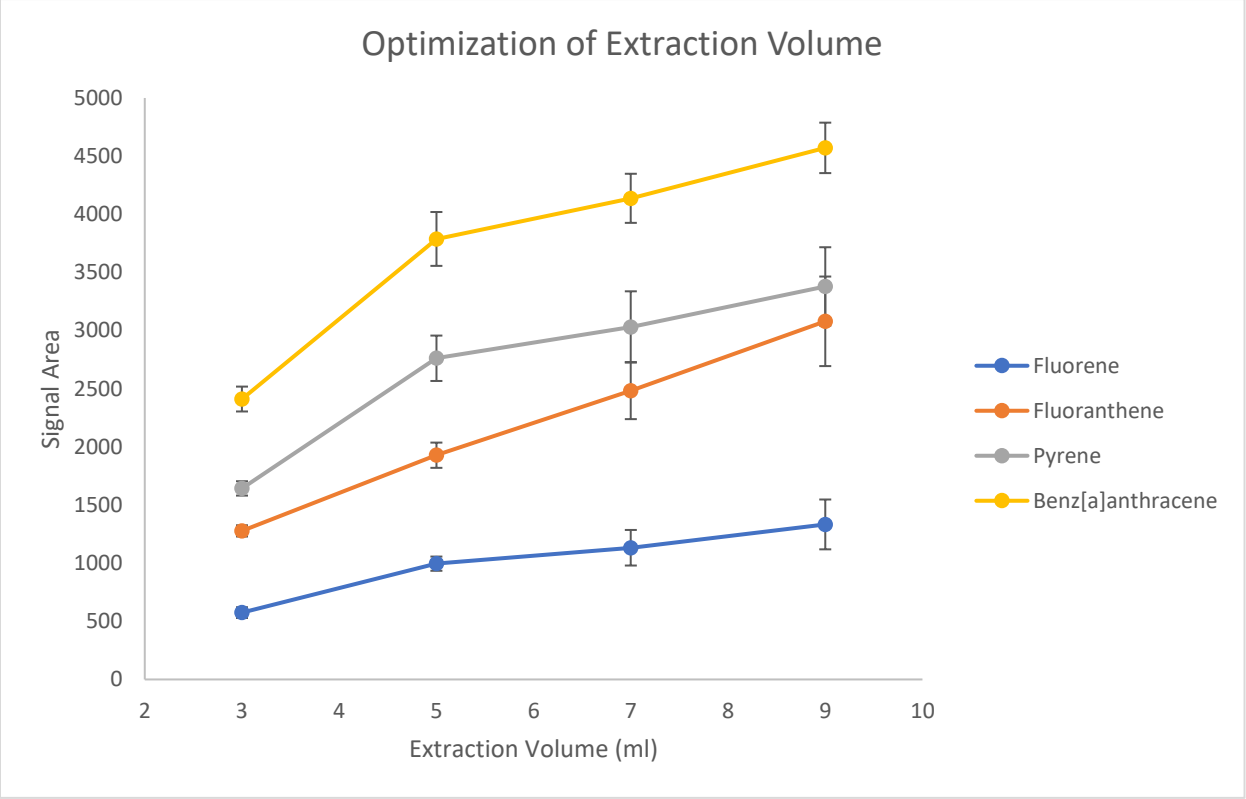

Figure 5.4 Optimization of temperature using 100 µg/L PAH mixture, 5 hours, 90 °C. Error bars are the standard deviations of the signal area from three trials. Signal area is the integrated peak area from the chromatogram.

5.3.3 Optimization of ionic strength

The ionic strength of the sample solution affects the volatility of PAHs. The magnitude and direction of the effect can depend on the polarity and size of the analyte. For polar compounds, the addition of salt usually lowers the solubility. This is known as the "salting out" effect. In an aqueous solution, analytes and salt ions are both stabilized by interactions with water molecules. An increase in salt ions will lead to less water molecules that are available to stabilize the analytes, thus lowering their solubility. However, in Figure 5.5, the opposite effect is seen. The addition of NaCl actually decreases the extraction efficiency, implying an increase in their solubility. For fluorene, the extraction efficiency is largely unaffected by ionic strength, but the signals decrease significantly for the other three analytes. This is because fluorene is the smallest and most polar molecule in the PAH mixture. The decrease in extraction efficiency for the other three analytes is likely due to the apolar nature of the molecules. It is possible that these apolar molecules are interacting with the salt ion, which will increase their polarity. This potential increase in polarity could either increase their solubility, or decrease the strength of interactions with the asphaltene coating. Both of these scenarios could explain the decrease in extraction efficiency with respect to ionic strength. For all subsequent experiments, no salt was added. However, real world samples might contain small amounts of salt. In most ocean and seawaters, the amount of salt present is less than 5%, and this will not have a large effect on the extraction efficiencies of medium-sized PAHs.

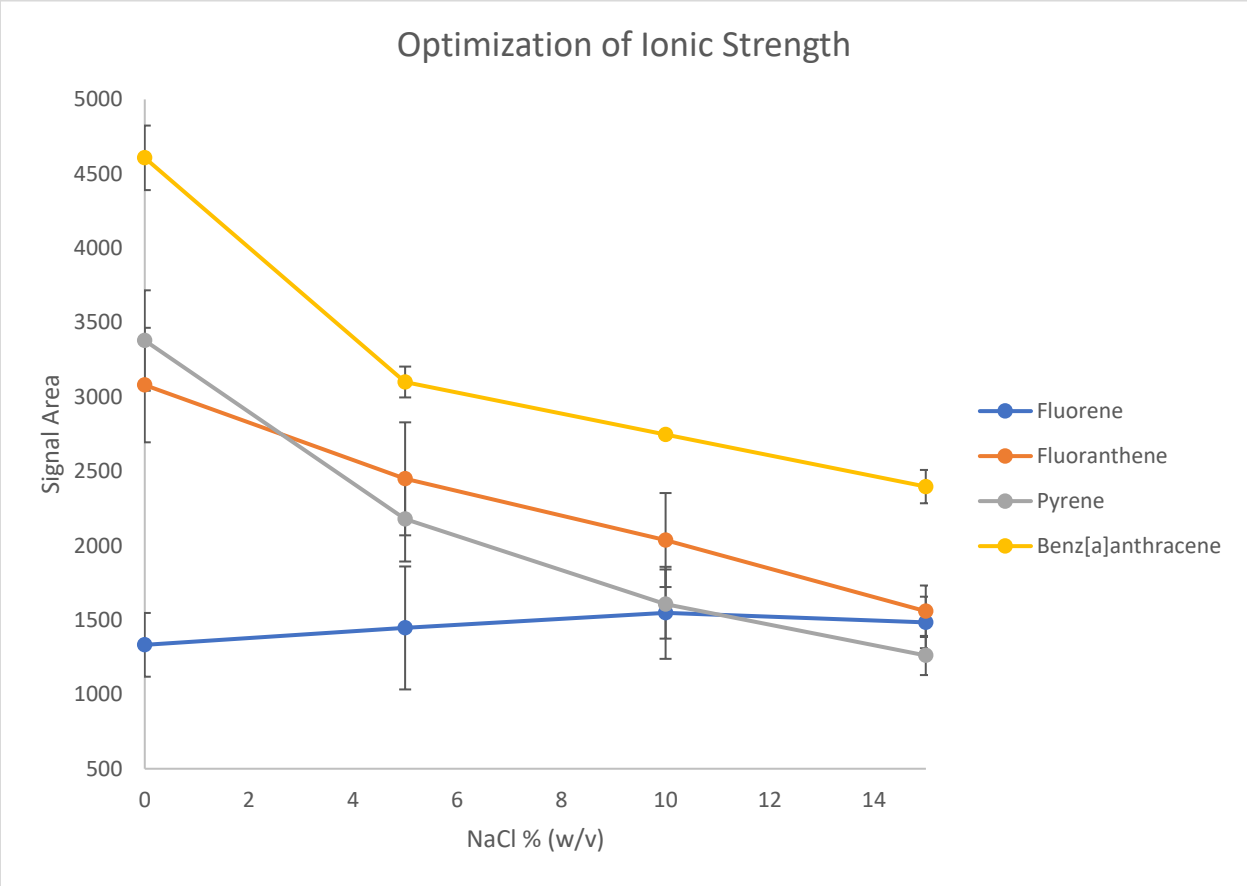

Figure 5.5 Optimization of ionic strength using 100 µg/L PAH mixture, 5 hours, 90 ^{o}C. Error bars are the standard deviations of the signal area from three trials. Signal area is the integrated peak area from the chromatogram.

5.3.4 Optimization of extraction time

Figure 5.6 shows the extraction curves as a function of time. Extraction was performed for 1, 3, 5, and 7 hours. The extraction efficiency steadily increases until 5 hours, except for fluorene, which plateaus after 3 hours. Extraction for 5 hours is sufficient to reach equilibrium under these conditions. Hence, 5 hours was chosen for all subsequent experiments. For comparison, HS-SPME of PAH mixtures using MWCNT and CNT/composite coatings require extraction times of 45 minutes to 1 hour to reach equilibrium.[16,17]

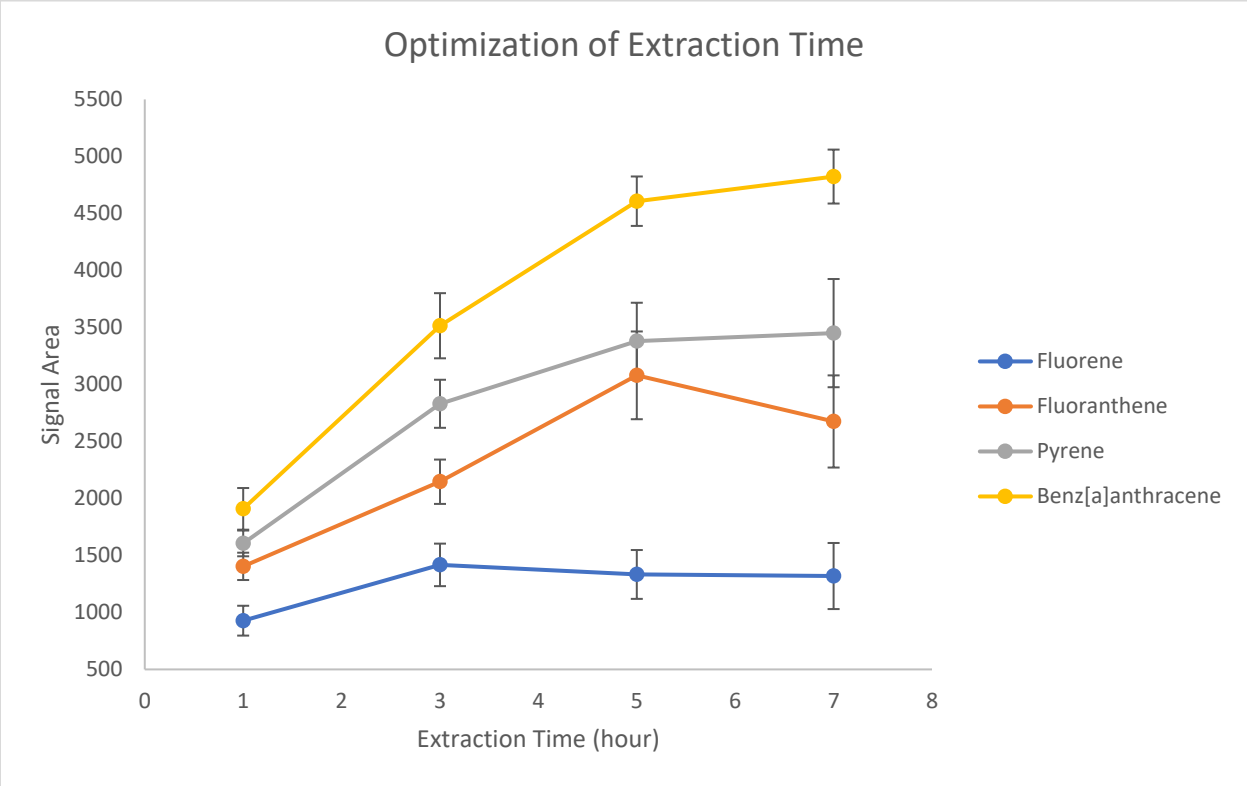

Figure 5.6 Optimization of extraction time using 100 μg/L PAH mixture, 0% NaCl, 90 ^{o}C. Error bars are the standard deviations of the signal area from three trials. Signal area is the integrated peak area from the chromatogram.

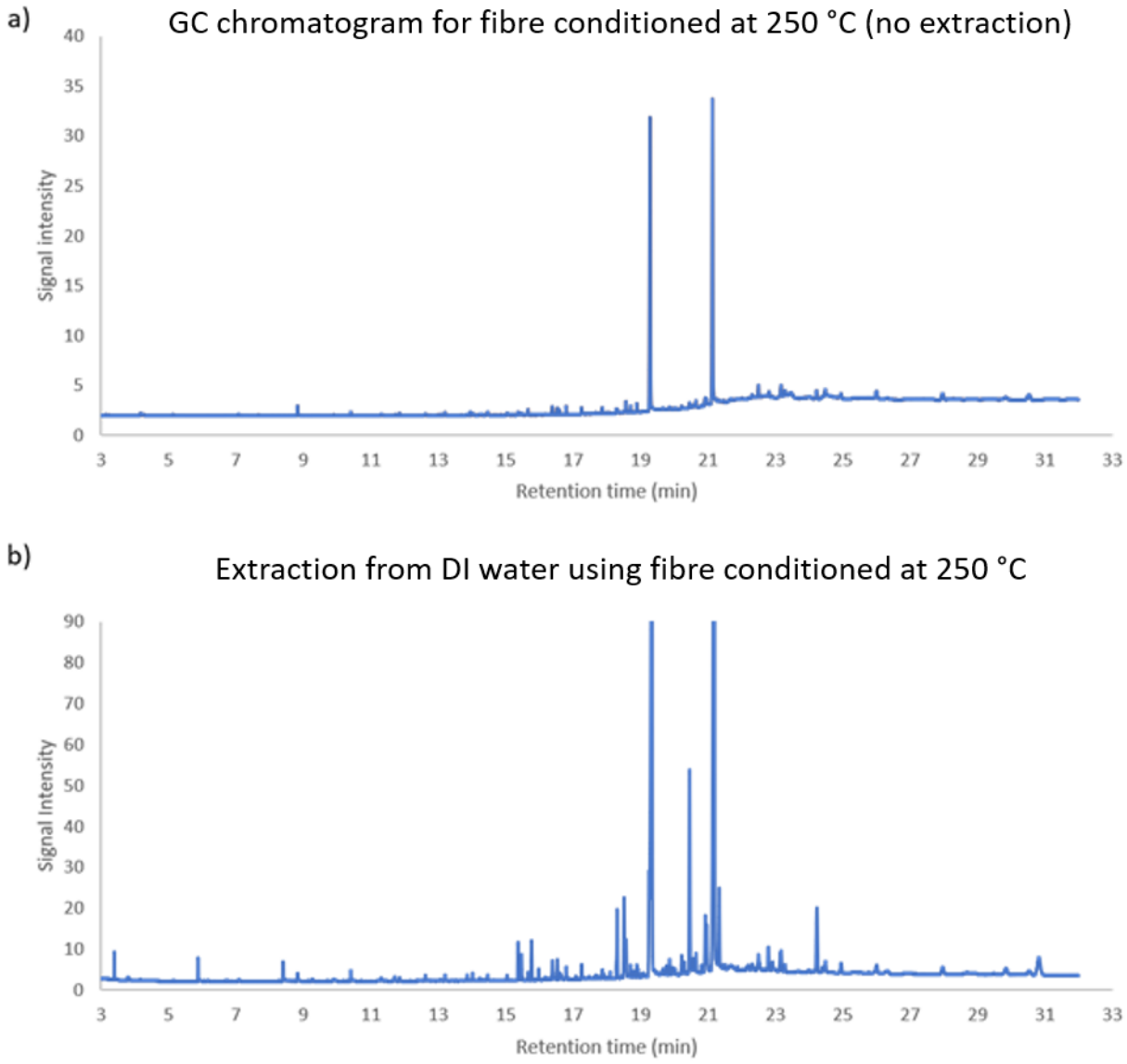

Figure 5.7 GC chromatogram for asphaltene-coated SPME fibre with a) no extraction b) extraction from deionized water (5 hours, 90 ^{o}C)

5.3.5 Optimization of conditioning temperatures

The conditioning temperature for the asphaltene coating is important for the amount of background signal. Ideally, a SPME coating should have a low background so that signals from the coating would not overlap or interfere with analyte signals. For previous optimizations (Figures 5.3-5.6), the asphaltene coating was conditioned at 250 ^{o}C. These optimizations were performed using a 100 μg/L PAH mixture, a relatively high concentration. The analyte signals are strong enough that the background does not cause interference. However, to detect very low concentrations, we must optimize for chemical noise and conditioning temperature.

Figure 5.7 shows the background for an asphaltene-coated SPME fibre conditioned at 250 ^{o}C. After conditioning at 250 ^{o}C, the fibre is directly inserted into the GC inlet for thermal desorption. The result is shown in Figure 5.7a. There are two large peaks at 19.3 and 21.1 minutes. Other than these two peaks, the background signal is fairly low. However, when the same fibre is used to extract from pure deionized water, the background becomes much more noisy. These extra signals do not come from the water, but rather from the asphaltene coating. Asphaltene is complex class of molecules that have a wide range of molecular weights, so it is not surprising to see these background peaks during a blank extraction. It is possible that during a blank extraction, moisture collects on the asphaltene coating, and dissolves a small amount of the coating, which then appears in the chromatogram during thermal desorption. Another explanation for these background peaks is that during thermal desorption in the GC inlet, the evaporation of moisture from the coating could dislodge small amounts of asphaltenes. This is not ideal for detection from a low concentration sample since these background peaks will interfere with the analyte.

In an attempt to reduce the background, the asphaltene-coated fibre was also conditioned at 300 ^{o}C and 330 ^{o}C. In Figure 5.8, asphaltene-coated fibres conditioned at different temperatures were used to extract from deionized water. The background for the 300 ^{o}C and 330 ^{o}C conditioned fibres are reduced dramatically compared to the 250 ^{o}C conditioned fibres. The two peaks at 19.3 and 21.1 minutes remain present, though they are reduced in intensity. This is not an issue for real samples as long as the analytes do not overlap with these two peaks. There is not much difference in background between 300 ^{o}C and 330 ^{o}C, so 300 ^{o}C is chosen as the optimal condition temperature for method development. Also, asphaltenes will begin to undergo rapid thermal degradation above 330 ^{o}C, so 300 ^{o}C is better for stability.

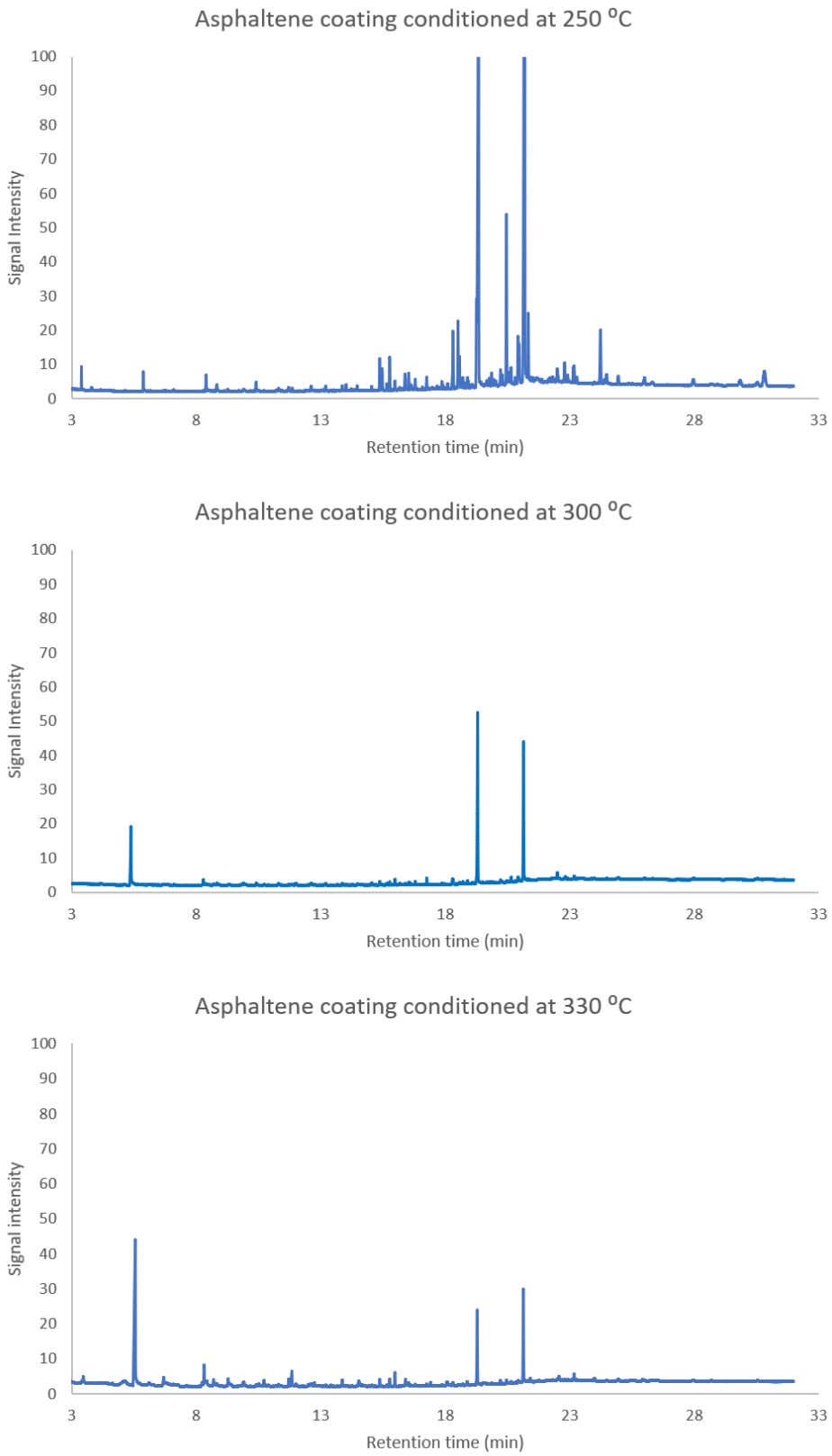

Figure 5.8 Extraction from deionized water using asphaltene-coated fibre conditioned at 250 °C, 300 °C, and 330 °C.

a)

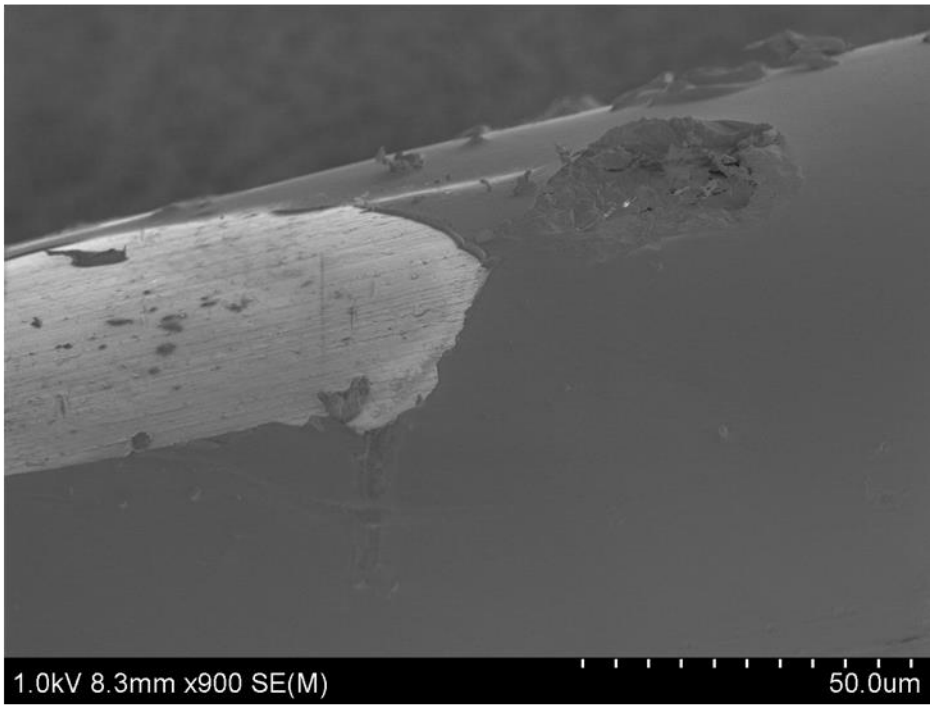

b)

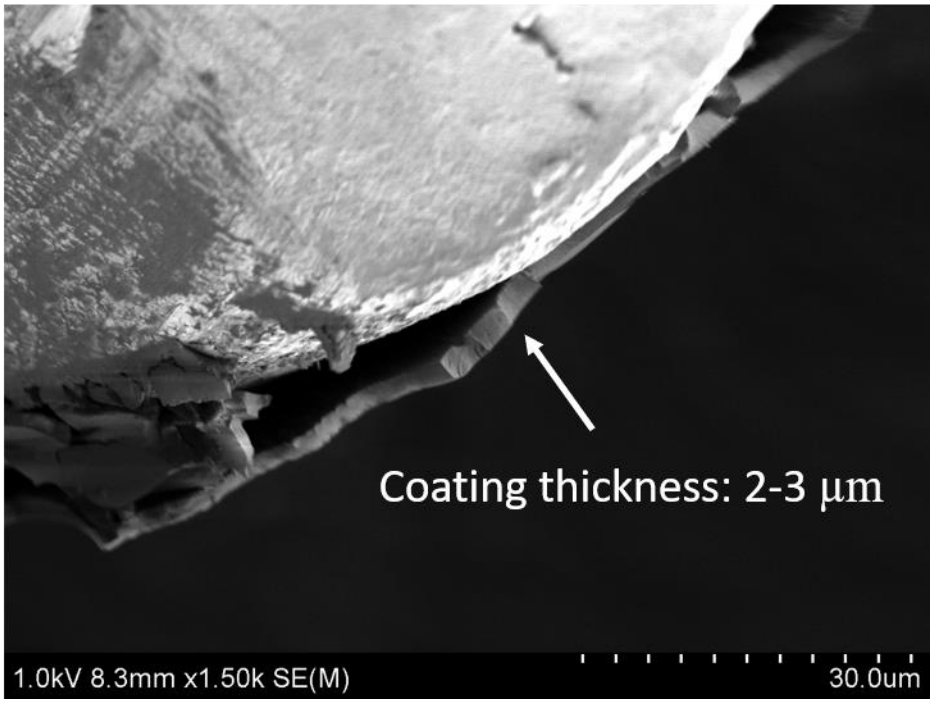

Figure 5.9 SEM image of asphaltene-coated fibre conditioned at 300 ^{o}C. a) top-view b) cross-sectional view.

5.3.6 SEM characterization

An asphaltene-coated fibre conditioned at 300 ^{o}C was imaged under SEM (Figure 5.9). The coating on the stainless-steel wire is smooth, with no discernible features, cracks, or abnormalities (the crack in the SEM image was purposely made to image the contrast between bare wire and the asphaltene coating). The fibre was also cut with a wire-cutter to image its cross-section. The asphaltene coating is clearly seen in the cross-sectional view, with the thickness being 2-3 μm. For comparison, commercially available PDMS coatings can range from 7 to 100 μm in thickness. Commercial polyacrylate or divinylbenzene coatings are also within this range in thickness.

5.3.7 Limits of detection

The limits of detection for a HS-SPME-GC method depend on various factors. Aside from the optimizations performed above, the ability to extract and detect analytes also heavily depends on the GC instrument and the detector. The same SPME coating, with the same extraction conditions, would exhibit a lower limit of detection using a two-dimensional GC separation rather than one-dimensional. The detector also plays an important role. A GC-MS instrument is typically more powerful than GC-FID because GC-MS can separate analytes not only in polarity, but also in mass. A flame-ionization detector is suitable for the detection of organic compounds, but it cannot be used differentiate analytes that have similar retention times. Hence, a discussion of the limits of detection must take into account the conditions under which the experiments are performed. Here, the limits of detection are presented in the context of the asphaltene coating, but other factors also play an important role.

During the optimization for the conditioning temperature, it was observed that the asphaltene coating itself contributes to the background of the chromatogram. This issue is especially concerning between 19 and 21 minutes on the chromatogram due to large signals from the asphaltenes. Two of the analytes, fluoranthene and pyrene, elute within this time frame and their limits of detection are affected by the background signal. Figure 5.10 shows the elution profile for fluoranthene. During a blank extraction with DI water, under the exact same conditions, there is a peak which elutes around 20.45 minutes. This peak comes from the asphaltene coating, and its intensity is fairly consistent across multiple SPME fibres. When the same extraction is done from a 100 ng/L PAH mixture, fluoranthene also elutes around 20.45 minutes. A conservative estimate of the limit of detection is calculated using the signal to noise ratio (equation 5.2). In this case, the intensity from the blank extraction is taken to be noise. At 100 ng/L, the signal to noise ratio is equal to 3, which is the limit of detection. Another method to estimate the limit of detection is the blank determination (equation 5.3).

$$LOD = 3\frac{S}{N} \qquad (5.2)$$

$$LOD = Blank + 3\sigma_B \qquad (5.3)$$

In the blank method, the limit of detection is the signal of the blank plus 3 times its standard deviation. For fluoranthene, the blank signal is the peak at 20.45 minutes from the DI water extraction. From three different SPME fibres, the average blank intensity is 17 with $\sigma_B =$

4. Using this method, the limit of detection is calculated to be 50 ng/L for fluoranthene (Figure 5.11).

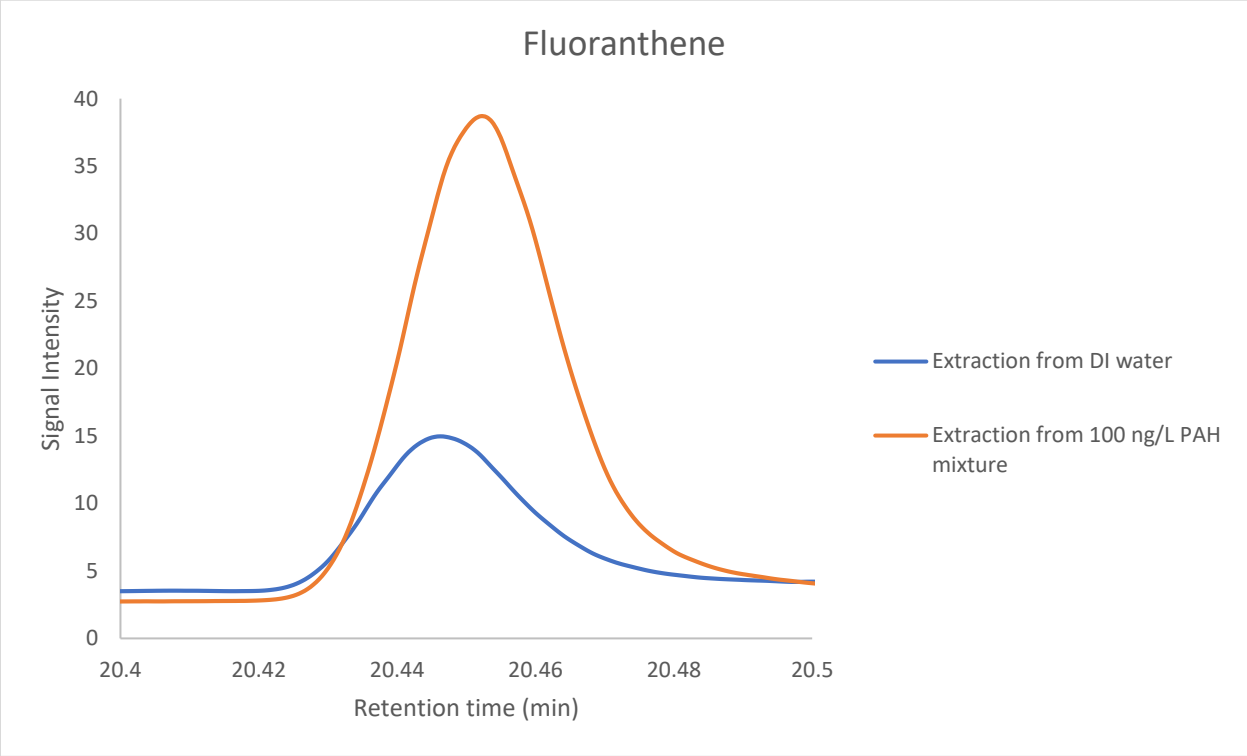

Figure 5.10 Extraction profile for fluoranthene peak with $LOD = 3S/N$.

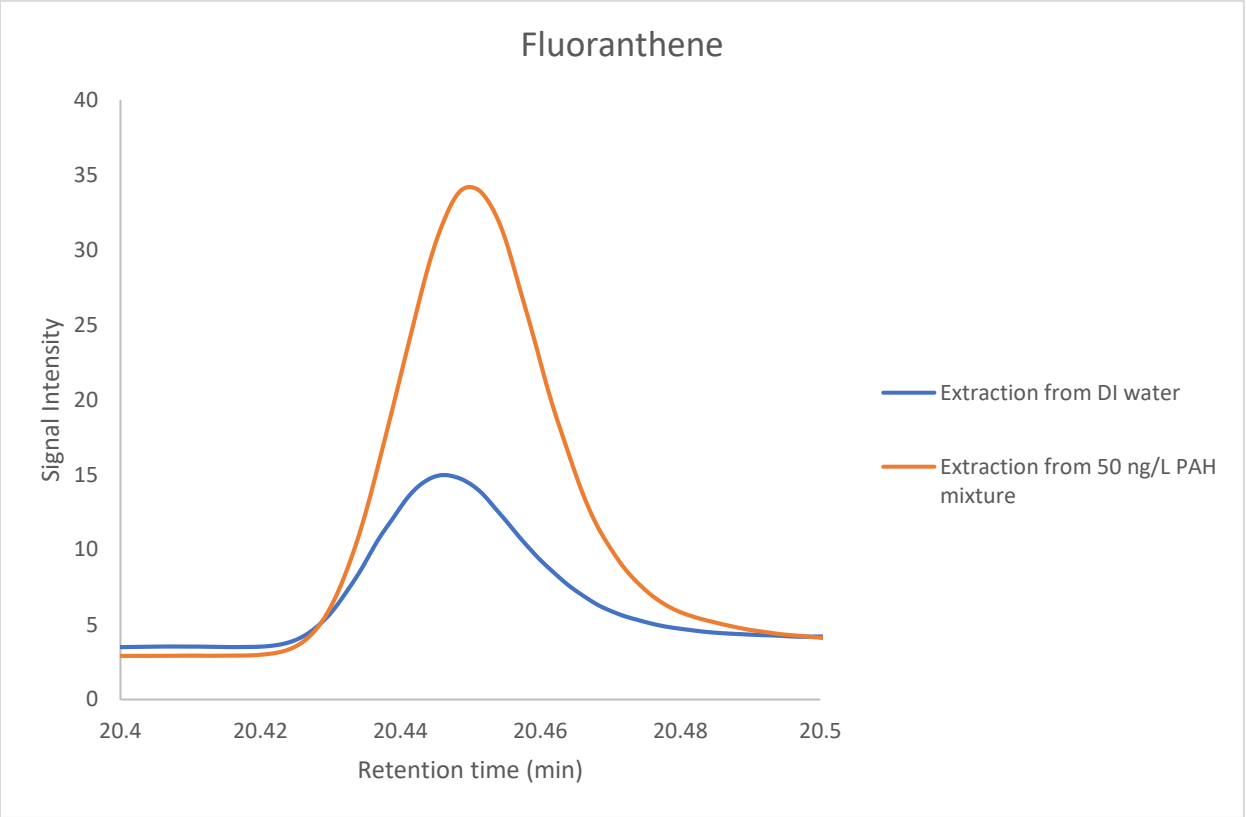

Figure 5.11 Extraction profile for fluoranthene peak with $LOD = Blank + 3\sigma_B$.

The calculation for the limit of detection for pyrene is complicated by the fact that pyrene elutes on the shoulder of a blank signal. Figure 5.12 shows the chromatograms for a blank extraction and an extraction from a 50 ng/L PAH mixture. In the blank extraction, there is a peak that elutes at 20.91 minutes with a small shoulder at 20.95 minutes. The actual pyrene peak also elutes at 20.95 minutes. At 50 ng/L, the pyrene peak is more than $3\sigma_B$ above the blank. However, when the concentration is less than 50 ng/L, the pyrene peak is less than this threshold. Therefore, the limit of detection for pyrene is determined to be 50 ng/L.

Both fluorene and benz[a]anthracene elute at quiet regions in the chromatogram. Figures 5.13 and 5.14 show the elution profiles for fluorene and benz[a]anthracene, respectively. The limits of detection for these two analytes are determined to be 20 ng/L and 10 ng/L, respectively. Table 5.1 summarizes the LOD for all four analytes including comparable values from literature. The comparisons from literature were all conducted using HS-SPME-GC-FID except for the graphene oxide-fused silica fibre, which was done using direct sampling. In Table 5.1, it is clear that commercial SPME fibres made from PDMS or PA do not have low limits of detection for these large, non-polar analytes. The LODs from commercial fibres range from 50 to 330 ng/L, which are all much higher than the asphaltene coating, as well as other coatings from literature. Even though fluoranthene and pyrene peaks were hindered by the blank, their LODs (50 ng/L) are lower than that from MWCNTs and CNT-composites.[16,17] By using microwave-assisted heating, which improves extraction time and sensitivity, fluoranthene and pyrene can be detected at as low as 30 ng/L with PDMS/PVB.[18,22] This is still comparable to the values obtained with the asphaltene coating. For both fluorene and benz[a]anthracene, the LODs from the asphaltene coating are the lowest among relevant literature. Benz[a]anthracene

is a 4-ring polycyclic compound, and these larger PAHs are not usually extracted using headspace-SPME. Larger PAHs have low vapour pressure and can only partition into the headspace at high temperatures. However, as discussed earlier, high temperature is detrimental to analyte adsorption onto the SPME coating. Microwave-assisted heating with PDMS/PVB had low LODs for fluoranthene and pyrene, but the LOD for benz[a]anthracene is 100 ng/L, which is an order of magnitude higher than that achieved using asphaltenes (10 ng/L). Only direct-sampling (which does not depend on the vapour pressure of analytes) with graphene oxide-fused silica achieved a comparable LOD for benz[a]anthracene.[14] Table 5.1 also shows the CCME environmental safety guidelines for the levels of fluorene, fluoranthene, pyrene, and benz[a]anthracene in fresh water. The LOD of the asphaltene coating is below the levels set by CCME for fluorene and benz[a]anthracene. Among the different coatings listed in Table 5.1, the asphaltene coating is the only example that can achieve a LOD below CCME's guideline using HS-SPME. These results show that the asphaltene coating is an excellent candidate for the extraction and detection of PAHs with HS-SPME-GC. This is not surprising since asphaltenes are non-polar with large polycyclic rings. The asphaltene coating shows superior performance in terms of its LOD compared to almost all "novel" coatings found in literature. Coatings such as carbon nanotubes require complicated, time-consuming, and costly manufacturing processes whereas the asphaltene coating can be fabricated in a matter of seconds using an inexpensive, easy process. This gives asphaltenes a tremendous advantage for any potential scale-up or commercialization.

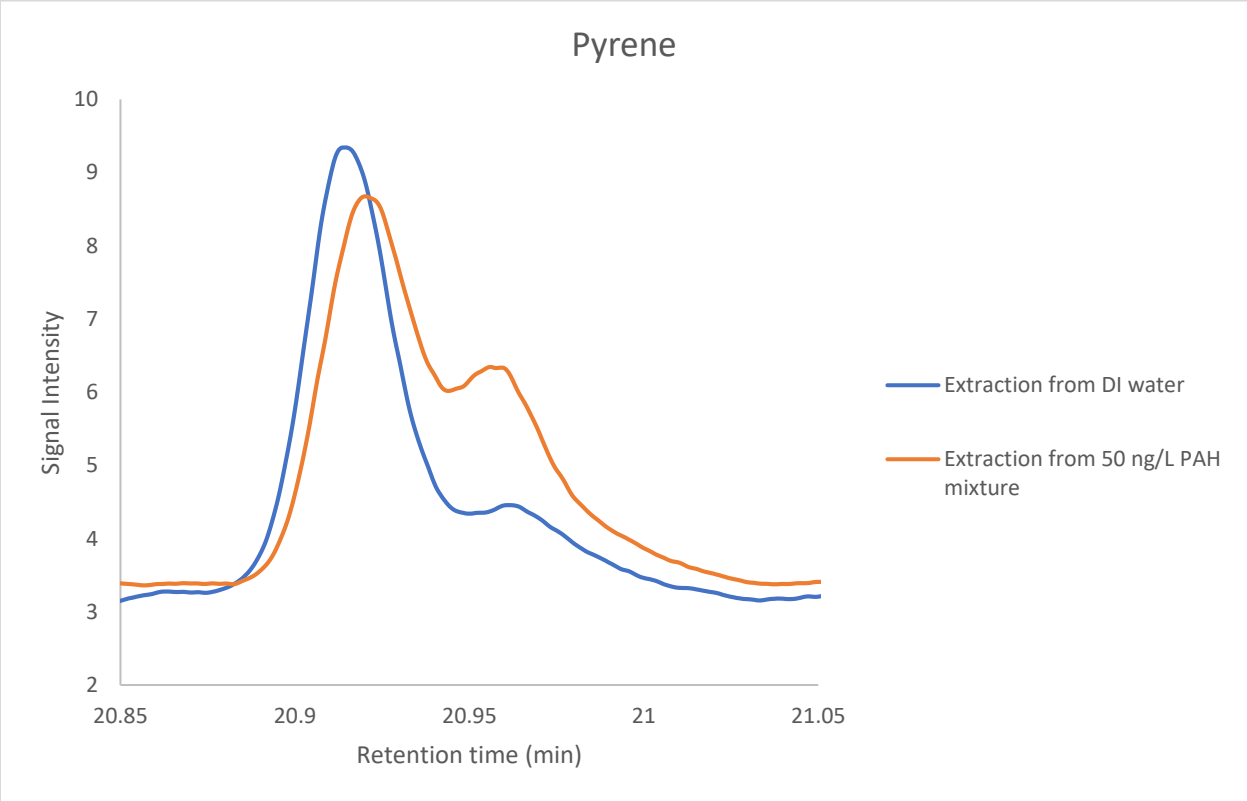

Figure 5.12 LOD for pyrene peak (20.95 min) showing extraction profiles from blank (water) and 50 ng/L PAH mixture.

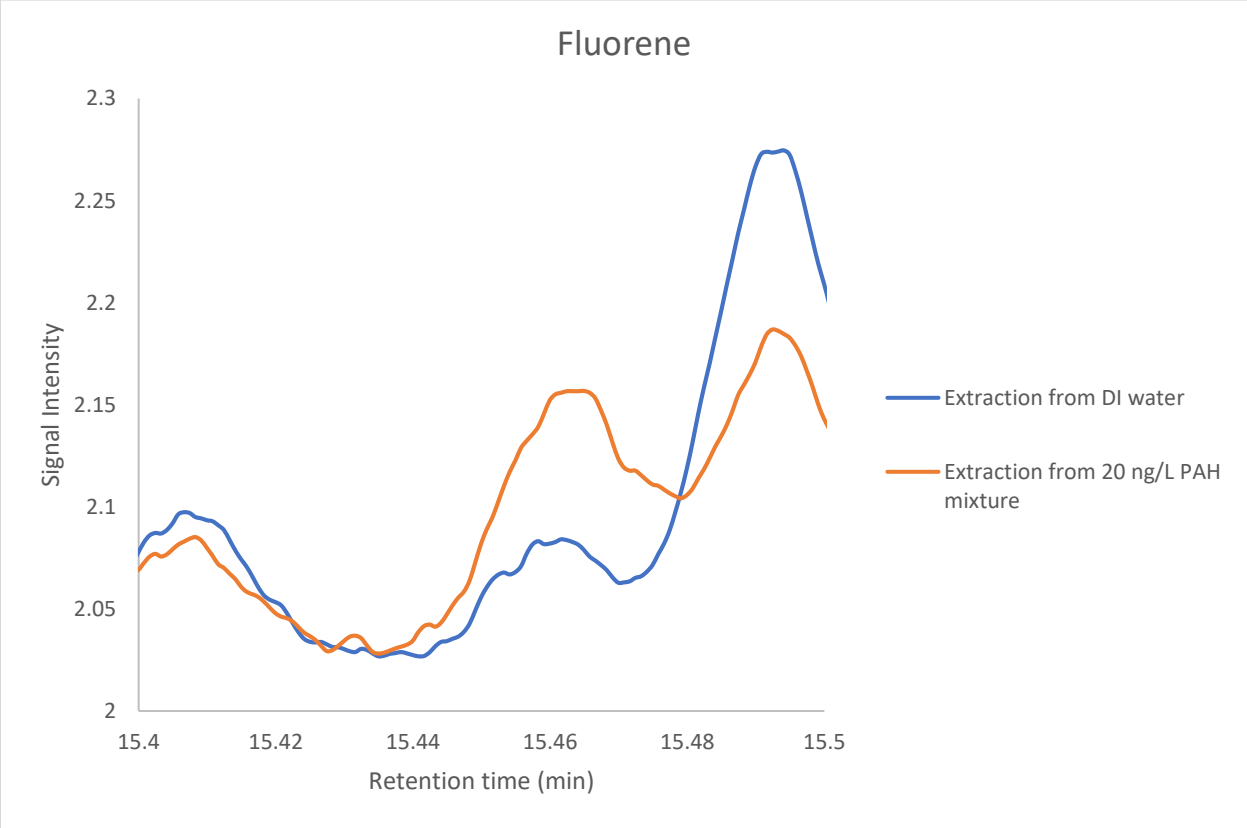

Figure 5.13 LOD for fluorene peak (15.46 min) showing extraction profiles from blank (water) and 20 ng/L PAH mixture.

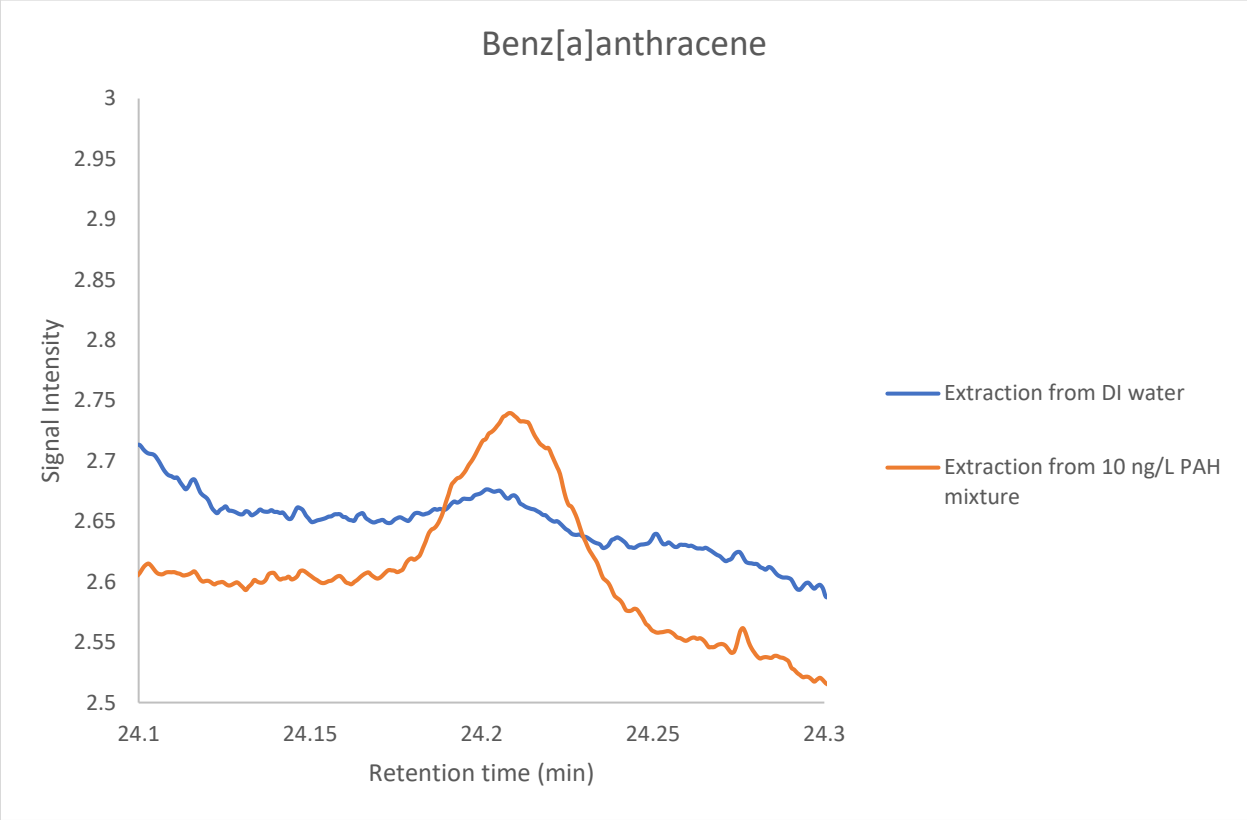

Figure 5.14 LOD for benz[a]anthracene peak (24.21 min) showing extraction profiles from blank (water) and 10 ng/L PAH mixture.

	CCME environmental safety guidelines for fresh water[6]	Asphaltene	MWCNTs[17]	CNTs/poly-ortho-phenylenediamine composite[16]	PDMS/PVB microwave assisted heating[18]	PDMS/PA[23]	Graphene oxide fused silica (not headspace)[14]
Fluorene	3000	20	40	20	80	80/80	40
Fluoranthene	40	50	70	70	30	250/170	
Pyrene	25	50		90	30	260/330	
Benz[a]anthracene	18	10			100	290/50	10

Table 5.1 Comparison of LODs (ng/L) for PAH using HS-SPME-GC-FID.

5.3.8 Linear range

Calibration curves for each of the four analytes are shown in Figure 5.15 and Table 5.2. The linear ranges for fluoranthene and pyrene are both 0.5-50 μg/L. Because of the interference from background peaks, the signals for fluoranthene and pyrene are not linear at low concentrations, even with background subtraction. However, the signal responses from fluorene and benz[a]anthracene are linear over four orders of magnitude, from 0.05-25 μg/L and 0.05-50 μg/L, respectively. Table 5.2 also shows the linear range of other SPME coatings from literature. There are some slight variations between coatings, but generally the lower end of the linearity ranges from 0.1 to 0.5 μg/L and the higher end ranges from 20-300 μg/L. This is very comparable to the asphaltene coating. One noticeable disadvantage for the asphaltene coating is that its linearity tops out at between 25-50 μg/L, whereas carbon nanotube-based coatings can achieve linearity up to 100-300 μg/L. This can be attributed to the fact that the asphaltene coating is a thin, smooth coating, but carbon nanotubes have a much higher surface area. However, despite this difference, the asphaltene coating performs impressively in terms of its linearity compared to more complicated, advanced, costly materials.

The linearity can be assessed using a residual plot, which plots the residuals (difference between actual signal area and fitted signal area) as a function of the fitted y-value. For a true linear relationship, a random distribution of residuals is expected. Figure 16 shows the residual plots for all four analytes. These residual plots seem to not show a true random distribution, but a U-shaped pattern instead. This suggests that the relationship is not completely linear, despite R^2 values that are close to 1 (Table 5.2). However, residual plots are most effective when the number of data points are large. With only 4 or 5 data points, such as in this case, it is difficult to discern whether the residuals are randomly distributed.

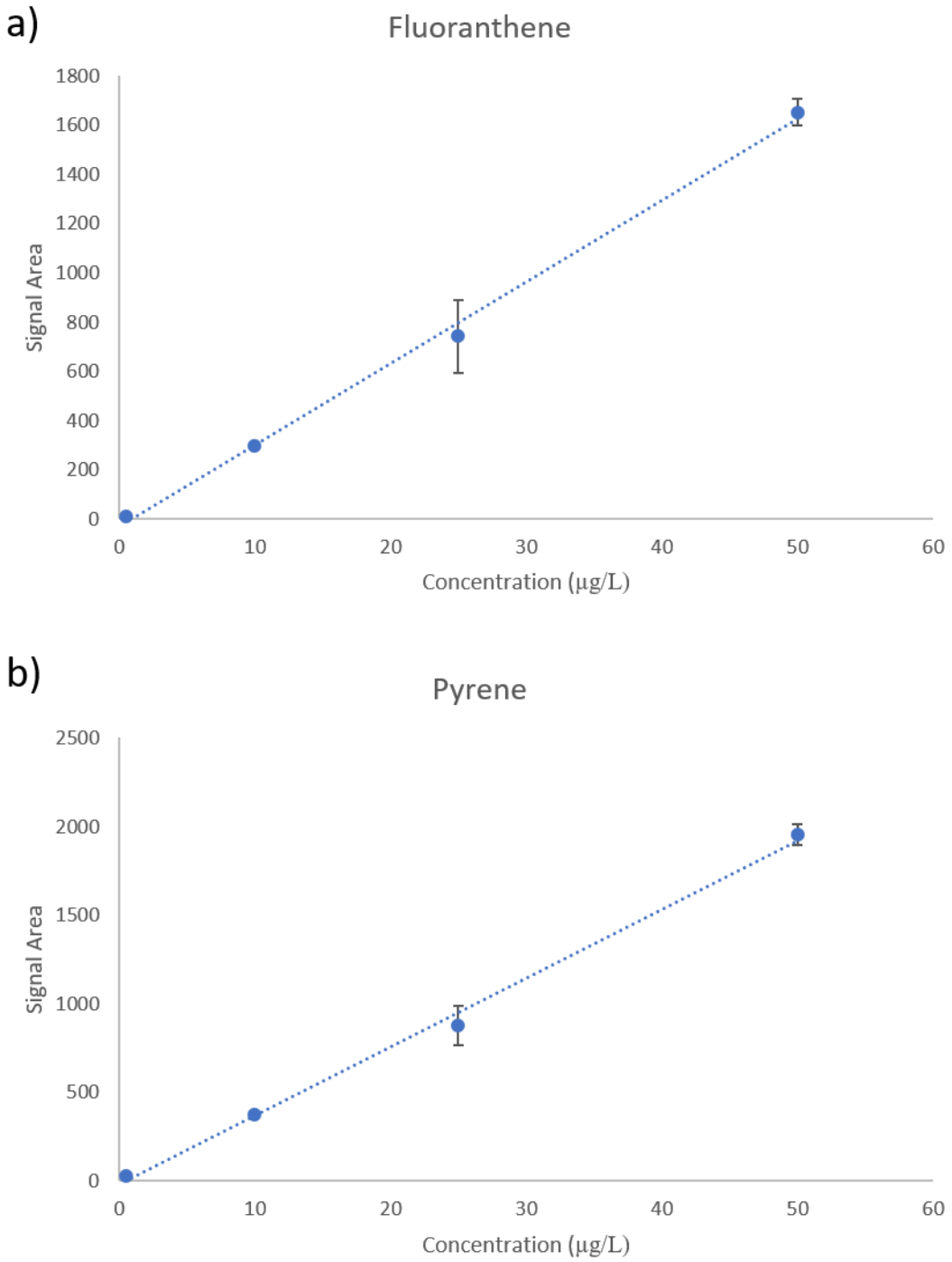

Figure 5.15 Linear range calibration curves for a) fluoranthene b) pyrene c) fluorene d) benz[a]anthracene. (*n=3*)

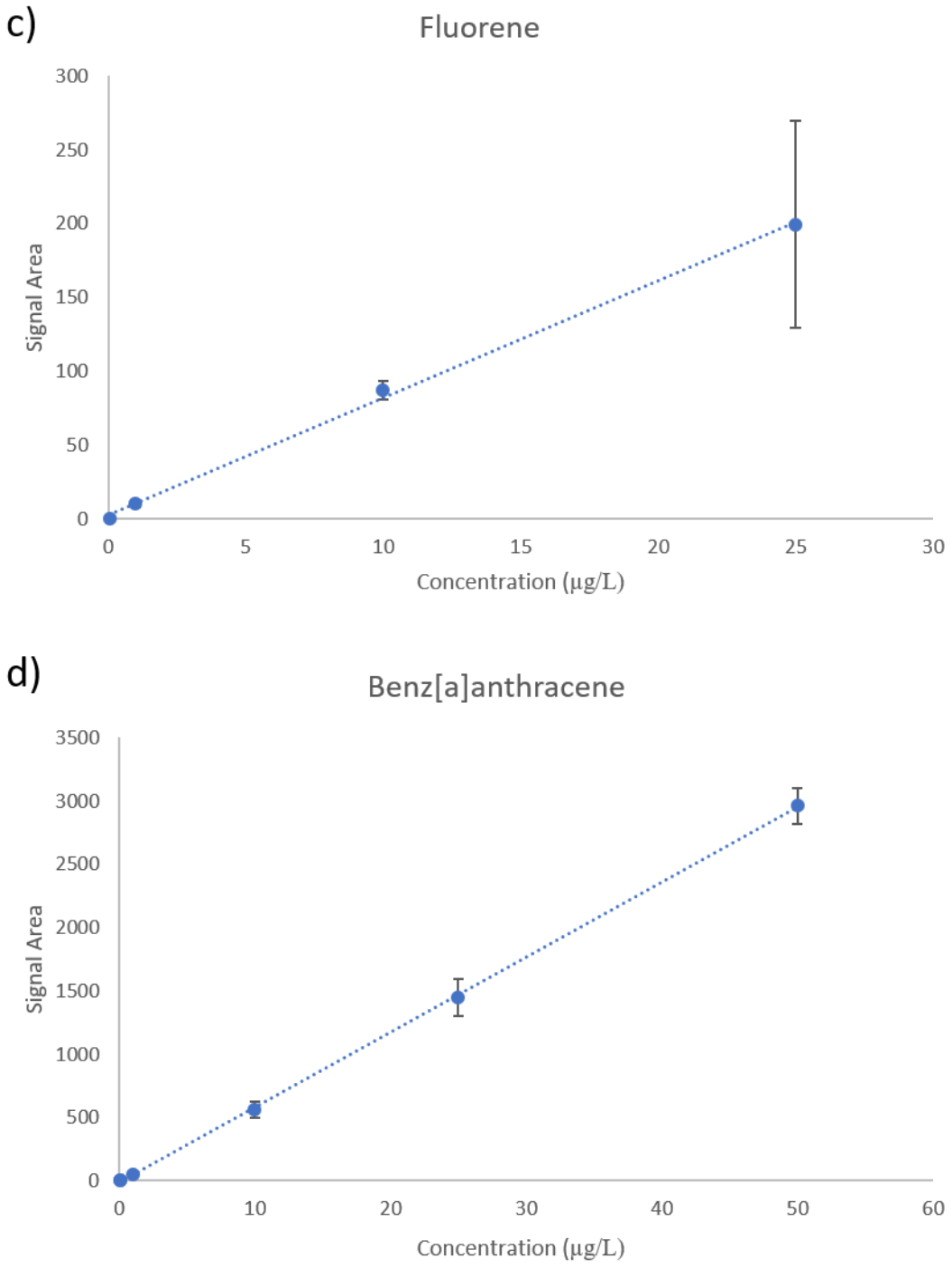

Figure 5.15 Linear range calibration curves for a) fluoranthene b) pyrene c) fluorene d) benz[a]anthracene. (*n=3*)

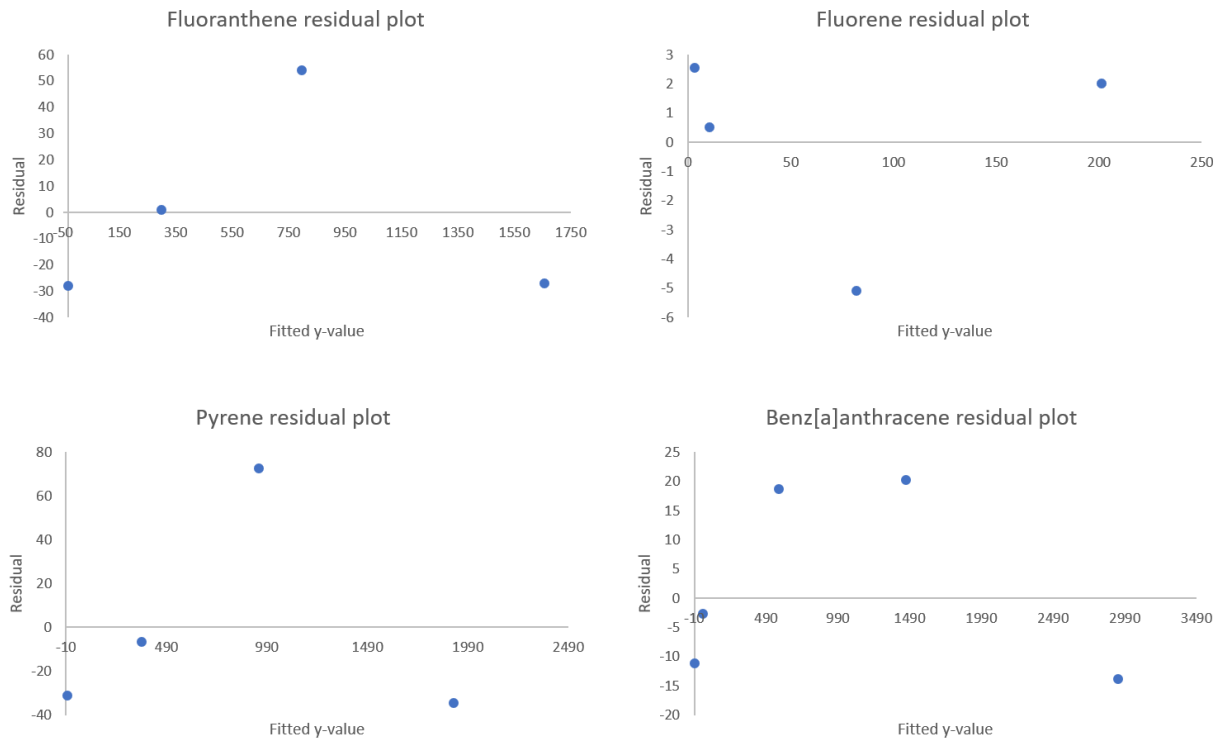

Figure 5.16 Residual plots to assess linearity.

	Linear range (µg/L) and R^2 for asphaltene coating	MWCNTs[17]	CNTs/poly-ortho-phenylenediamine composite[16]	PDMS/PVB microwave assisted heating[18]
Fluorene	0.05-25 (0.9985)	0.1-100	0.1-100	0.5-100
Fluoranthene	0.5-50 (0.9971)	0.5-50	0.5-300	0.1-20
Pyrene	0.5-50 (0.9965)		0.5-300	0.1-20
Benz[a]anthracene	0.05-50 (0.9998)			0.5-100

Table 5.2 Linear ranges and coefficients of determination for asphaltene SPME coating with comparisons from literature.

5.3.9 Reproducibility

	Intra-fibre relative STDEV	Inter-fibre relative STDEV
Fluorene	16±8%	16±7%
Fluoranthene	11±3%	5±3%
Pyrene	9±3%	5±3%
Benz[a]anthracene	10±1%	6±4%

Table 5.3 Intra- and inter-fibre relative standard deviation for asphaltene coating.

The reproducibility of these asphaltene-coated SPME fibres was investigated by extracting from a 10 μg/L PAH mixture on 6 different days, using 3 different SPME fibres each time. The intra-fibre relative standard deviation, which is the day-to-day variation in a single fibre, is approximately 10% for all analytes except for fluorene, which has a relative standard deviation of 16±8%. A similar trend is seen for inter-fibre relative standard deviation, which is the variation across multiple fibres on a single day. The inter-fibre relative standard deviation is approximately 5% for all analytes except for fluorene, which has a relative standard deviation of 16±7%. Overall, the relative standard deviations are standard compared to other works in literature.

5.4 Conclusion

A simple, cost-effective method of producing SPME fibres using asphaltenes was developed for the extraction and detection of polycyclic aromatic hydrocarbons. The limits of detection for fluorene, fluoranthene, pyrene, and benz[a]anthracene range from 10 to 50 ng/L. This matches, or even surpasses, the performance of other SPME coatings. One disadvantage of the asphaltene coating is the background noise due to leeching during a separation. However, even with this disadvantage, the performance (LOD and linear range) is excellent compared to more complicated and expensive materials, such as carbon nanotubes. The simplicity and performance of the asphaltene coating suggests asphaltenes has tremendous potential as an extraction tool. Asphaltenes can be used not only for the detection of PAHs, but for other classes of analytes as well. In ambient detection of molecules, where there is no solution involved, the asphaltene coating can potentially show even more impressive performance. In ambient extraction, leeching of the coating itself will not be a problem, which means the adsorption power of asphaltenes will not be hindered by background.

5.5 References

1. Phillips, D. H. & Grover, P. L. Polycyclic hydrocarbon activation: Bay regions and beyond. *Drug Metab. Rev.* **26,** 443–467 (1994).

2. Lima, A. L. C., Farrington, J. W. & Reddy, C. M. Combustion-derived polycyclic aromatic hydrocarbons in the environment - A review. *Environ. Forensics* **6,** 109–131 (2005).

3. Boffetta, P., Jourenkova, N. & Gustavsson, P. Cancer risk from occupational and environmental exposure to polycyclic aromatic hydrocarbons. *Cancer Causes Control* **8,** 444–72 (1997).

4. Phillips, D. H. Polycyclic aromatic hydrocarbons in the diet. *Mutat. Res.* **443,** 139–147 (1999).

5. Kelly, E. N. *et al.* Oil sands development contributes polycyclic aromatic compounds to the Athabasca River and its tributaries. *Proc. Natl. Acad. Sci.* **106,** 22346–22351 (2009).

6. CCME. *CARCINOGENIC AND OTHER POLYCYCLIC AROMATIC HYDROCARBONS (PAHs) (Environmental and Human Health Effects)*. *Canadian Council of Ministers of the Environment* (2010).

7. US EPA. *EPA Method 8270D: Semivolatile organic compounds by gas chromatography/mass spectrometry SW-846*. (2014).

8. Arthur, C. L. & Pawliszyn, J. Solid Phase Microextraction with Thermal Desorption Using Fused Silica Optical Fibres. *Anal. Chem.* **62,** 2145–2148 (1990).

9. Hernandez, F., Beltran, J., Lopez, F. J. & Gaspar, J. V. Use of solid-phase microextraction for the quantitative determination of herbicides in soil and water samples. *Anal. Chem.* **72,** 2313–2322 (2000).

10. Fucci, N., De Giovanni, N. & Chiarotti, M. Simultaneous detection of some drugs of abuse in saliva samples by SPME technique. *Forensic Sci. Int.* **134,** 40–45 (2003).

11. Nacham, O., Clark, K. D. & Anderson, J. L. Extraction and Purification of DNA from Complex Biological Sample Matrices Using Solid-Phase Microextraction Coupled with Real-Time PCR. *Anal. Chem.* **88,** 7813–7820 (2016).

12. Bagheri, H., Babanezhad, E. & Es-haghi, A. An aniline-based fibre coating for solid phase microextraction of polycyclic aromatic hydrocarbons from water followed by gas chromatography-mass spectrometry. *J. Chromatogr. A* **1152,** 168–174 (2007).

13. Bagheri, H., Akbarinejad, A. & Aghakhani, A. A highly thermal-resistant electrospun-based polyetherimide nanofibres coating for solid-phase microextraction Microextraction Techniques. *Anal. Bioanal. Chem.* **406,** 2141–2149 (2014).

14. Xu, L., Feng, J., Li, J., Liu, X. & Jiang, S. Graphene oxide bonded fused-silica fibre for solid-phase microextraction-gas chromatography of polycyclic aromatic hydrocarbons in

water. *J. Sep. Sci.* **35,** 93–100 (2012).

15. Banitaba, M. H., Hosseiny Davarani, S. S. & Kazemi Movahed, S. Comparison of direct, headspace and headspace cold fibre modes in solid phase microextraction of polycyclic aromatic hydrocarbons by a new coating based on poly(3,4-ethylenedioxythiophene)/graphene oxide composite. *J. Chromatogr. A* **1325,** 23–30 (2014).

16. Behzadi, M., Noroozian, E. & Mirzaei, M. A novel coating based on carbon nanotubes/poly-ortho-phenylenediamine composite for headspace solid-phase microextraction of polycyclic aromatic hydrocarbons. *Talanta* **108,** 66–73 (2013).

17. Maghsoudi, S. & Noroozian, E. HP-SPME of volatile polycyclic aromatic hydrocarbons from water using multiwalled carbon nanotubes coated on a steel fibre through electrophoretic deposition. *Chromatographia* **75,** 913–921 (2012).

18. Wei, M. C. & Jen, J. F. Determination of polycyclic aromatic hydrocarbons in aqueous samples by microwave assisted headspace solid-phase microextraction and gas chromatography/flame ionization detection. *Talanta* **72,** 1269–1274 (2007).

19. Ghiasvand, A. R., Hosseinzadeh, S. & Pawliszyn, J. New cold-fibre headspace solid-phase microextraction device for quantitative extraction of polycyclic aromatic hydrocarbons in sediment. *J. Chromatogr. A* **1124,** 35–42 (2006).

20. Mullins, O. C. The Modified Yen Model. *Energy & Fuels* **24,** 2179–2207 (2010).

21. Gorecki, T. & Pawliszyn, J. Effect of sample volume on quantitative analysis by solid-phase microextraction. Part 1. Theoretical considerations. *Anal. (Cambridge, United Kingdom)* **122,** 1079–1086 (1997).

22. Jocelyn Paré, J. R., Bélanger, J. M. R. & Stafford, S. S. Microwave-assisted process (MAP™): a new tool for the analytical laboratory. *Trends Anal. Chem.* **13,** 176–184 (1994).

23. Doong, R. a, Chang, S. M. & Sun, Y. C. Solid-phase microextraction for determining the distribution of sixteen US Environmental Protection Agency polycyclic aromatic hydrocarbons in water samples. *J. Chromatogr. A* **879,** 177–188 (2000).

Chapter 6

Conclusion, Outlook, and Future Direction

6.1 General outlook

Asphaltene is not an obscure or niche topic of research in chemistry. On the contrary, asphaltene has a very long history in the literature and its scope has been increasing dramatically in recent years. Part of the reason for this increase is that asphaltene is a ubiquitous fraction of heavy oils, and as the world's dependence on oil increases, as well as a shift from light to heavy crudes, the need to understand the chemistry of asphaltenes is imperative. In Figure 6.1, we can see the trend for the growing number of publications associated with asphaltenes since 1990. It is impossible to go through every single publication to read what it is about, but a simple analysis can be done by reading the title of each publication in 2018. Out of 372 publications in 2018 (as of November, research articles only), only 4 publications are investigating potential applications of asphaltenes.[1–4] Furthermore, out of these 4 publications, there are duplicates of very similar papers from the same research group, such as "Effect of Natural Macromolecule Filler on the Properties of High-Density Polyethylene (HDPE)" and "Use of asphaltene filler to improve low-density polyethylene properties". This means that out of the total number of publications involving asphaltenes, the number of unique papers using asphaltenes for practical applications is somewhere between 1 and 2%. The vast majority of publications, by far, is concerned about the chemistry, structure, and the behaviour of asphaltenes. Why are there so few publications and does this mean asphaltenes have no real potential for other uses? On the contrary, asphaltenes have tremendous potential, and not only for a single application. This is because asphaltenes have different properties that can be exploited, in particularly its high carbon content and its adsorptive properties. The lack of relevant research in this area is not a reflection of its

potential, but is rather due to neglect. Even today, the most basic, fundamental properties of asphaltenes, its structure and composition, are still up to debate. It is difficult to research the applications of a material when there are so much that are still not understood. Hence, it is not surprising that the majority of the research into asphaltenes is related to better understanding this material. However, this thesis has shown that even without a complete understanding of the material, possible applications can still be explored.

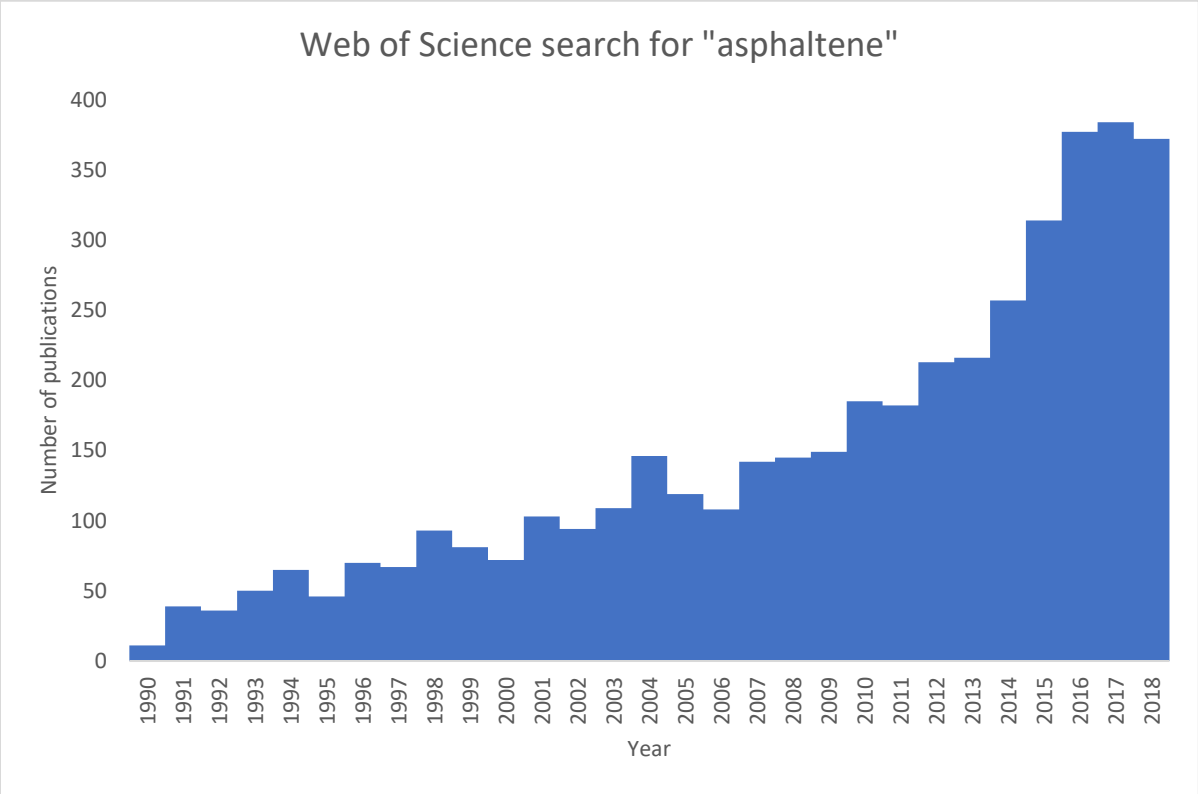

Figure 6.1 Web of Science search for “asphaltene” from 1990 to 2018.

6.2 Asphaltene as a carbon precursor

Even though the exact structures of asphaltenes are a source of controversy, one fact is undeniably true. Asphaltenes are predominately composed of carbon atoms. Because asphaltenes are organic molecules, they can be used as a precursor for other carbonaceous materials. Previous chapters have shown that graphitic electrodes and composite fibres can be made from asphaltenes. The performance of asphaltene-derived thin film electrodes was shown to be comparable to that of glassy carbon. Hence, how viable is using asphaltenes as a precursor for graphitic electrodes? From a cost perspective, asphaltenes have a tremendous advantage. Typical precursors for glassy carbon are polymers such as phenolic resins and poly(furfuryl) alcohol. For reference, the commercial cost of furfuryl alcohol is $86 CAD per kilogram (Sigma-Aldrich, as of November 2018). Asphaltenes are not commercially available for purchase, so a direct comparison cannot be made. However, an estimate can be made by using the price of bitumen. The price of Western Canadian Select, which is a heavy bitumen blend, ranges from $13.44 to $58.49 per barrel (159 L) in a one-year period. Taking the high end of this price range, this heavy oil blend sells for $0.36 per liter (~1 kg). Obviously, heavy oil is only composed of 10-20% asphaltenes, but we can get an idea of the price difference between polymer resins and asphaltenes. Currently, asphaltenes are considered to be a waste product. It is not purposefully manufactured for sale. Asphaltenes are removed from bitumen prior to refinement, or are spontaneously precipitated during recovery, transport, or refinement. There is currently no market for asphaltenes so it is a negative cost for the oil industry. This means that no additional processing is required for the production of asphaltenes, since it is made as a by-product. This further enhances the economic advantage of asphaltenes.

The performance of asphaltene-derived thin film electrodes has already been discussed previously. The conductivity and electron-transfer kinetics of these films mainly depend on the temperature and conditions during pyrolysis, whereas the starting material doesn't matter as much. This is why asphaltenes pyrolyzed at 1000 ^{o}C behave similarly to photoresist treated at the same temperature. This suggests that the most important factors, other than performance, for a viable precursor is carbon content and cost. Asphaltenes have a high carbon content, approximately 80%. This is advantageous because high carbon content leads to higher yield after pyrolysis. This was especially apparent when electrospun asphaltene-composite fibres were pyrolyzed. Electrospun composite fibres with asphaltenes as an additive led to greater yield after carbonization. There has been no research in literature for using asphaltenes as an additive for producing high carbon content materials. Even though we showed asphaltenes can be used, and has a positive impact on yield, there is no data on the effects of asphaltenes on the mechanical properties or electrochemical properties of these electrospun fibres. One active area of research is using carbonized, electrospun fibres in energy-related applications such as supercapacitors or anodes. However, one issue is the carbon yield after pyrolysis. Currently, polyacrylonitrile is the polymer of choice because it can be thermally stabilized, can be electrospun easily, and has a relatively high carbon yield at around 50% after pyrolysis. We have shown evidence that asphaltenes can increase the yield to above 50%, but so far there is no data on the performance of these fibres. It would be interesting and worthwhile to conduct mechanical, and electrochemical studies, such as measuring the capacitance of pyrolyzed PAN fibres compared to pyrolyzed PAN-asphaltene composite fibres.

6.3 Asphaltene as an adsorptive device

Asphaltene's main problem in industry is its tendency to precipitate and adsorb onto surfaces. However, this can also be asphaltene's most exploitable feature. If asphaltenes adsorb onto other surfaces, then molecules can adsorb onto asphaltenes as well. The previous chapter had shown that asphaltenes can be used as a coating for the extraction and detection of organic analytes. Not only was asphaltenes capable of this, the performance was on-par, or in some cases, even superior to more advanced nano-materials. The impressive performance is very promising for using asphaltenes as an analytical tool. There are a few examples of this in literature as well. The adsorptive feature of asphaltenes was used to remove dye compounds from water.[5] Despite the very small amount of research, we can see the power and potential of exploiting the adsorption of asphaltenes.

One issue in using asphaltenes for headspace-SPME is the leeching of the coating, and the large background it causes. This was somewhat diminished by thermally treating the coating at 300 ^{o}C, but the problem still persists. There are a couple of methods to potentially further lower the background. One method is to use a crosslinking agent to crosslink asphaltene molecules. Asphaltenes contain oxygen and sulfur functional groups, which can undergo covalent crosslinking reactions. Crosslinking agents have been used to reduce the aqueous solubility of electrospun fibres.[6–9] It could be possible to perform similar reactions on asphaltenes to reduce leeching into the moisture that condenses on the surface of the coating during headspace extraction. However, unlike simple polymers such as poly(vinyl) alcohol or collagen, asphaltenes are composed of countless different structures. There is no single monomer building block, or predictable locations of functional groups. The use of crosslinking

agents will be more complicated in this case. A trial and error approach will be required by trying different crosslinking agents such as glutaraldehyde, formaldehyde, etc. Another method to reduce the background is by thermal treatment. This works similarly to chemical agents because heat can also be used to crosslink molecules. A basic heat treatment at 300 ^{o}C was performed, but a more comprehensive study would be helpful, including slow temperature ramps, heat treatment for longer periods of time, and heat treatment in different atmospheres. A combination of these techniques could further improve the limit of detection and sensitivity of this SPME coating.

6.5 References

1. Siddiqui, M. N., Redhwi, H. H., Younas, M., Hussain, S. & Achilias, D. S. Use of asphaltene filler to improve low-density polyethylene properties. *Pet. Sci. Technol.* **36,** 756–764 (2018).

2. Pereira, M. L. D. O., Grasseschi, D. & Toma, H. E. Photocatalytic Activity of Reduced Graphene Oxide-Gold Nanoparticle Nanomaterials: Interaction with Asphaltene and Conversion of a Model Compound. *Energy and Fuels* **32,** 2673–2680 (2018).

3. Siddiqui, M. N. *et al.* Effect of Natural Macromolecule Filler on the Properties of High-Density Polyethylene (HDPE). *Macromol. Symp.* **380,** 1800072 (2018).

4. Lee, K. S., Park, C. W. & Kim, J. D. Synthesis of ZnO/activated carbon with high surface area for supercapacitor electrodes. *Colloids Surfaces A Physicochem. Eng. Asp.* **555,** 482–490 (2018).

5. Siddiqui, M. N. Developing an effective adsorbent from asphaltene for the efficient removal of dyes in aqueous solution. *Desalin. Water Treat.* **67,** 20450 (2017).

6. Luo, X. *et al.* Study on structure, mechanical property and cell cytocompatibility of electrospun collagen nanofibres crosslinked by common agents. *Int. J. Biol. Macromol.* **113,** 476–486 (2018).

7. Quinn, J. A., Yang, Y., Buffington, A. N., Romero, F. N. & Green, M. D. Preparation and characterization of crosslinked electrospun poly(vinyl alcohol) nanofibrous membranes. *Polymer (Guildf).* **134,** 275–281 (2018).

8. Mashayekhi, M., Mirzadeh, H. & Bagheri-khoulenjani, S. Effects of Crosslinking and Neutralization Agents on the Morphology of Chitosan Electrospun Scaffolds. **29,** 521–531 (2017).

9. Lu, T. & Olesik, S. V. Electrospun polyvinyl alcohol ultra-thin layer chromatography of amino acids. *J. Chromatogr. B Anal. Technol. Biomed. Life Sci.* **912,** 98–104 (2013).

Complete list of references

Acevedo, S. *et al.* Importance of asphaltene aggregation in solution in determining the adsorption of this sample on mineral surfaces. *Colloids Surfaces A Physicochem. Eng. Asp.* **166,** 145–152 (2000).

Acevedo, S., Ranaudo, M. A., García, C., Castillo, J. & Fernández, A. Adsorption of asphaltenes at the toluene-silica interface: A kinetic study. *Energy and Fuels* **17,** 257–261 (2003).

Aisenberg, S. & Chabot, R. Ion-beam deposition of thin films of diamondlike carbon. *J. Appl. Phys.* **42,** 2953–2958 (1971).

Ali, M. F. & Saleem, M. Thermal Decomposition of Saudi Crude Oil Asphaltenes. *Fuel Sci. Technol. Int.* **9,** 461–484 (1991).

Aliabadi, M., Irani, M., Ismaeili, J., Piri, H. & Parnian, M. J. Electrospun nanofibre membrane of PEO/Chitosan for the adsorption of nickel, cadmium, lead and copper ions from aqueous solution. *Chem. Eng. J.* **220,** 237–243 (2013).

Aluigi, A. *et al.* Structure and properties of keratin/PEO blend nanofibres. *Eur. Polym. J.* **44,** 2465–2475 (2008).

Arthur, C. L. & Pawliszyn, J. Solid Phase Microextraction with Thermal Desorption Using Fused Silica Optical Fibres. *Anal. Chem.* **62,** 2145–2148 (1990).

Aurbach, D., Markovsky, B., Weissman, I., Levi, E. & Ein-Eli, Y. On the correlation between surface chemistry and performance of graphite negative electrodes for Li ion batteries. *Electrochim. Acta* **45,** 67–86 (1999).

Bagheri, H. & Aghakhani, A. Novel nanofiber coatings prepared by electrospinning technique for headspace solid-phase microextraction of chlorobenzenes from environmental samples. *Anal. Methods* **3,** 1284–1289 (2011).

Bagheri, H., Aghakhani, A., Baghernejad, M. & Akbarinejad, A. Novel polyamide-based nanofibres prepared by electrospinning technique for headspace solid-phase microextraction of phenol and chlorophenols from environmental samples. *Anal. Chim. Acta* **716,** 34–39 (2012).

Bagheri, H., Akbarinejad, A. & Aghakhani, A. A highly thermal-resistant electrospun-based polyetherimide nanofibres coating for solid-phase microextraction. *Anal. Bioanal. Chem.* **406,** 2141–2149 (2013).

Bagheri, H., Babanezhad, E. & Es-haghi, A. An aniline-based fibre coating for solid phase microextraction of polycyclic aromatic hydrocarbons from water followed by gas chromatography-mass spectrometry. *J. Chromatogr. A* **1152,** 168–174 (2007).

Baker, R. T. K., Barber, M. A., Harris, P. S., Feates, F. S. & Waite, R. J. Nucleation and growth of carbon deposits from the nickel catalyzed decomposition of acetylene. *J. Catal.* **26,** 51–62 (1972).

Baltzis, D., Orfanidis, S., Lekatou, A. & Paipetis, A. S. Stainless steel coupled with carbon nanotube- modified epoxy and carbon fibre composites : Electrochemical and mechanical study Stainless steel coupled with carbon nanotube- modified epoxy and carbon fibre composites : *Plast. Rubber Compos.* **8011,** 95–105 (2016).

Banitaba, M. H., Hosseiny Davarani, S. S. & Kazemi Movahed, S. Comparison of direct, headspace and headspace cold fibre modes in solid phase microextraction of polycyclic aromatic hydrocarbons by a new coating based on poly(3,4-ethylenedioxythiophene)/graphene oxide composite. *J. Chromatogr. A* **1325,** 23–30 (2014).

Bard, R. J., Baxman, H. R., Bertino, J. P. & O'Rourke, J. A. Pyrolytic Carbons Deposited in Fluidized Beds At 1200 To 1400 ° C From Various Hydrocarbons. *Carbon N. Y.* **6,** 603–616 (1967).

Bashir, Z. A critical review of the stabilisation of polyacrylonitrile. *Carbon N. Y.* **29,** 1081–1090 (1991).

Behzadi, M., Noroozian, E. & Mirzaei, M. A novel coating based on carbon nanotubes/poly-ortho-phenylenediamine composite for headspace solid-phase microextraction of polycyclic aromatic hydrocarbons. *Talanta* **108,** 66–73 (2013).

Beilby, A. L. & Carlsson, A. A pyrolytic carbon film electrode for voltammetry. *J. Electroanal. Chem. Interfacial Electrochem.* **248,** 283–304 (1988).

Bergshoef, M. M. & Vancso, G. J. Transparent nanocomposites with ultrathin, electrospun nylon-4,6 fibre reinforcement. *Adv. Mater.* **11,** 1362–1365 (1999).

Bi, X.-X. *et al.* Nanoscale carbon blacks produced by CO2 laser pyrolysis. *J. Mater. Res.* **10,** 2875–2884 (1995).

Bishop, A., Balázsi, C., Yang, J. H. & Gouma, P. I. Biopolymer-hydroxyapatite composite coatings prepared by electrospinning. *Polym. Adv. Technol.* **17,** 395–418 (2006).

Blackstock, J. J. *et al.* Ultraflat carbon film electrodes prepared by electron beam evaporation. *Anal. Chem.* **76,** 2544–2552 (2004).

Boffetta, P., Jourenkova, N. & Gustavsson, P. Cancer risk from occupational and environmental exposure to polycyclic aromatic hydrocarbons. *Cancer Causes Control* **8,** 444–72 (1997).

Brabec, Christoph J., et al. Origin of the open circuit voltage of plastic solar cells. *Adv. Funct. Mater.* **11,** 374–380. (2001).

Byrne, C. E. & Nagle, D. C. Carbonization of wood for advanced materials applications. *Carbon N. Y.* **35,** 259–266 (1997).

CCME. *CARCINOGENIC AND OTHER POLYCYCLIC AROMATIC HYDROCARBONS (PAHs)*

(Environmental and Human Health Effects). *Canadian Council of Ministers of the Environment* (2010).

Chandra, S., Das, P., Bag, S., Laha, D. & Pramanik, P. Synthesis, functionalization and bioimaging applications of highly fluorescent carbon nanoparticles. *Nanoscale* **3,** 1533 (2011).

Chen, C., Kennel, E. B., Stiller, A. H., Stansberry, P. G. & Zondlo, J. W. Carbon foam derived from various precursors. *Carbon N. Y.* **44,** 1535–1543 (2006).

Chen, P. & McCreery, R. L. Control of Electron Transfer Kinetics at Glassy Carbon Electrodes by Specific Surface Modification. *Anal. Chem.* **68,** 3958–3965 (1996).

Chen, Z. *et al.* High-performance supercapacitors based on hierarchically porous graphite particles. *Adv. Energy Mater.* **1,** 551–556 (2011).

Chronakis, I. S. Novel nanocomposites and nanoceramics based on polymer nanofibers using electrospinning process - A review. *J. Mater. Process. Technol.* **167,** 283–293 (2005).

Conley, R. T. & Bieron, J. F. Examination of the oxidative degradation of polyacrylonitrile using infrared spectroscopy. *J. Appl. Polym. Sci.* **7,** 1757–1773 (1963).

Dalton, A. B. *et al.* Super-tough carbon-nanotube fibres. *Nature* **423,** 703–703 (2003).

Danumah, C., Myles, A. J. & Fenniri, H. Graphitic Carbon Nanoparticles from Asphaltenes. *MRS Proc.* **1312,** (2011).

Datta, M. K. *et al.* Amorphous silicon – carbon based nano-scale thin film anode materials for lithium ion batteries. *Electrochim. Acta* **56,** 4717–4723 (2014).

Davini, P. Desulphurization properties of active carbons obtained from petroleum pitch pyrolysis. *Carbon N. Y.* **37,** 1363–1371 (1999).

Deakin, M. R., Kovach, P. M., Stutts, K. J. & Wightman, R. M. Heterogeneous Mechanisms of the Oxidation of Catechols and Ascorbic Acid at Carbon Electrodes. *Anal. Chem.* **58,** 1474–1480 (1986).

Dong, Q. *et al.* Ultrasound-assisted preparation of electrospun carbon nanofibre/graphene composite electrode for supercapacitors. *J. Power Sources* **243,** 350–353 (2013).

Doong, R. a, Chang, S. M. & Sun, Y. C. Solid-phase microextraction for determining the distribution of sixteen US Environmental Protection Agency polycyclic aromatic hydrocarbons in water samples. *J. Chromatogr. A* **879,** 177–188 (2000).

Du, R., Ssenyange, S., Aktary, M. & McDermott, M. T. Fabrication and characterization of graphitic carbon nanostructures with controllable size, shape, and position. *Small* **5,** 1162–1168 (2009).

Dubey, S. . & Waxman, M. . Asphaltene Adsorption and Desorption From Mineral Surfaces. *SPE Reserv. Eng.* **6,** 389–395 (1991).

Dudášová, D., Silset, A. & Sjöblom, J. Quartz crystal microbalance monitoring of asphaltene adsorption/ deposition. *J. Dispers. Sci. Technol.* **29,** 139–146 (2008).

Duley, W. W. Refractive indices for amorphous carbon. *Astrophys. J.* **287,** 694–696 (1984).

DuVall, S. H. & McCreery, R. L. Control of catechol and hydroquinone electron-transfer kinetics on native and modified glassy carbon electrodes. *Anal. Chem.* **71,** 4594–4602 (1999).

Duvall, S. H. & McCreery, R. L. Self-catalysis by catechols and quinones during heterogeneous electron transfer at carbon electrodes. *J. Am. Chem. Soc.* **122,** 6759–6764 (2000).

Endo, M. & Pimenta, M. A. Origin of dispersive effects of the raman d band in carbon materials. *Phys. Rev. B - Condens. Matter Mater. Phys.* **59,** R6585–R6588 (1999).

Endo, M. *et al.* Anode performance of a Li ion battery based on graphitized and B-doped milled mesophase pitch-based carbon fibres. *Carbon N. Y.* **37,** 561–568 (1999).

Fan, Z. *et al.* A three-dimensional carbon nanotube/graphene sandwich and its application as electrode in supercapacitors. *Adv. Mater.* **22,** 3723–3728 (2010).

Fang, X. & Reneker, D. H. DNA fibers by electrospinning. *J. Macromol. Sci. Part B* **36,** 169–173 (1997).

Fialkov, A. S., Baver, A. I., Sidorov, N. M., Chaikun, M. I., & Rabinovich, S. M. Pyrographite (preparation, structure, properties). *Russ. Chem. Rev.* **34,** 46–58 (1965).

Fitzer, E., Schaefer, W. & Yamada, S. The formation of glasslike carbon by pyrolysis of polyfurfuryl alcohol and phenolic resin. *Carbon N. Y.* **7,** 643–648 (1969).

Fochler, H. S., Mooney, J. R., Ball, L. E., Boyer, R. D. & Grasselli, J. G. Infrared and NMR spectroscopic studies of the thermal degradation of polyacrylonitrile. *Spectrochim. Acta Part A Mol. Spectrosc.* **41,** 271–278 (1985).

Formhals, A. Artificial Thread and Method of Producing Same. **16187,** (1940).

Formhals, A. Methods and apparatus for Spinning. 1–5 (1944).

Formhals, A. Production of artifcial fibres from fibre forming liquids. 2–5 (1943).

Fucci, N., De Giovanni, N. & Chiarotti, M. Simultaneous detection of some drugs of abuse in saliva samples by SPME technique. *Forensic Sci. Int.* **134,** 40–45 (2003).

Gao, W. *et al.* Direct laser writing of micro-supercapacitors on hydrated graphite oxide films. *Nat. Nanotechnol.* **6,** 496–500 (2011).

Ge, J. J. *et al.* Assembly of well-aligned multiwalled carbon nanotubes in confined polyacrylonitrile environments: Electrospun composite nanofibre sheets. *J. Am. Chem. Soc.* **126,** 15754–15761 (2004).

George, R., Kashyap, K. T., Rahul, R. & Yamdagni, S. Strengthening in carbon nanotube/aluminium (CNT/Al) composites. *Scr. Mater.* **53,** 1159–1163 (2005).

Ghiasvand, A. R., Hosseinzadeh, S. & Pawliszyn, J. New cold-fibre headspace solid-phase microextraction device for quantitative extraction of polycyclic aromatic hydrocarbons in sediment. *J. Chromatogr. A* **1124,** 35–42 (2006).

Gojny, F. H., Wichmann, M. H. G., Köpke, U., Fiedler, B. & Schulte, K. Carbon nanotube-reinforced epoxy-composites: Enhanced stiffness and fracture toughness at low nanotube content. *Compos. Sci. Technol.* **64,** 2363–2371 (2004).

Gorecki, T. & Pawliszyn, J. Effect of sample volume on quantitative analysis by solid-phase microextraction. Part 1. Theoretical considerations. *Anal. (Cambridge, United Kingdom)* **122,** 1079–1086 (1997).

Gray, M. R., Tykwinski, R. R., Stryker, J. M. & Tan, X. Supramolecular assembly model for aggregation of petroleum asphaltenes. *Energy and Fuels* **25,** 3125–3134 (2011).

Groenzin, H. & Mullins, O. C. Petroleum asphaltene molecular size and structure. *ACS Div. Fuel Chem. Prepr.* **44,** 728–732 (1999).

Hadi, M., Rouhollahi, A. & Yousefi, M. Chemical Nanocrystalline graphite-like pyrolytic carbon film electrode for electrochemical sensing of hydrazine. *Sensors Actuators B. Chem.* **160,** 121–128 (2011).

Hebert, N. E., Snyder, B., McCreery, R. L., Kuhr, W. G. & Brazill, S. A. Performance of pyrolyzed photoresist carbon films in a microchip capillary electrophoresis device with sinusoidal voltammetric detection. *Anal. Chem.* **75,** 4265–4271 (2003).

Hernandez, F., Beltran, J., Lopez, F. J. & Gaspar, J. V. Use of solid-phase microextraction for the quantitative determination of herbicides in soil and water samples. *Anal. Chem.* **72,** 2313–2322 (2000).

Hirono, S., Umemura, S., Tomita, M. & Kaneko, R. Superhard conductive carbon nanocrystallite films. *Appl. Phys. Lett.* **80,** 425–427 (2002).

Hou, H. & Reneker, D. H. Carbon Nanotubes on Carbon Nanofibers: A Novel Structure Based on Electrospun Polymer Nanofibers. *Adv. Mater.* **16,** 69–73 (2004).

Hou, H. *et al.* Electrospun polyacrylonitrile nanofibres containing a high concentration of well-aligned multiwall carbon nanotubes. *Chem. Mater.* **17,** 967–973 (2005).

Hu, I. F. & Kuwana, T. Oxidative Mechanism of Ascorbic Acid at Glassy Carbon Electrodes. *Anal. Chem.* **58,** 3235–3239 (1986).

Jada, A. & Debih, H. Hydrophobation of clay particles by asphaltenes adsorption. *Compos. Interfaces* **16,** 219–235 (2009).

Jain, S., Sharma, A. & Basu, B. Vertical electric field stimulated neural cell functionality on porous amorphous carbon electrodes. *Biomaterials* **34,** 9252–9263 (2013).

Ji, L., Jung, K.-H., Medford, A. J. & Zhang, X. Electrospun polyacrylonitrile fibers with dispersed Si

nanoparticles and their electrochemical behaviors after carbonization. *J. Mater. Chem.* **19,** 4992 (2009).

Ji, L., Jung, K.-H., Medford, A. J. & Zhang, X. Electrospun polyacrylonitrile fibres with dispersed Si nanoparticles and their electrochemical behaviors after carbonization. *J. Mater. Chem.* **19,** 4992 (2009).

Ji, X., Banks, C. E., Crossley, A. & Compton, R. G. Oxygenated edge plane sites slow the electron transfer of the ferro-/ferricyanide redox couple at graphite electrodes. *ChemPhysChem* **7,** 1337–1344 (2006).

Jia, J. *et al.* Structure and Electrochemical Properties of Carbon Films Prepared by a Electron Cyclotron Resonance Sputtering Method. *Anal. Chem.* **79,** 893–900 (2007).

Jocelyn Paré, J. R., Bélanger, J. M. R. & Stafford, S. S. Microwave-assisted process (MAP^{TM}): a new tool for the analytical laboratory. *Trends Anal. Chem.* **13,** 176–184 (1994).

Jönsson, G. & Gorton, L. An amperometric glucose sensor made by modification of a graphite electrode surface with immobilized glucose oxidase and adsorbed mediator. *Biosensors* **1,** 355–368 (1985).

Jönsson, G. & Gorton, L. An electrochemical sensor for hydrogen peroxide based on peroxidase adsorbed on a spectrographic graphite electrode. *Electroanalysis* **1,** 465–468 (1989).

Kampalanonwat, P. & Supaphol, P. Preparation and adsorption behavior of aminated electrospun polyacrylonitrile nanofiber mats for heavy metal ion removal. *ACS Appl. Mater. Interfaces* **2,** 3619–3627 (2010).

Karimi, A. *et al.* Quantitative Evidence for Bridged Structures in Asphaltenes by Thin Film Pyrolysis. *Energy & Fuels* **25,** 3581–3589 (2011).

Karu, A. E. & Beer, M. Pyrolytic formation of highly crystalline graphite films. *J. Appl. Phys.* **37,** 2179–2181 (1966).

Kashiwagi, T. *et al.* Thermal degradation and flammability properties of poly(propylene)/carbon nanotube composites. *Macromol. Rapid Commun.* **23,** 761–765 (2002).

Kelemen, S. R. & Freund, H. XPS Characterization of Glassy-Carbon Surfaces Oxidized by O2, CO2, and HNO3. *Energy and Fuels* **2,** 111–118 (1988).

Kelly, E. N. *et al.* Oil sands development contributes polycyclic aromatic compounds to the Athabasca River and its tributaries. *Proc. Natl. Acad. Sci.* **106,** 22346–22351 (2009).

Kiema, G. K. & Brett, M. J. Electrochemical Characterization of Carbon Films with Porous Microstructures. *J. Electrochem. Soc.* **150,** E342 (2003).

Kim, C. *et al.* Fabrication of electrospinning-derived carbon nanofibre webs for the anode material of lithium-ion secondary batteries. *Adv. Funct. Mater.* **16,** 2393–2397 (2006).

Kim, C. *et al.* Self-sustained thin Webs consisting of porous carbon nanofibers for supercapacitors via the electrospinning of polyacrylonitrile solutions containing zinc chloride. *Adv. Mater.* **19,** 2341–2346 (2007).

Kim, C., Choi, Y. O., Lee, W. J. & Yang, K. S. Supercapacitor performances of activated carbon fibre webs prepared by electrospinning of PMDA-ODA poly(amic acid) solutions. *Electrochim. Acta* **50,** 883–887 (2004).

Knight, D. S. & White, W. B. Characterization of diamond films by Raman spectroscopy. *J. Mater. Res.* **4,** 385–393 (1989).

Ko, F. *et al.* Electrospinning of continuous carbon nanotube-filled nanofiber yarns. *Adv. Mater.* **15,** 1161–1165 (2003).

Kugatov, P. V & Zhirnov, B. S. Porous carbon / carbon composites produced from carbon black and petroleum pitch. *J. Porous Mater.* **20,** 875–882 (2013).

Lee, K. S., Park, C. W. & Kim, J. D. Synthesis of ZnO/activated carbon with high surface area for supercapacitor electrodes. *Colloids Surfaces A Physicochem. Eng. Asp.* **555,** 482–490 (2018).

Leontaritis, K. J. Asphaltene Deposition: A Comprehensive Description of Problem Manifestations and Modeling Approaches. *SPE Prod. Oper. Symp.* (1989).

Li, W. *et al.* Core – Shell Si / C Nanospheres Embedded in Bubble Sheet-like Carbon Film with Enhanced Performance as Lithium Ion Battery Anodes. *Small* **11,** 1345–1351 (2015).

Lima, A. L. C., Farrington, J. W. & Reddy, C. M. Combustion-derived polycyclic aromatic hydrocarbons in the environment - A review. *Environ. Forensics* **6,** 109–131 (2005).

Lu, T. & Olesik, S. V. Electrospun polyvinyl alcohol ultra-thin layer chromatography of amino acids. *J. Chromatogr. B Anal. Technol. Biomed. Life Sci.* **912,** 98–104 (2013).

Luo, X. *et al.* Study on structure, mechanical property and cell cytocompatibility of electrospun collagen nanofibres crosslinked by common agents. *Int. J. Biol. Macromol.* **113,** 476–486 (2018).

Mack, J. J. *et al.* Graphite nanoplatelet reinforcement of electrospun polyacrylonitrile nanofibers. *Adv. Mater.* **17,** 77–80 (2005).

Maghsoudi, S. & Noroozian, E. HP-SPME of volatile polycyclic aromatic hydrocarbons from water using multiwalled carbon nanotubes coated on a steel fibre through electrophoretic deposition. *Chromatographia* **75,** 913–921 (2012).

Malladi, K., Wang, C. & Madou, M. Fabrication of suspended carbon microstructures by e-beam writer and pyrolysis. *Carbon N. Y.* **44,** 2602–2607 (2006).

Mani, R. C. *et al.* Nanocrystalline graphite for electrochemical sensing. *J. Electrochem. Soc.* **152,** E154–E159 (2005).

Mashayekhi, M., Mirzadeh, H. & Bagheri-khoulenjani, S. Effects of Crosslinking and Neutralization Agents on the Morphology of Chitosan Electrospun Scaffolds. **29,** 521–531

(2017).

Matsubara, H., Yamaguchi, Y., Shioya, J. & Murakami, S. Preparation and properties of graphite grown in vapor phase. *Synth. Met.* **18,** 503–507 (1987).

McCreery, R. L. Advanced carbon electrode materials for molecular electrochemistry. *Chem. Rev.* **108,** 2646–2687 (2008).

McDermott, M. T., Kneten, K. & McCreery, R. L. Anthraquinonedisulfonate Adsorption, Electron-Transfer Kinetics, and Capacitance on Ordered Graphite-Electrodes: The Important Role of Surface Defects. *J. Phys. Chem.* **96,** 3124–3130 (1992).

McDermott, M. T., McDermott, C. a. & McCreery, R. L. Scanning Tunneling Microscopy of Carbon Surfaces - Relationships Between Electrode-Kinetics, Capacitance, and Morphology for Glassy-Carbon Electrodes. *Anal. Chem.* **65,** 937–944 (1993).

McFadden, C. F., Russell, L. L., Melaragno, P. R. & Davis, J. A. Low-Temperature Pyrolytic Carbon Films: Electrochemical Performance and Surface Morphology as a Function of Pyrolysis Time, Temperature, and Substrate. *Anal. Chem.* **64,** 1521–1527 (1992).

McNally, T. *et al.* Polyethylene multiwalled carbon nanotube composites. *Polymer (Guildf).* **46,** 8222–8232 (2005).

Mohri, M. *et al.* Rechargeable lithium battery based on pyrolytic carbon as a negative electrode. *J. Power Sources* **26,** 545–551 (1989).

Mullins, O. C. The Modified Yen Model. *Energy & Fuels* **24,** 2179–2207 (2010).

Nacham, O., Clark, K. D. & Anderson, J. L. Extraction and Purification of DNA from Complex Biological Sample Matrices Using Solid-Phase Microextraction Coupled with Real-Time PCR. *Anal. Chem.* **88,** 7813–7820 (2016).

Nam, S. H. *et al.* Ag or Au nanoparticle-embedded one-dimensional composite TiO2nanofibres prepared via electrospinning for use in lithium-ion batteries. *ACS Appl. Mater. Interfaces* **2,** 2046–2052 (2010).

Natarajan, A., Mahavadi, S. C., Natarajan, T. S., Masliyah, J. H. & Xu, Z. Preparation of Solid and Hollow Asphaltene Fibers by Single Step Electrospinning. *J. Eng. Fiber. Fabr.* **6,** 1–6 (2011).

Nemanich, R. J., Glass, J. T., Lucovsky, G. & Shroder, R. E. Raman scattering characterization of carbon bonding in diamond and diamondlike thin films. *J. Vac. Sci. Technol. A Vacuum, Surfaces, Film.* **6,** 1783–1787 (1988).

Newsome, T. E. & Olesik, S. V. Electrospinning silica/polyvinylpyrrolidone composite nanofibres. *J. Appl. Polym. Sci.* **131,** 1–9 (2014).

Nicholson, R. S. Theory and Application of Cyclic Voltammetry for Measurement of Electrode Reaction Kinetics. *Anal. Chem.* **37,** 1351–1355 (1965).

Nlwa, O. & Tabel, H. Voltammetric Measurements of Reversible and Quasi-Reversible Redox Species Using Carbon Film Based Interdigitated Array Microelectrodes. *Anal. Chem.* **66,** 285–289 (1994).

Obraztsov, A. N. *et al.* Raman scattering characterization of CVD graphite films. *Carbon N. Y.* **46,** 963–968 (2008).

Obraztsov, A. N., Obraztsova, E. A., Tyurnina, A. V. & Zolotukhin, A. A. Chemical vapor deposition of thin graphite films of nanometer thickness. *Carbon N. Y.* **45,** 2017–2021 (2007).

Ohnishi, T., Murase, I., Noguchi, T. & Hirooka, M. Preparation of graphite film by pyrolysis of polymers. *Synth. Met.* **18,** 497–502 (1987).

Onozuka, K. *et al.* Electrospinning processed nanofibrous TiO2 membranes for photovoltaic applications. *Nanotechnology* **17,** 1026–1031 (2006).

Orlanducci, S. *et al.* Chemical/structural characterization of carbon nanoparticles produced by laser pyrolysis and used for nanotube growth. *Mater. Chem. Phys.* **87,** 190–195 (2004).

Pan, H., Li, L., Hu, L. & Cui, X. Continuous aligned polymer fibers produced by a modified electrospinning method. *Polymer (Guildf).* **47,** 4901–4904 (2006).

Park, B. Y., Taherabadi, L., Wang, C., Zoval, J. & Madou, M. J. Electrical Properties and Shrinkage of Carbonized Photoresist Films and the Implications for Carbon Microelectromechanical Systems Devices in Conductive Media. *J. Electrochem. Soc.* **152,** J136 (2005).

Peining, Z., Nair, A. S., Shengjie, P., Shengyuan, Y. & Ramakrishna, S. Facile Fabrication of TiO2 − Graphene Composite with Enhanced Photovoltaic and Photocatalytic Properties by Electrospinning. *Appl. Mater. Interfaces* **4,** 581–585 (2012).

Peled, E. Improved Graphite Anode for Lithium-Ion Batteries Chemically. *J. Electrochem. Soc.* **143,** L4 (1996).

Pereira, M. L. D. O., Grasseschi, D. & Toma, H. E. Photocatalytic Activity of Reduced Graphene Oxide-Gold Nanoparticle Nanomaterials: Interaction with Asphaltene and Conversion of a Model Compound. *Energy and Fuels* **32,** 2673–2680 (2018).

Pham, Q. P., Sharma, U. & Mikos, A. G. Electrospinning of Polymeric Nanofibers for Tissue Engineering Applications: A Review. *Tissue Eng.* **0,** 60509065116001 (2006).

Phillips, D. H. & Grover, P. L. Polycyclic hydrocarbon activation: Bay regions and beyond. *Drug Metab. Rev.* **26,** 443–467 (1994).

Phillips, D. H. Polycyclic aromatic hydrocarbons in the diet. *Mutat. Res.* **443,** 139–147 (1999).

Presland, A. E. B. & Walker, P. L. Growth of single-crystal graphite by pyrolysis of acetylene over metals. *Carbon* **7,** 1–8 (1969).

Qian, D., Dickey, E. C., Andrews, R. & Rantell, T. Load transfer and deformation mechanisms in carbon nanotube-polystyrene composites. *Appl. Phys. Lett.* **76,** 2868 (2000).

Qin, X. H. Structure and property of electrospinning PAN nanofibers by different preoxidation temperature. *J. Therm. Anal. Calorim.* **99,** 571–575 (2010).

Quinn, J. A., Yang, Y., Buffington, A. N., Romero, F. N. & Green, M. D. Preparation and characterization of crosslinked electrospun poly(vinyl alcohol) nanofibrous membranes. *Polymer (Guildf).* **134,** 275–281 (2018).

Ra, E. J., Raymundo-Piñero, E., Lee, Y. H. & Béguin, F. High power supercapacitors using polyacrylonitrile-based carbon nanofibre paper. *Carbon N. Y.* **47,** 2984–2992 (2009).

Ranganathan, S., Kuo, T. C. & McCreery, R. L. Facile preparation of active glassy carbon electrodes with activated carbon and organic solvents. *Anal. Chem.* **71,** 3574–3580 (1999).

Ranganathan, S., Mccreery, R., Majji, S. M. & Madou, M. Photoresist-Derived Carbon for Microelectromechanical Systems and Electrochemical Applications. *J. Electrochem. Soc.* **147,** 277–282 (2000).

Ranganathan, S., Steidel, I., Anariba, F. & Mccreery, R. L. Covalently Bonded Organic Monolayers on a Carbon Substrate : A New Paradigm for Molecular Electronics. *Nano Lett.* **1,** 491–494 (2001).

Ray, S. C., Saha, A., Jana, N. R. & Sarkar, R. Fluorescent carbon nanoparticles: Synthesis, characterization, and bioimaging application. *J. Phys. Chem. C* **113,** 18546–18551 (2009).

Redfern, B. US3109712 A. (1960).

Reina, A. *et al.* Large area, few-layer graphene films on arbitrary substrates by chemical vapor deposition. *Nano Lett.* **9,** 30–35 (2009).

Reneker, D. H. & Chun, I. Nanometer diameter fibers of polymer, produced by electrospinning. *Nanotechnology* **7,** 216–223 (1996).

Rode, A. V., Luther-Davies, B. & Gamaly, E. G. Ultrafast ablation with high-pulse-rate lasers. Part II: Experiments on laser deposition of amorphous carbon films. *J. Appl. Phys.* **85,** 4222–4230 (1999).

Rojo, A., Rosenstratten, A. & Anjo, D. Characterization of a Conductive Carbon Film Electrode for Voltammetry. *Anal. Chem.* **58,** 2988–2991 (1986).

Rossnagel, S. M., Russak, M. A. & Cuomo, J. J. Pressure and plasma effects on the properties of magnetron sputtered carbon films. *J. Vac. Sci. Technol. A Vacuum, Surfaces, Film.* **5,** 2150–2153 (1987).

Sandler, J. K. W., Kirk, J. E., Kinloch, I. A., Shaffer, M. S. P. & Windle, A. H. Ultra-low electrical percolation threshold in carbon-nanotube-epoxy composites. *Polymer (Guildf).* **44,** 5893–5899 (2003).

Sato, T., Furuno, S., Iguchi, S. & Hanabusa, M. Deposition of Diamond-like Carbon Films by Pulsed-Laser Evaporation. *Jpn. J. Appl. Phys.* **26,** L1487 (1987).

Savage, P. E., Klein, M. T. & Kukes, S. G. Asphaltene Reaction Pathways. 1. Thermolysis. *Ind. Eng. Chem. Process Des. Dev.* **24,** 1169–1174 (1985).

Sawyer, W. E. & Man, A. Patent US229335. (1880).

Schadler, L. S., Giannaris, S. C. & Ajayan, P. M. Load transfer in carbon nanotube epoxy composites. *Appl. Phys. Lett.* **73,** 3842–3844 (1998).

Schlesinger, R., Bruns, M. & Ache, H. J. Development of thin film electrodes based on sputtered amorphous carbon. *J. Electrochem. Soc.* **144,** 6–15 (1997).

Schueller, O. J. A., Brittain, S. T. & Whitesides, G. M. Fabrication of glassy carbon microstructures by pyrolysis of microfabricated polymeric precursors. *Adv. Mater.* **9,** 477–480 (1997).

Schwan, J., Ulrich, S., Batori, V., Ehrhardt, H. & Silva, S. R. P. Raman spectroscopy on amorphous carbon films. *J. Appl. Phys.* **80,** 440–447 (1996).

Sen, R. *et al.* Preparation of single-walled carbon nanotube reinforced polystyrene and polyurethane nanofibres and membranes by electrospinning. *Nano Lett.* **4,** 459–464 (2004).

Siddiqui, M. N. Developing an effective adsorbent from asphaltene for the efficient removal of dyes in aqueous solution. *Desalin. Water Treat.* **67,** 20450 (2017).

Siddiqui, M. N. *et al.* Effect of Natural Macromolecule Filler on the Properties of High-Density Polyethylene (HDPE). *Macromol. Symp.* **380,** 1800072 (2018).

Siddiqui, M. N., Redhwi, H. H., Younas, M., Hussain, S. & Achilias, D. S. Use of asphaltene filler to improve low-density polyethylene properties. *Pet. Sci. Technol.* **36,** 756–764 (2018).

Sill, T. J. & von Recum, H. A. Electrospinning: Applications in drug delivery and tissue engineering. *Biomaterials* **29,** 1989–2006 (2008).

Simm, W. Apparatus for the production of filters by electrostatic fibre spinning. (1976).

Singh, A., Jayaram, J., Madou, M. & Akbar, S. Pyrolysis of Negative Photoresists to Fabricate Carbon Structures for Microelectromechanical Systems and Electrochemical Applications. *J. Electrochem. Soc.* **149,** E78 (2002).

Stanislaus, A. Coke formation on catalysts during the hydroprocessing of heavy oils ’. *Appl. Catal.* **72,** 193–215 (1991).

Tatchell, J. J. Manufacture of carbon filaments. *U.S. Patent No. 3,663,170* (1972).

Taylor, G. Electrically Driven Jets. *Proc. R. Soc. A Math. Phys. Eng. Sci.* **313,** 453–475 (1969).

Taylor, G. Studies in Electrohydrodynamics. I. The Circulation Produced in a Drop by Electrical Field. *Proc. R. Soc. A Math. Phys. Eng. Sci.* **291,** 159–166 (1966).

Thostenson, E. T., Ren, Z. & Chou, T.-W. Advances in the science and technology of carbon nanotubes and their composites: a review. *Compos. Sci. Technol.* **61,** 1899–1912 (2001).

Tripatanasuwan, S., Zhong, Z. & Reneker, D. H. Effect of evaporation and solidification of the charged jet in electrospinning of poly(ethylene oxide) aqueous solution. *Polymer (Guildf).* **48,** 5742–5746 (2007).

US EPA. *EPA Method 8270D: Semivolatile organic compounds by gas chromatography/mass spectrometry SW-846*. (2014).

Wang, C. & Madou, M. From MEMS to NEMS with carbon. *Biosens. Bioelectron.* **20,** 2181–2187 (2005).

Wang, C., Li, Y., Ding, G., Xie, X. & Jiang, M. Preparation and characterization of graphene oxide/poly(vinyl alcohol) composite nanofibres via electrospinning. *J. Appl. Polym. Sci.* **127,** 3026–3032 (2013).

Wang, M. X., Huang, Z. H., Shimohara, T., Kang, F. & Liang, K. NO removal by electrospun porous carbon nanofibers at room temperature. *Chem. Eng. J.* **170,** 505–511 (2011).

Wang, P. *et al.* Mesoporous carbon nanofibres with a high surface area electrospun from thermoplastic polyvinylpyrrolidone. *Nanoscale* **4,** 7199–7204 (2012).

Wang, T., Geng, A. & Li, X. Pyrolysis of one crude oil and its asphaltenes: Evolution of gaseous hydrocarbons and carbon isotope. *J. Pet. Sci. Eng.* **71,** 8–12 (2010).

Wang, Y., Alsmeyer, D. C. & McCreery, R. L. Raman Spectroscopy of Carbon Materials: Structural Basis of Observed Spectra. *Chem. Mater.* **2,** 557–563 (1990).

Wang, Y., Pham, L., Vasconcellos, G. P. S. de & Madou, M. Fabrication and characterization of micro PEM fuel cells using pyrolyzed carbon current collector plates. *J. Power Sources* **195,** 4796–4803 (2010).

Wei, M. C. & Jen, J. F. Determination of polycyclic aromatic hydrocarbons in aqueous samples by microwave assisted headspace solid-phase microextraction and gas chromatography/flame ionization detection. *Talanta* **72,** 1269–1274 (2007).

Wen, Z. S., Yang, J., Wang, B. F., Wang, K. & Liu, Y. High capacity silicon / carbon composite anode materials for lithium ion batteries. *Electrochem. commun.* **5,** 165–168 (2003).

Wilson, S. D. R. & Hulme, A. Stress recrystallization of graphite. *Proc. R. Soc. A Math. Phys. Eng. Sci.* **266,** 20–32 (1962).

Wu, H., Zhang, R., Liu, X., Lin, D. & Pan, W. Electrospinning of Fe, Co, and Ni nanofibers:

synthesis, assembly, and magnetic properties. *Chemistry of materials* **19,** 3506–3511 (2007).

Wu, M., Wang, Q., Li, K., Wu, Y. & Liu, H. Optimization of stabilization conditions for electrospun polyacrylonitrile nanofibres. *Polym. Degrad. Stab.* **97,** 1511–1519 (2012).

Xie, K. & Karan, K. Kinetics and Thermodynamics of Asphaltene Adsorption on Metal Surfaces: A Preliminary Study. *Energy & fuels* **14,** 1252–1260 (2005).

Xu, C. L. *et al.* Fabrication of aluminum / carbon nanotube composites and their electrical properties. *Carbon N. Y.* **37,** 855–858 (1999).

Xu, L., Feng, J., Li, J., Liu, X. & Jiang, S. Graphene oxide bonded fused-silica fibre for solid-phase microextraction-gas chromatography of polycyclic aromatic hydrocarbons in water. *J. Sep. Sci.* **35,** 93–100 (2012).

Xu, X. *et al.* Biodegradable electrospun poly(l-lactide) fibres containing antibacterial silver nanoparticles. *Eur. Polym. J.* **42,** 2081–2087 (2006).

Yajima, S., Satow, T. & Hirai, T. Mechanism of the pyrolytic graphite formation. *J. Nucl. Mater.* **17,** 116–126 (1965).

Yang, Y. *et al.* Highly porous electrospun polyvinylidene fluoride (PVDF)-based carbon fibre. *Carbon N. Y.* **49,** 3395–3403 (2011).

Yen, T. F. Structure of Petroleum Asphaltene and Its Significance. *Energy Sources* **1,** 447–463 (1974).

Yoshino, K. *et al.* Graphite film prepared by pyrolysis of bacterial cellulose. *J. Appl. Phys.* **68,** 1720–1725 (1990).

Yoshio, M., Wang, H., Fukuda, K., Hara, Y. & Adachi, Y. Effect of Carbon Coating on Electrochemical Performance of Treated Natural Graphite as Lithium-Ion Battery Anode Material. *J. Electrochem. Soc.* **147,** 1245 (2000).

You, T. *et al.* Reductive H2O2 Detection at Nanoparticle Iridium/Carbon Film Electrode and Its Application as L-Glutamate Enzyme Sensor. *Electroanalysis* **16,** 54–59 (2004).

You, T., Niwa, O., Tomita, M. & Hirono, S. Characterization of platinum nanoparticle-embedded carbon film electrode and its detection of hydrogen peroxide. *Anal. Chem.* **75,** 2080–2085 (2003).

Yu, D. & Dai, L. Self-assembled graphene/carbon nanotube hybrid films for supercapacitors. *J. Phys. Chem. Lett.* **1,** 467–470 (2010).

Yu, D. G. *et al.* Oral fast-dissolving drug delivery membranes prepared from electrospun polyvinylpyrrolidone ultrafine fibres. *Nanotechnology* **20,** (2009).

Yu, D. G., Zhang, X. F., Shen, X. X., Brandford-White, C. & Zhu, L. M. Ultrafine ibuprofen-loaded polyvinylpyrrolidone fibre mats using electrospinning. *Polym. Int.* **58,** 1010–1013 (2009).

Yu, Y., Yang, Q., Teng, D., Yang, X. & Ryu, S. Reticular Sn nanoparticle-dispersed PAN-based carbon nanofibers for anode material in rechargeable lithium-ion batteries. *Electrochem. commun.* **12,** 1187–1190 (2010).

Zahabi, A., Gray, M. R. & Dabros, T. Kinetics and properties of asphaltene adsorption on surfaces. *Energy and Fuels* **26,** 1009–1018 (2012).

Zali, S., Jalali, F., Es-haghi, A. & Shamsipur, M. Electrospun nanostructured polystyrene as a new coating material for solid-phase microextraction: Application to separation of multipesticides from honey samples. *J. Chromatogr. B Anal. Technol. Biomed. Life Sci.* **1002,** 387–393 (2015).

Zanganeh, P. *et al.* Asphaltene deposition during CO 2 injection and pressure depletion: A visual study. *Energy and Fuels* **26,** 1412–1419 (2012).

Zewe, J. W., Steach, J. K. & Olesik, S. V. Electrospun Fibers for Solid-Phase Microextraction. *Anal. Chem.* **82,** 5341–5348 (2010).

Zhang, D. *et al.* Asphaltenes — Problematic but Rich in Potential. *Oilf. Rev.* 22–43 (2007).

Zhang, K., Choi, H. J. & Kim, J. H. Preparation and Characteristics of Electrospun Multiwalled Carbon Nanotube/Polyvinylpyrrolidone Nanocomposite Nanofibre. *J. Nanosci. Nanotechnol.* **11,** 5446–5449 (2011).

Zhang, W. J. A review of the electrochemical performance of alloy anodes for lithium-ion batteries. *J. Power Sources* **196,** 13–24 (2011).

Zhang, W. X., Wang, Y. Z. & Sun, C. F. Characterization on oxidative stabilization of polyacrylonitrile nanofibres prepared by electrospinning. *J. Polym. Res.* **14,** 467–474 (2007).

Zhang, X. *et al.* Electrospun TiO 2-graphene composite nanofibres as a highly durable insertion anode for Lithium ion batteries. *J. Phys. Chem. C* **116,** 14780–14788 (2012).

Zhao, Y., Wei, F. & Yu, Y. Effects of reaction time and temperature on carbonization in asphaltene pyrolysis. *J. Pet. Sci. Eng.* **74,** 20–25 (2010).

Zoccola, M. *et al.* Study on cast membranes and electrospun nanofibers made from keratin/fibroin blends. *Biomacromolecules* **9,** 2819–2825 (2008).

Zussman, E. *et al.* Mechanical and structural characterization of electrospun PAN-derived carbon nanofibers. *Carbon N. Y.* **43,** 2175–2185 (2005).